

https://dspace.org/

Partial Data Offloading with Mobile Edge Computing to Address Joint Challenges in Latency and Energy Efficiency

Singh, Kiren

2025
University of the Witwatersrand, Johannesburg
https://hdl.handle.net/10539/47638

Singh, Kiren . (2025). Partial Data Offloading with Mobile Edge Computing to Address Joint Challenges in Latency and Energy Efficiency [Master`s dissertation, University of the Witwatersrand, Johannesburg]. WIReDSpace. https://hdl.handle.net/10539/47638

Downloaded from a DSpace repository. https://dspace.org/

IMPACT OF LOW VOLTAGE RIDE THROUGH CAPABILITY OF IBT ON VOLTAGE STABILITY OF AN INTERCONNECTED POWER SYSTEM



UNIVERSITY OF THE
WITWATERSRAND,
JOHANNESBURG

Prepared by:

Ronald Henry Marais

1805127

Master dissertation in fulfilment of the requirements for the degree of

Master of Science in Engineering

School of Electrical & Information Engineering

University of the Witwatersrand

Prepared for:

Professor John Van Coller

May 2025

Declaration

I know the meaning of plagiarism and declare that all the work in the document, save for the properly acknowledged, is my own. I confirm that my supervisor has seen my report and any concerns revealed by such have been resolved with my supervisor.

Student name: Ronald Henry Marais



Signature:

Date: 2025/05/14

ACKNOWLEDGEMENTS

I would like to express my gratitude to Professor John Van Coller for his supervision during this research. His input greatly enhanced my understanding of research and the research process. I would also like to thank my wife for her encouragement and support. Additionally, I want to thank my friends and colleagues for their support during the period I worked on this research.

ABSTRACT

Impact of low voltage-ride-through on voltage stability for an interconnected power system

This research investigates the impact of the Inverter-Based-Technology (IBT) response during Low-Voltage-Ride-Through (LVRT) events on the classical P-V steady-state voltage collapse analysis. The response of the IBT Renewable-Energy-Sources (RES) during LVRT events has the form of a reduction in the IBT RES active-power export which is not considered in classical P-V steady-state voltage collapse analysis. The relationship between the transmission (Tx) voltage depression due to a fault on a Tx busbar and the IBT RES active-power export reduction is examined in this research. The classical P-V steady-state voltage collapse grid active-power transfer limits are compared between a conventional synchronous generator scenario (synchronous scenario) and a scenario where both synchronous generators and IBT RES are present (IBT RES scenario) using the Cigre Nordic voltage collapse test network. A novel prediction model is developed to approximate the IBT RES active-power reduction characteristic response to LVRT. Finally, it is shown that both the IBT RES LVRT active-power export response and the IBT RES LVRT reactive-power response impact the Tx-corridor active-power transfer limits and the Tx-corridor reactive-power export requirements not observed in the classical P-V steady-state voltage collapse analysis.

TABLE OF CONTENTS

CHAPTER 1: INTRODUCTION 13

1.1 Background 13
1.2 Research motivation 14
1.3 Research objective 15
1.4 Research contributions 16
1.5 Research structure and limitations 16

CHAPTER 2: LITERATURE REVIEW 20

2.1 Voltage stability 20
2.1.1 Power system stability classification 20
2.1.2 P-V Analysis techniques 22
2.1.2.1 P-V AND V-Q ANALYSIS 23
2.2 Low Voltage Ride Through (LVRT) events and international requirements 29
2.2.1 Standards 30
2.2.2 Grid Code 30
2.2.3 LVRT Grid Code Compliance used in this study 31
2.3 IBT RES Models 33
2.3.1 Power flow – simple single-generator model 33
2.3.2 Dynamic – 2nd RE generation models 34
2.4 The limitation of classical P-V steady-state voltage stability analysis 35

CHAPTER 3: TASK 1: IBT RES ACTIVE-POWER EXPORT RESPONSE FOR A 400 KV TX VOLTAGE DEPRESSION 37

3.1 LVRT response test system and system condition 37
3.2 System conditions impacting LVRT 38
3.3 System strength (Short Circuit Ratio (SCR)) 40
3.4 Simulation scenarios 41
3.5 Network variables impacting voltage depressions 42
3.6 Steady-state model 43
3.7 Dynamic models 44

3.7.1 Inverter model 44
3.8 Simulation results 47
3.8.1 Simulation Results - IBT RES responses 48
3.8.2 IBT RES responses for a fault at the Tx busbar 48
3.8.3 System strength - Tx fault admittance vs active-power. 50
3.9 Developing a robust Tx voltage versus active-power export reduction model 59
CHAPTER 4: TASK 2: CLASSICAL P-V STEADY-STATE ANALYSIS WITH AND WITHOUT IBT RES PRESENT (NO TX FAULT AND HENCE NO IBT RES LVRT RESPONSE) FOR THE CIGRE NORDIC VOLTAGE COLLAPSE TEST NETWORK 64
4.1 Cigre Nordic Test Network 65
4.2 Synchronous scenario: P-V steady-state curve analysis 67
4.2.1 Synchronous scenario: P-V steady-state analysis results 68
4.3 IBT RES scenario: P-V steady-state analysis 71
4.3.1 IBT RES scenario: P-V steady-state analysis results 72
4.4 Comparison between synchronous scenario and the IBT RES scenario P-V steady-state results 76
CHAPTER 5: TASK 3: EFFECT OF THE IBT RES LVRT RESPONSE DURING A 400 KV TX FAULT ON THE TX-CORRIDOR ACTIVE-POWER TRANSFER. 79
5.1 Phase 1 of task 3: a 400 kV Tx fault does not cause voltage collapse 79
5.1.1 Network initial conditions 80
5.1.2 Synchronous scenario 82
5.1.3 IBT RES scenario 83
5.1.4 Analysis of results 85
5.1.5 Synchronous scenario: active-power and reactive-power response. 86
5.1.6 IBT RES scenario: active-power and reactive-power response. 88
5.1.7 Approximate IBT RES characteristic response model prediction 91
5.2 Phase 2 of task 3: Set the study-area demand (load) for the Tx-corridor P-V active-power transfer limit for the limiting network contingencies in Table V and Table VII including the 5% margin 94

5.2.1 Network initial conditions....94
5.2.2 Results for the synchronous scenario....97
5.2.3 Results for the IBT RES scenario....98
5.2.4 Results for marginal stable condition (step 4)....101
5.2.5 Analysis of results....103
5.2.6 Synchronous scenario: active-power and reactive-power response....103
5.2.7 IBT RES scenario: active-power and reactive-power response for the marginal step case 105

CHAPTER 6: CONCLUSIONS 108

6.1 Research conclusions.... 108
6.2 Recommended for future research.... 109

ANNEXURE: LITERATURE PLATFORMS 110

ANNEXURE: SIMPLE MODEL - PSSE LOAD FLOW DATA 111

ANNEXURE: WECC 2ND GENERATION - PSSE DYNAMICS DATA 113

ANNEXURE: IBT RESPONSE – SAMPLE FOR SCR LOW, ACTIVE-POWER 1.PU, PF 1 AND LINE 1 117

ANNEXURE: VOLTAGE VS ACTIVE-POWER FOR INITIAL IBT ACTIVE-POWER 1P.U. AND 0.5P.U. 119

REFERENCES.... 123

LIST OF FIGURES

Figure 1 - Research structure 17
Figure 2 – Thesis layout 19
Figure 3 – Revised power system stability classification [PES-TR77] 21
Figure 4 – Voltage stability analysis techniques 23
Figure 5 – Voltage stability analysis: P-V curve 24
Figure 6 – Classical P-V curves and classical voltage stability definitions 25
Figure 7 – Classical P-V curves including two contingencies 25
Figure 8 – No IBT RES 27
Figure 9 – IBT RES present but remains connected during contingency 27
Figure 10 – IBT RES present but disconnects during the network contingency 28
Figure 11 – IBT RES LVRT with delayed return of active-power 28
Figure 12 – Typical LVRT profile 30
Figure 13 – RSA Renewable Grid Code Voltage Ride Through Capability requirement [37] 31
Figure 14 – SAGCRPP requirements for reactive-current export ΔIq/In, during low-voltage and high-voltage events at the POC [37] 32
Figure 15 – Post-fault active-power ramp up 33
Figure 16 – Typical Single-Generator Equivalent Power Flow Representation [28] 34
Figure 17 - Dynamic Model Evolution 35
Figure 18 – Simulation model 38
Figure 19 – System conditions that were varied and the variables that were monitored 40
Figure 20 – IBT RES active-power vs LVRT procedure 42
Figure 21 – PSSE Model 43
Figure 22 - Inverter Current (I) characteristic (active and reactive current) 45
Figure 23 - IBT RES active current (ip) and reactive current (iq) priority (left) and active-power export (P) and reactive-power export (Q) as a function of the voltage at the IBT RES POC (assuming inverter initially exporting zero reactive-power and initially exporting maximum active-power) 46
Figure 24 – iq and ip Grid Code requirement versus WECC dynamic model (assuming inverter initially exporting zero reactive current and exporting maximum active current) 47
Figure 25 - IBT RES response for fault initial conditions 48

Figure 26 - Nine faults with different fault admittance values causing different Tx busbar voltage dip depths (left) and different IBT RES active-power exports (right) 49
Figure 27 – Transmission voltage depression for high, medium and low system strength 49
Figure 28 – Active-power export reduction for varied fault admittances for high, medium and low system strengths for various initial conditions of active-power and reactive-power. 51
Figure 29 – Impact of active-power export reduction for varied fault admittance for high, medium and low system strengths for various initial conditions of active-power and reactive-power 52
Figure 30 – Active-power export reduction for varied fault admittances for high, medium and low system strengths for various initial conditions. 55
Figure 31 – Active-power export reduction for varied system strengths: high, medium and low for various fixed reactive-power initial conditions. 57
Figure 32 – Tx voltage vs active-power export reduction for the same pf with varying system strengths. 58
Figure 33 – Average Tx busbar voltage vs active-power export reduction for active-power output 1p.u. 60
Figure 34 – Average Tx voltage versus active-power export reduction for initial active-power export of 0.5pu 61
Figure 35 - Average characteristic response of 1pu and 0.5pu initial IBT RES active-power export curves to determine the Tx voltage vs active-power export characteristic model 62
Figure 36 – Characteristic model versus collector network response 63
Figure 37 – Cigre Nordic voltage collapse test network 65
Figure 38 – Tx-Corridor (for contingency analysis) 66
Figure 39 – Synchronous scenario: Load (MW) and generation (MW) location 68
Figure 40 – Synchronous scenario: P-V steady-state analysis for base and contingencies 69
Figure 41 – Synchronous scenario: P-V steady-state analysis with 5% reactive-power safety margin and limit 69
Figure 42 – Synchronous scenario: P-V steady-state analysis for Tx margin (still safe for limiting network contingency) and network limit (voltage collapse for worst network contingencies) 70

Figure 43 – Synchronous scenario: P-V steady-state analysis Tx-corridor margin and limit 71
Figure 44 – IBT RES scenario: Synchronous (MW) and IBT RES (MW) location 72
Figure 45 – IBT RES scenario: P-V steady-state analysis for base and contingencies... 73
Figure 46 – IBT RES scenario: P-V steady-state analysis with 5% reactive-power safety margin and limit 74
Figure 47 – IBT RES scenario: P-V steady-state analysis for Tx margin (still safe for limiting network contingency) and network limit (voltage collapse for worst network contingencies)..... 75
Figure 48 – IBT RES scenario: P-V steady-state analysis Tx-corridor margin and limit75
Figure 49 - P-V curve comparison of the synchronous scenario (blue) and of the IBT RES scenario (green) for the base network (solid lines) and worst contingency (dashed lines)..... 77
Figure 50 – Reactive-power comparison of the synchronous scenario (blue) and of the IBT RES scenario (green) for the limiting network contingency (dashed lines) ... 77
Figure 51 – Fault level comparison for the synchronous scenario and for the IBT RES scenario..... 78
Figure 52 – Synchronous Scenario: Initial steady-state conditions and load flow results 81
Figure 53 – IBT RES Scenario: Initial steady-state conditions and load flow results 81
Figure 54 – Synchronous scenario 82
Figure 55 – IBT RES scenario 84
Figure 56 – IBT RES scenario cumulative active-power and reactive-power 84
Figure 57 – Active-power balance 85
Figure 58 – Synchronous scenario: active-power response 86
Figure 59 – Synchronous scenario: reactive-power response. 87
Figure 60 – IBT RES scenario: active-power response 88
Figure 61 – IBT RES scenario: reactive-power response. 89
Figure 62 – IBT RES scenario active-power responses (using an accurate network model)..... 90
Figure 63 – Synchronous scenario: Network P-V limits condition and load flow..... 96
Figure 64 – IBT RES scenario: Network P-V limits and load flow..... 96
Figure 65 – Synchronous scenario: P-V network results 97
Figure 66 – Step 1-4 results 99

Figure 67 – Cumulative reduction of active-power export scaling factor and collapse margin for steps 1-4 100
Figure 68 – IBT RES scenario: bus voltages, active-power and reactive-power 102
Figure 69 – IBT RES scenario: IBT RES active-power and reactive-power 102
Figure 70 – Synchronous scenario active-power disturbance. 103
Figure 71 – Synchronous scenario reactive-power response. 104
Figure 72 – IBT RES scenario active-power response 105
Figure 73 – IBT RES active-power response 106
Figure 74 – IBT RES scenario reactive-power response 107

LIST OF TABLES

Table I– Network variables impacting the 132 kV POC voltage dip depth seen by the IBT RES 39
Table II – SCRs at the 132 kV Tx busbar and at the 132 kV IBT RES busbar 40
Table III– Network variables impacting by the voltage depressions 43
Table IV– Synchronous scenario: initial conditions 67
Table V– Synchronous scenario: P-V steady-state analysis results 68
Table VI– IBT RES scenario: initial conditions 71
Table VII– IBT RES scenario: P-V steady-state analysis results 73
Table VIII– Comparison of P-V steady-state results for the synchronous scenario and for the IBT RES scenario 76
Table IX– Initial steady-state conditions and limits 80
Table X– System response at instant of Tx-corridor peak active-power transfer (using a accurate network model)(IBT RES scenario)(Figure 60 A) 90
Table XI– IBT RES scenario approximate IBT RES characteristic response model prediction 91
Table XII– Steady-state scenario conditions and limits 95
Table XIII– Voltage collapse margin 98
Table XIV– Voltage collapse margin. 101
Table XV– Active-power disturbances at the time of the Tx-corridor maximum active-power flow 106

List of Acronyms and Definitions

COI:	Centre of Inertia
Electrical 'closeness'	The electrical 'closeness' is the relationship between a system event at a bus bar and the relative change in voltage at any busbar in the system. If the busbar experiences a similar voltage depression it is considered electrically close to the event.
IBT RES :	Inverter-Based-Technology Renewable-Energy-Source
IEA	International Energy Agency
IEEE	Institute of Electrical and Electronic Engineers
LVRT:	Low Voltage Ride Through
Momentary cessation	Temporarily cease to export active-power and reactive-power into an electric power system, while connected to the area electric power system, in response to a disturbance of the applicable voltages or the system frequency, with the capability of immediate restoration of output when the applicable voltages and the system frequency return to within defined ranges.
NSIP	Non-Synchronous Instantaneous Penetration
PAJ:	Phase-Angle-Jump
PV	Solar PhotoVoltaic
P-V	Active-power versus voltage characteristic
SCR	Short Circuit Ratio – system strength (the three-phase short circuit ratio e.g. IBT RES MVA / Three-phase short circuit MVA)
REDz:	Renewable Energy Development zones
REIPPP:	Renewable Energy Independent Power Producer Procurement Programme
RES	Renewable Energy Source
RoCoF:	Rate of Change of Frequency
SAGCRPP	South African Grid Code for Renewable Power Plants
SEA	Strategic Environmental Assessment
SI	System Inertia
SNSP	System Non-Synchronous Penetration
Tx	Transmission
VDIFD:	Voltage Dip Induced Frequency Deviation

CHAPTER 1: Introduction

1.1 Background

Voltage instability and voltage collapse have resulted in many blackouts [1]. Extensive literature on voltage stability in synchronous generator-based systems (synchronous scenario) has resulted in a theoretical and practical understanding of this phenomena in interconnected power systems [2]. It is well established that sufficient reactive-power support at specific network locations is required to maintain healthy grid voltage profiles. However this does not guarantee voltage stability, as voltage stability is not only a static phenomenon but also a dynamic phenomenon. However, to deal with the multiple potential contingencies, steady-state analysis is used to establish the Tx-corridor active-power transfer margin and the physical location of the voltage collapse point. This enables the system operator and the system planner to determine the Tx-corridor active-power transfer limit during normal operation (N) and to ensure the system can withstand the failure of any single Tx component (N-1) without voltage collapse.

Voltage stability risks will likely increase as more active-power needs to be transferred along Tx-corridors due to the increased integration of RES [3]. Although the Tx line impedance does not change the total impedance increases because of the reduction of the short-circuit current with the removal of the synchronous generators. This increases the total Tx-corridors impedance reducing the active-power transfer limit. The future grid will no longer be dominated by synchronous generators as RES, such as wind energy and solar energy, dominates new energy sources due to the declining costs of wind energy and solar energy sources and increasing RES capacity factors [4]. Technology improvements have accompanied the cost reductions [5] and IBT now dominates the renewable industry [6]. The rapid growth IBT RES increases the penetration of non-synchronous energy sources into a traditionally synchronous system and synchronous scenario (synchronous generators only). Power systems are transitioning away from the well-understood synchronous scenario [7], with growing implications for their stability [8] [9].

1.2 Research motivation

Voltage stability analysis has been extensively studied [1, 12-14]. The analysis techniques enable power system operation and planning to determine the Tx-corridor active-power transfer margin and physical location of voltage instability through analysis based on P–V curve analysis, V–Q curve analysis, Jacobian matrix analysis, eigenvalue analysis and load flow analysis [11]. Reference [11] reviews analytical methods of voltage stability analysis in IBT RES-dominant power systems and concludes that the mainstream method for voltage stability analysis is steady-state analysis. Although voltage collapse is a dynamic event, steady-state analysis has provided an adequate assessment of the risk of voltage instability for the synchronous scenario. However, with an increase in IBT RES (IBT RES scenario), the system dynamics have changed and various international events reported IBT RES disconnection as a result of grid faults [9-12]. The change in dynamics comes from the control action of the IBT RES replacing the dynamic behaviour of synchronous generators. To address this shortcoming, international standards and grid codes introduced IBT LVRT requirements [15, 16] which require IBT RES control action to ensure that the IBT RES remains connected to the grid during a grid fault and after the grid fault is cleared. The control action usually increases the IBT RES reactive-power export during the LVRT event and usually reduces the IBT RES active-power export during the LVRT event. The IBT RES active-power export ramps back up once the system voltage recovers [17, 18]. One of the challenges in the modern grid is the delayed IBT RES active-power export recovery following a network fault [10]. The reduction in IBT RES active-power export during the LVRT event and the IBT RES active-power export ramping up after the grid fault is cleared and the IBT RES reactive-power ramping down after the grid fault is cleared changes the system dynamics. Classical P-V steady-state voltage stability analysis does not consider the IBT RES response during and after the LVRT event. Voltage stability of power systems, when considering fault conditions, inducing the IBT RES LVRT response, is investigated in this research to determine the system response compared with classical P-V steady-state voltage stability analysis and the impact on Tx-corridor active-power transfer limits (for the limiting network contingency).

1.3 Research objective

In this research it is investigated whether classical Tx-corridor P-V steady-state active-power transfer limits (for the limiting network contingency) remain valid in an increased IBT RES interconnected power system. The researched questions are provided in the tasks below:

1. The first task is to derive an approximate relationship between the IBT RES active-power export reduction as a function of the Tx voltage depression, distance of the IBT RES from the Tx substation and the grid operating condition at the time of the Tx fault.
2. The second task is to investigate the difference between the classical P-V steady-state Tx-corridor active-power transfer limits (for the limiting network contingency) for the synchronous scenario and for the IBT RES scenario (no Tx fault present). For the synchronous scenario, the Tx-corridor active-power transfer limits (for the limiting network contingency) are expected to be higher because of the greater voltage support provided by synchronous generators compared with IBT RES.
3. The third task is to examine the P-V Tx-corridor active-power transfer during an LVRT event (now adding a Tx fault causing an IBT RES LVRT response including the ramping up of the active-power export after the Tx fault is cleared). To ensure no voltage collapse, the network condition is set to well below the classical Tx-corridor P-V steady-state active-power transfer limit (for the limiting network contingency) determined in the second task above. This allows observation of the Tx-corridor active-power transfer during the LVRT event. The reduction in the IBT RES active-power export during the Tx fault is determined by the Tx voltage depression versus the IBT RES active-power export reduction characteristic (the approximate relationship derived in the first task above) which is adjusted to the response observed with the accurate network model. This adjusted (more accurate) characteristic is used with the classical P-V steady-state analysis results to predict potential exceedance of the Tx-corridor P-V steady-state active-power transfer limits during the LVRT event. To test the Tx-corridor P-V steady-state active-power transfer limit (for the limiting network contingency) the downstream study-area demand (load) is set to the Tx-corridor P-V steady-state active-power transfer limit (for the limiting network

contingency) determined in the second task (no Tx fault present) and then by varying the Tx fault impedance in steps, changing the depth of the Tx voltage depression which in turn changes the IBT RES active-power export reduction. The IBT RES active-power export is predicted for each step using the adjusted (using the accurate grid model) characteristic response (determined in the third task). This enables the prediction of possible exceedance of the Tx-corridor P-V active-power transfer margins leading to voltage collapse.

1.4 Research contributions

- Classical P-V steady-state voltage collapse analysis is deficient when determining the Tx-corridor active-power transfer margins when IBT RES is present.
- The IBT RES active-power export during the LVRT event increases the Tx-corridor reactive-power requirement, which is not considered in the classical P-V steady-state voltage collapse analysis.
- An approximate IBT RES characteristic model is developed that can predict the relationship between the Tx voltage depression and the IBT RES active-power export reduction. This can be used as an initial scanning tool to determine the risk of Tx-corridor P-V steady-state active-power transfer limit exceedance with increased IBT RES.

1.5 Research structure and limitations

The research is divided into four sections and three tasks as indicated below

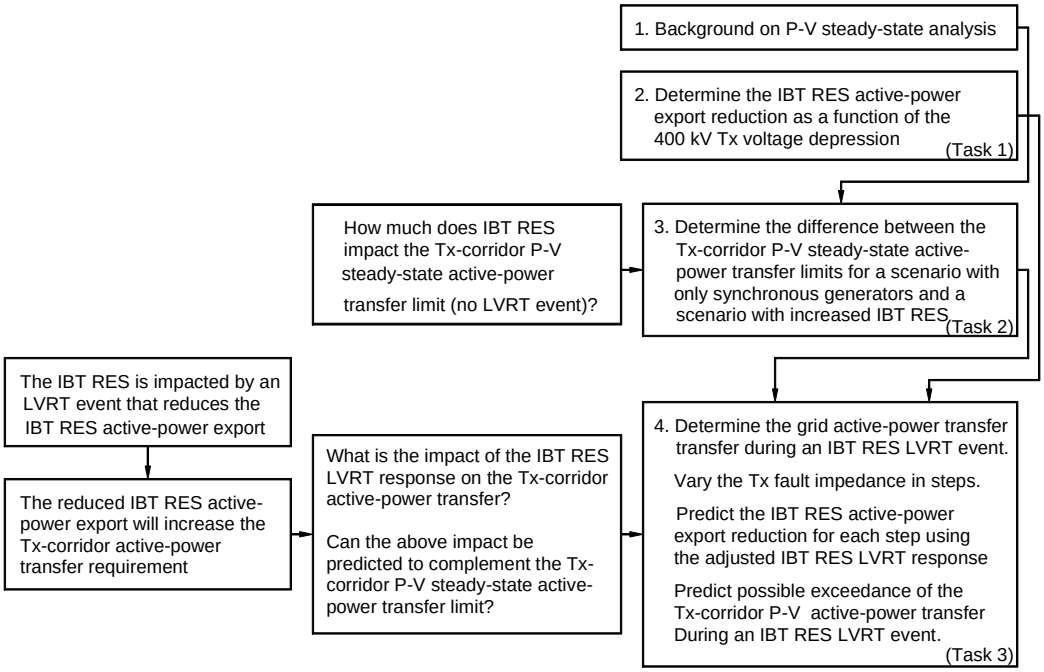

Figure 1 - Research structure

In the first section, the classical Tx-corridor P-V steady-state active-power transfer limits, LVRT standards and Grid Code implications are reviewed.

In the second section, IBT active-power export reduction for 400kV Tx voltage depressions is modelled.

In the third section, the IBT RES impact on classical P-V steady-state voltage collapse analysis is investigated (no Tx fault yet). This section applies P-V steady-state voltage collapse analysis to the Cigre Nordic voltage-collapse test network for both the synchronous scenario and for the IBT RES scenario (no Tx-fault yet and hence no IBT RES LVRT response yet). The grid initial conditions and contingencies are identical for both cases. P-V steady-state curves are generated, considering grid voltage collapse, Tx-corridor reactive-power margins and Tx-corridor safe operating limits (for the limiting network contingency). The Cigre Nordic voltage-collapse test network, initially comprising synchronous generators, is modified in the IBT RES scenario by substituting synchronous generators with the equivalent IBT RES. The Tx-corridor P-V steady-state active-power transfer limits (for the limiting network contingency) obtained in this

section are compared to establish if these limits remain valid for increased IBT RES integration.

In the fourth section, simulation of IBT RES LVRT response impacts on Tx-corridor active-power transfer is performed (in this section, in contrast with the third section above, a Tx-level fault is now added, including modelling of the IBT RES LVRT response). The simulations in section four are conducted in two phases, each subdivided into the synchronous scenario and into the IBT RES scenario.

The first phase of the investigation in the fourth section (now with a Tx fault), tested conditions where voltage collapse does not occur. Insights into the IBT RES LVRT active-power export reduction, IBT RES LVRT reactive-power response, Tx-corridor active-power transfer response and the impacts on Tx-corridor active-power transfer limits (for the limiting network contingency) for both scenarios were obtained. The ability to predict the IBT RES active-power export reduction for Tx faults was investigated using the approximate IBT RES characteristic response developed in the second section above with the simulated Tx bus voltage depression as input.

The second phase of the investigation in the fourth section (also now with a Tx fault), examined if the Tx-corridor P-V steady-state voltage collapse active-power transfer limits (for the limiting network contingency) determined in the third section (no Tx fault yet) are valid when a Tx fault is applied. In the second phase, in contrast to the first phase above, the loading in each scenario was increased from the initial load in the first phase above, to the Tx-corridor P-V steady-state active-power transfer limit (for the limiting network contingency).

The final section provides conclusions on the impact of the IBT RES LVRT response on classical P-V steady-state voltage collapse analysis.

The thesis layout is as follows:

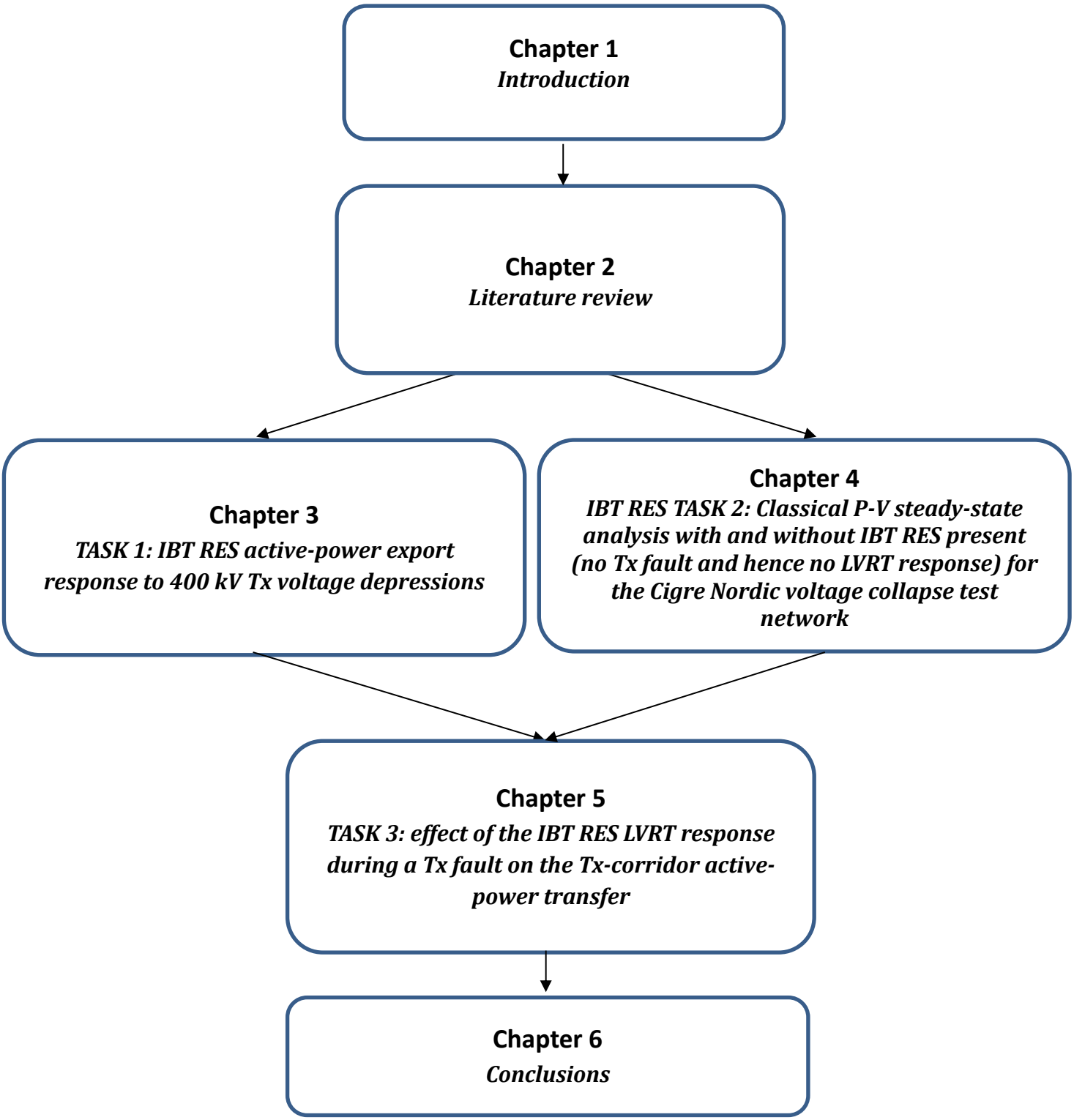

Figure 2 – Thesis layout

Chapter 2: Literature Review

This chapter presents a literature review of information relevant to the research, including the current knowledge base, sources of literature and knowledge gaps to be filled. The review covers voltage stability, classification, and analysis techniques, LVRT events and international requirements for IBT RES LVRT. Further, literature on LVRT standards, Grid Codes and compliance are reviewed. Finally, the literature on the dynamic model of IBT RES is reviewed. The relevance of the literature related to the research is discussed in each review section. The literature source is provided in Annexure: Literature platforms.

2.1 Voltage stability

Voltage stability is the ability of a power system to maintain acceptable voltages at all busbars under normal operating conditions and after being subjected to a disturbance [7]. Voltage stability is of greater concern for long transmission distances [19]. A condition for voltage stability is a positive voltage increase for a reactive-power injection at any busbar. Voltage collapse is a complex sequence of events resulting in low voltages over a wide area of the network. Voltage instability normally involves large disturbances and resulting large increases in power transfer or increase in load [2].

2.1.1 Power system stability classification

Power system stability classification in the last century assumed a synchronous system (synchronous generators only). Understanding the historical classification enables better scrutiny of the impact of high penetration IBT RES. This section provides a review of the traditional classification and the recent amendments to the classification to include IBT RES stability. However, the focus of this study is to better understand if the traditional methods for voltage stability are still valid with the IBT RES LVRT response especially in high IBT RES penetration grids.

It is recognised that power system stability is important to ensure a secure power supply [20] to avoid major blackouts. Kundur et al [21] describe the stability in the power system as essentially a single problem. However, subdividing the single problem into specific types of stability facilitates analysis. The stability type enables simplifying the system representation and consequently appropriate analytical techniques. The assumptions to analyse specific types of instability use an appropriate degree of system detail. For this reason, synchronous generation stability analysis is classified into three types (Figure 3 first three from the left). The three types are described in [20-22] and well-articulated in literature on the subject [2, 7, 23].

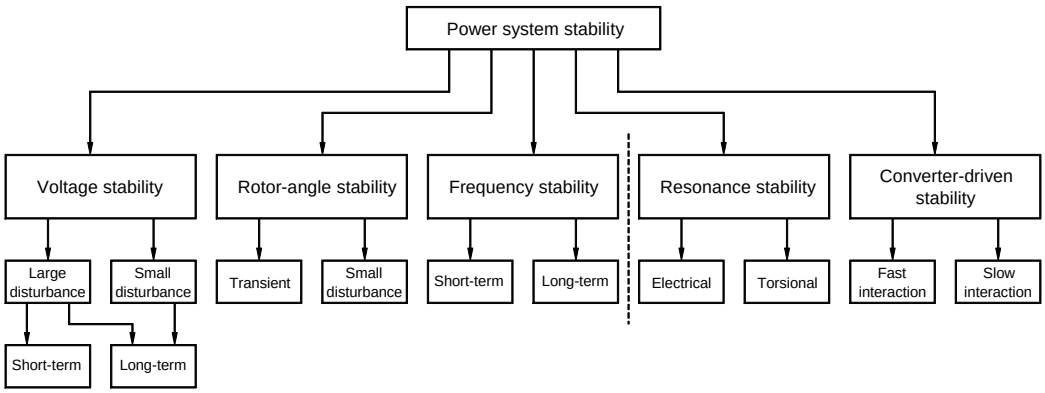

Figure 3 – Revised power system stability classification [PES-TR77]

The first type is based on the physical nature of the resulting mode observed in the main system variable in which instability can be observed, e.g. rotor angle, voltage or frequency. The second type considers the size of the disturbance as this influences the method of calculation and prediction of stability. The third type is the time span taken into consideration to assess stability. The three categories all consider the initial state, devices and processes. The traditional power system classification is shown in the blue shaded area (left) in Figure 3. The joint working group of IEEE and CIGRE generic definition is “Power system stability is the ability of an electric power system, for a given initial operating condition, to regain a state of operating equilibrium after being subjected to a physical disturbance, with most system variables bounded so that practically the entire system remains intact.” [21]

Key to stability is the transient condition associated with an event (e.g. a system disturbance such as a fault) for a particular initial condition. The transient condition can be a small or large disturbance. The impact on stability varies in duration. The transient event causes changes to the system rotor angle, frequency and voltage. In a synchronous system these three variables are sub-classified into discreet stability events for ease of study. However, emphasis is placed on the fact that all the characteristic of the system are in a transient state. This study focuses on large short-term system events which will initiate LVRT.

After closely examining the practical ramifications of increased IBT RES the IEEE Energy Society (PES) committee and CIGRE published a technical report to address the issue of stability definition and classification in power systems from a fundamental viewpoint. The Power System Dynamic Performance (PSDP) Committee Task Force on Stability in April 2020 published technical report PES-TR77 “Stability definitions and characterization of dynamic behaviour in systems with high penetration of power-electronic-interfaced-technologies” [24, 25]. PES-TR77 introduces two additional stability classifications for IBT RES namely, resonance and converter-driven stability, highlighted in the right side in Figure 3.

This thesis focuses on short-term large-disturbance voltage stability (first from the left in Figure 3). Transmission System Operators (TSOs) study voltage stability to ensure network transfer remains within acceptable active-power transfer limits to prevent voltage collapse and hence major blackouts.

2.1.2 P-V Analysis techniques

Although satisfactory voltage profiles are essential to voltage regulation, they do not provide certainty as to how close the grid is to voltage collapse. Analysis is required to determine the Tx-corridor active-power transfer margin to voltage collapse, the network contingency triggering voltage collapse, the reactive-power margin to network reactive-power capacity limits and the Tx-corridor active-power and reactive-power transfer conditions prior to the contingency. Voltage analysis techniques are broadly categorized into steady-state analysis and dynamic analysis indicated in Figure 4.

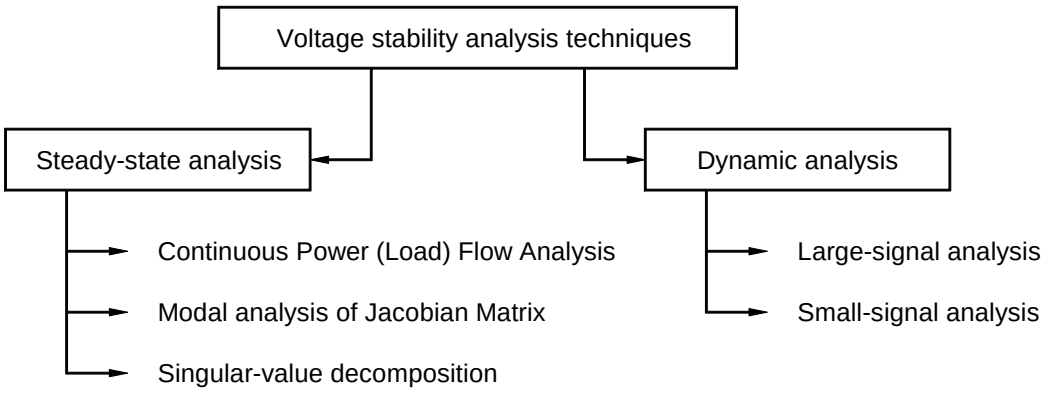

Figure 4 – Voltage stability analysis techniques

Various analysis techniques have been proposed [2, 11, 19, 26] to identify key indicators for evaluating Tx-corridor active-power transfer limits (for the limiting network contingency). In studies conducted by [17, 27], models were developed to simulate inadequacies in the European power system, which has high levels of renewable generation. These models confirmed that utilities use conventional load flow (steady-state) P-V and V-Q voltage collapse analysis.

2.1.2.1 P-V and V-Q analysis

To analyse the Tx-corridor active-power transfer limit, the receiving-end active-power (P) can be varied while observing the network receiving-end voltage (V) through P-V curve analysis. The voltage stability receiving-end reactive-power (Q) margin at a particular active-power transfer level is determined with V-Q curves. A simple two-bus system with a sending-end rms line voltage (E), receiving-end rms line voltage (V), line inductive reactance (X) and power angle (δ) is used. The active-power and reactive-power transfer equations below can be used to develop the P-V curve equation [19]

$$P = \frac{\mathrm{EV}}{\mathrm{X}} sin(\delta) \tag{2-1}$$

$$Q = \frac{\mathrm{EV}\cos(\delta) \; - \; V^2}{\mathrm{X}} \tag{2-2}$$

The receiving-end P-V curve equation is obtained from the above two equations [19]

$$V = \sqrt{\frac{E^2}{2} - QX \pm \sqrt{\frac{E^4}{4} - P^2X^2 - E^2QX}} \tag{2-3}$$

Equation 2-3 is used to plot the Tx-corridor active-power transfer limit for a constant power factor load (Figure 5). The voltage has two solutions indicated by the blue and orange curves. The blue line is calculated using the positive root in equations 2-3 and the orange with the negative root.

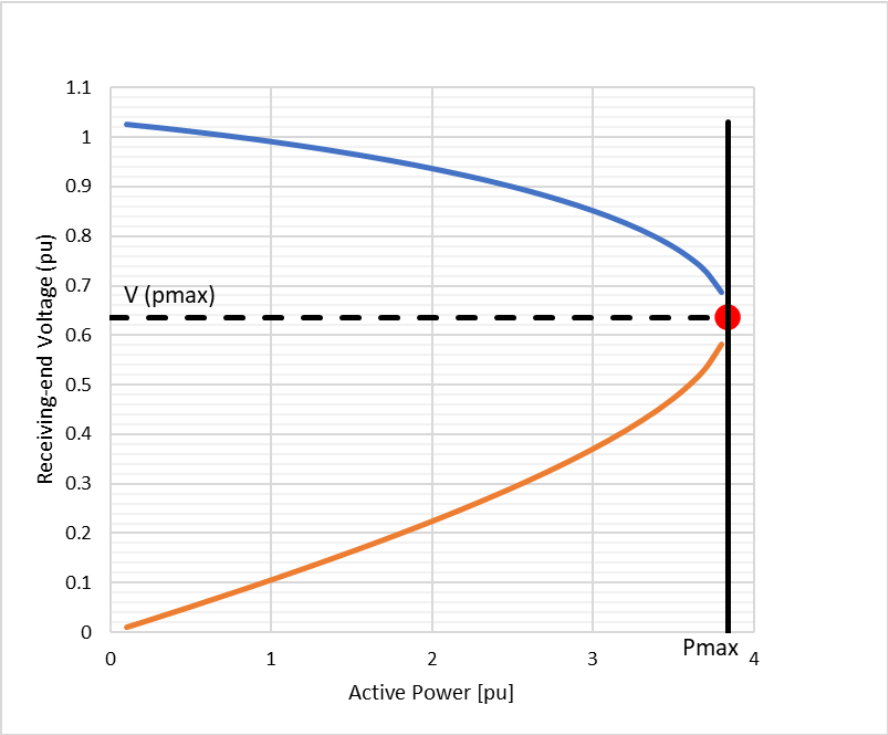

Figure 5 – Voltage stability analysis: P-V curve

The P-V curve knee point, indicated by the red dot, is the maximum Tx-corridor active-power (P_{max}) transfer and associated voltage ($V_{(pmax)}$) and can be calculated from

$$P_{max} = \frac{1}{X}\sqrt{\frac{E^4}{4} - E^2 QX} = \frac{E^2}{2X}\frac{\cos\delta}{1+\sin\delta} \tag{2-4}$$

$$V_{(pmax)} = \sqrt{\frac{E^2}{2} - QX} = \frac{E}{\sqrt{2}}\frac{1}{\sqrt{1+\sin\delta}} \tag{2-5}$$

Various network conditions, including different generation conditions, different voltage control device conditions (type and state) and different grid contingencies can be studied. The network is stable when dV/dP is less than 1 and unstable if dV/dP is greater than 1 (Figure 6).

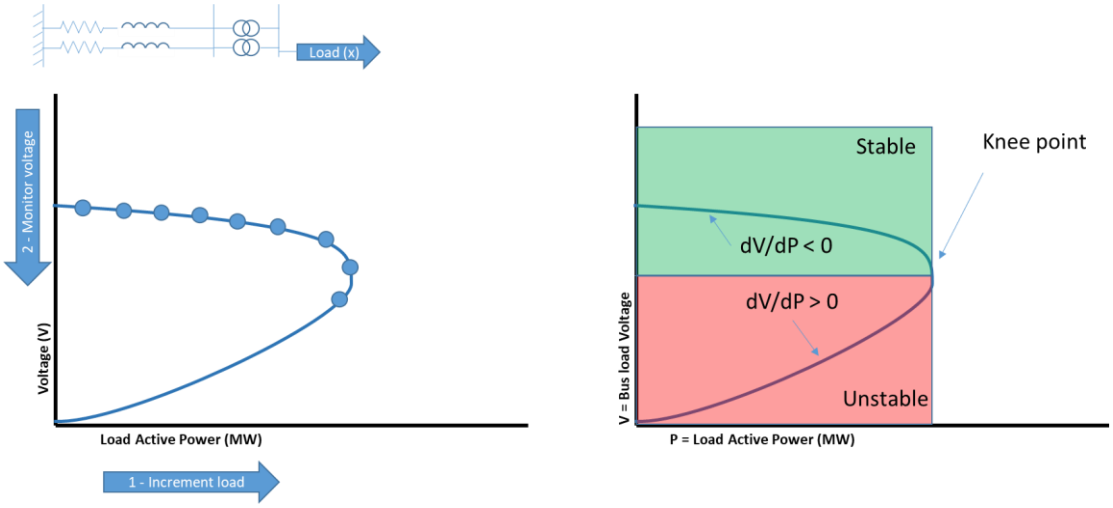

Figure 6 – Classical P-V curves and classical voltage stability definitions

The process is repeated for all credible contingencies and P-V curves are plotted (Figure 7), where the red and grey lines indicate the P-V curves for two contingency events. The knee point of each curve determines the maximum Tx-corridor active-power transfer for that state of the network. The lowest knee point, less some margin for uncertainty, normally 5%, is considered the maximum Tx-corridor active-power transfer capability (Pmax). That is, the grey P-V curve is the maximum Tx-corridor active-power transfer limit of the network.

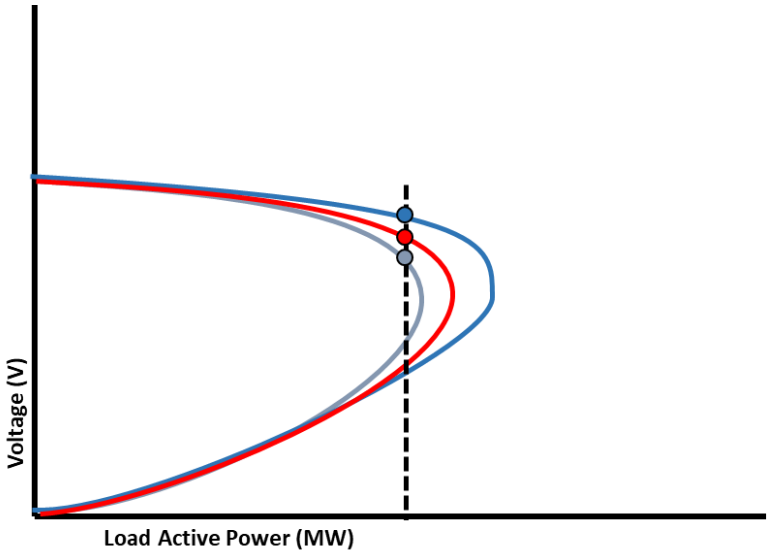

Figure 7 – Classical P-V curves including two contingencies

Various factors influence the Tx-corridor active-power transfer limit, including the load power factor, the type and state of the reactive-power devices, reactive-power capability of local generation, initial conditions and the load P-V characteristic.

P-V analysis is predominantly used for classical voltage stability. This method considers steady-state system conditions to construct the P-V curve. The impact of the Tx voltage depression caused by the Tx fault, which is subsequently cleared, is not considered. The active-power margin [27] is

$$Active\text{-}power\ margin = \frac{P_{max} - P_0}{P_{max}} \qquad (2\text{-}6)$$

- where P_0 is the maximum Tx-corridor active-power flow allowed.

When considering the IBT RES LVRT active-power reduction during the Tx fault, this significantly increases the Tx-corridor active-power transfer requirements during the LVRT active-power restoration [28], illustrated in Figure 8 to Figure 11. The $P_{load(max)}$ in Figure 8 is less than the lowest N-1 network contingency knee point to accommodate uncertainty margins.

Local IBT RES will reduce the net load as indicated in Figure 9 if the IBT RES remains connected as in steady-state studies. However, if the IBT RES disconnects, the net load $P_{load(max)}$ increases as indicated in Figure 10. In a delayed active-power IBT RES response – the major interest in this research - the net load $P_{load(max)}$ will also be increased as in Figure 11.

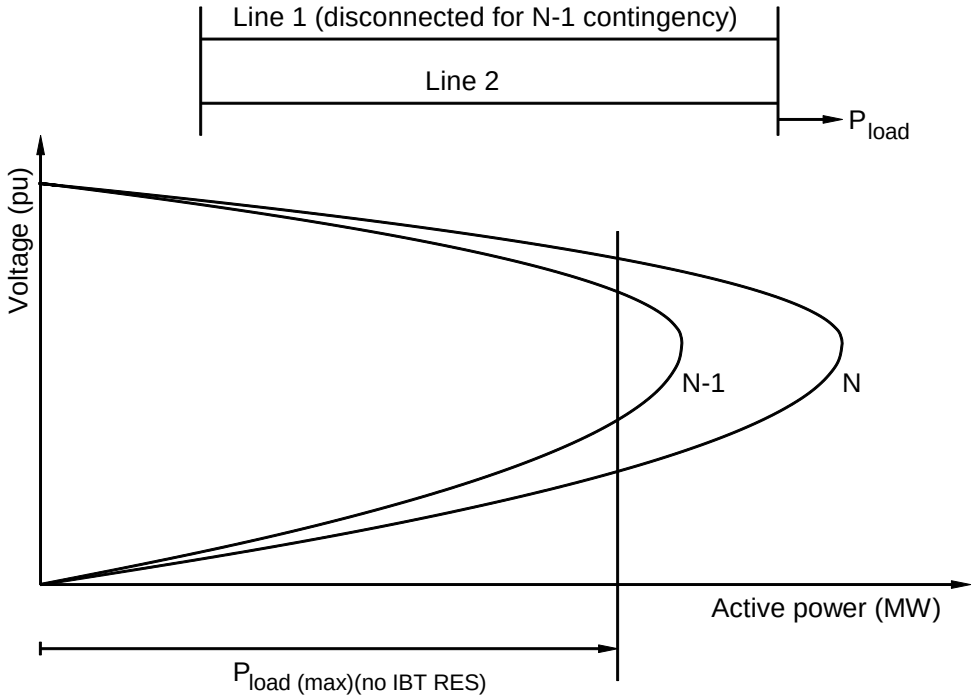

Active-power flow along line constrained by no voltage collapse for N-1 conditior

Figure 8 – No IBT RES

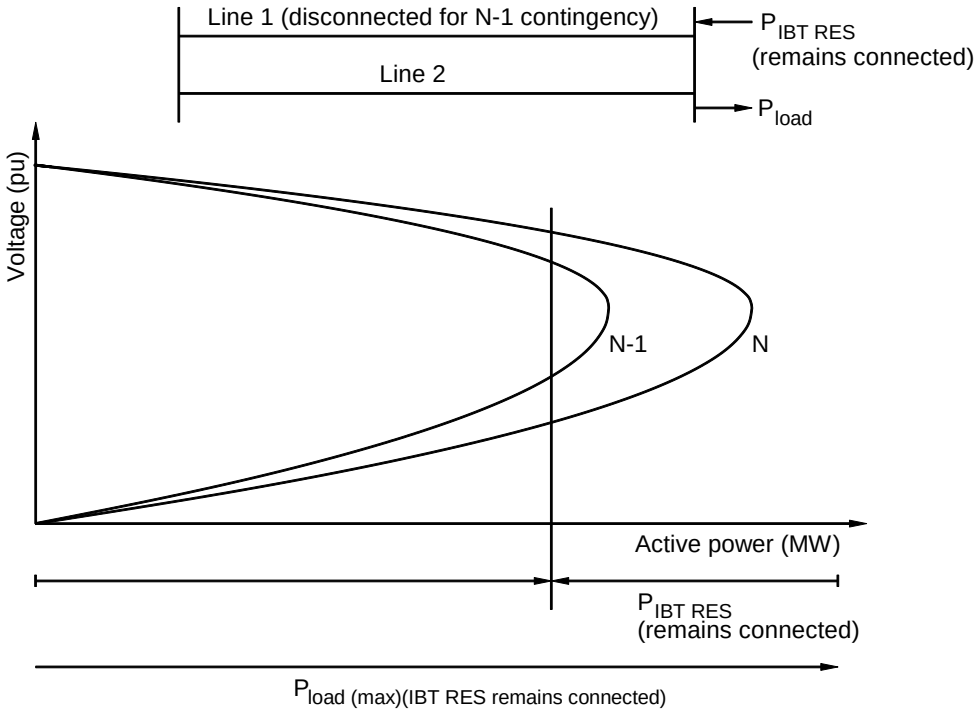

Active-power flow along line constrained by no voltage collapse for N-1 condition

Figure 9 – IBT RES present but remains connected during contingency

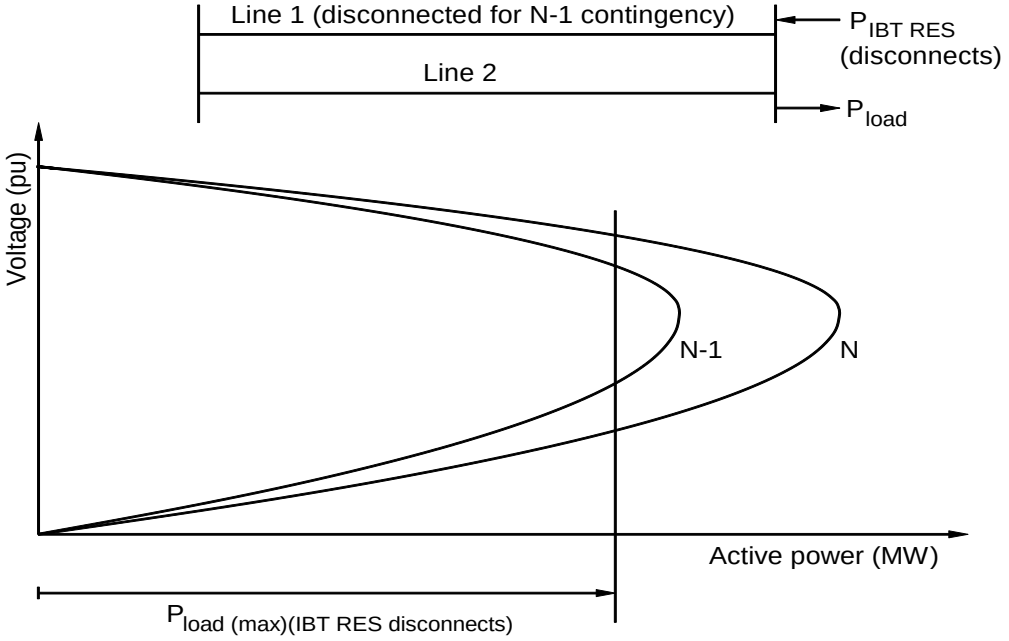

Active-power flow along line constrained by no voltage collapse for N-1 condition

Figure 10 – IBT RES present but disconnects during the network contingency

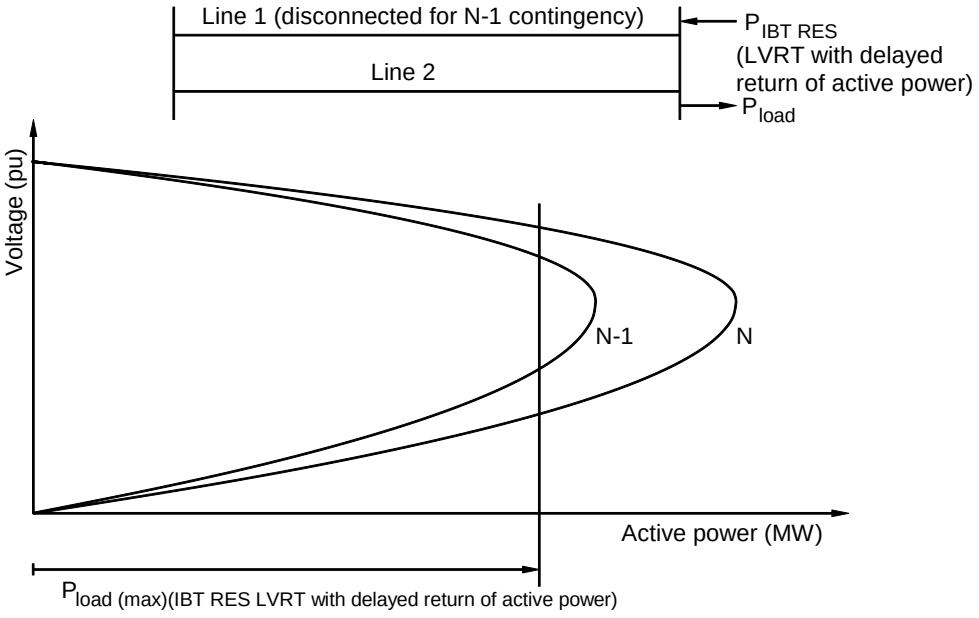

Active-power flow along line constrained by no voltage collapse for N-1 condition

Figure 11 – IBT RES LVRT with delayed return of active-power

2.2 Low Voltage Ride Through (LVRT) events and international requirements

Both synchronous generators and IBT RES are required to remain connected to the grid during and following the most common grid faults. Four key international events highlighted the vulnerability of IBT RES to low-voltage events. The events included Germany (2012) [29], Southern California (2016) [30], Australia (2016) [31] and Southern California (2017) [32, 33]. NREL presented the impact on voltage profiles for faults affecting IBT RES [35]. NREL refers to the phenomena as Fault Induced Delayed Voltage Recovery (FIDVR). The delay in voltage recovery delays the recovery of the IBT RES active-power export. To address this problem, international standards and grid codes have introduced LVRT requirements [15, 16] for fault events that cause voltage depressions outside of the normal operating voltage range. Fault-ride-through is defined as the ability to withstand voltage or frequency disturbances inside defined limits and to continue operating as specified [28]. The LVRT response during the low-voltage event increases the reactive-power export and reduces the active-power export to operate within the IBT RES current rating. The active-power export ramps back up once the grid voltage recovers. Coordinated voltage control at the Point of Connection (POC) requires fast reactive-power response during a voltage dip (voltage < 0.9pu). The typical voltage profile for LVRT compliance is shown Figure 12 (a): the IBT RES shall not trip (shaded green area) and the IBT RES is allowed to trip (shaded red area). The priority for weak grids is reactive-current export, Iq (in pu), during system low-voltage events (Figure 12 (b)). Alternatively active-power export is prioritised [36]. Prioritisation of reactive-power export is assumed in this study.

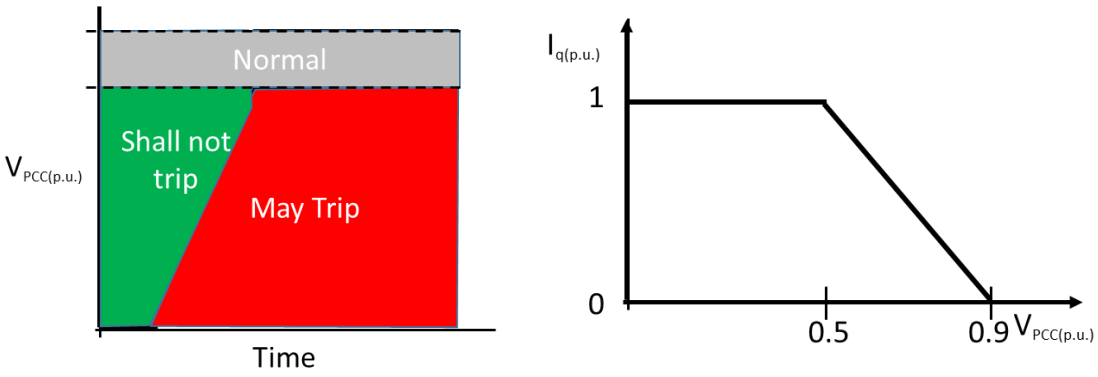

(a) (b)

$$iq(p.u.) = \begin{cases} 1 & : V_{PCC(p.u.)} < 0,5 \\ 2,5(0,9 - V_{PCC(p.u.)}) & : 0,5 \geq V_{PCC(p.u.)} \leq 0.9 \\ 0 & : V_{PCC(p.u.)} > 0,9 \end{cases} \quad (2\text{-}7)$$

Figure 12 – Typical LVRT profile

2.2.1 Standards

IEEE Std 1547 [28] is considered the international standard for LVRT for IBT RES. The requirements have evolved over the years. Initially (2003) with low IBT RES penetration the IBT RES was required not to actively regulate voltage and may trip on abnormal voltage/frequency events . In 2014 the requirement changed to where the IBT RES may actively regulate the voltage and shall ride through abnormal voltage and frequency events. In 2018 with higher IBT RES penetration and system experience, the requirements changed to where the IBT RES shall be capable of actively regulating voltage and shall ride through abnormal voltage/frequency events [28].

2.2.2 Grid Codes

Grid code LVRT requirements for many countries are similar to those in the IEEE 1547 standard; however they are not identical. The LVRT response prioritizes either reactive-power export or active-power export during a low-voltage event to support the

grid voltage, with most countries prioritizing reactive-power export. Grid code requirements can be divided into two parts: connection consistency and reactive-current export requirements during low-voltage events. Connection consistency requires the IBT RES to remain connected to the grid for a specific low-voltage event voltage profile. Reactive-current export requirements define the response of the reactive-power export as a function of the POC voltage. The response of the active-power export during these conditions is not defined. However, post-fault the IBT RES returns to pre-fault active-power, or a percentage of pre-fault active-power is defined.

2.2.3 LVRT Grid Code Compliance used in this study

The literature review indicates two key compliance requirements related to low-voltage events and active-power export. The specific requirements used for this study are from the South African Grid Code for Renewable Power Plants (SAGCRPP) version 3.1 [37] where large IBT RES (Figure 13) are required to export reactive-power during low-voltage events (Figure 14). In Figure 13, the IBT RES must remain connected to the grid in areas A,B (low voltage ride through) and D (high voltage ride through). In area C the IBT RES may disconnect from the grid.

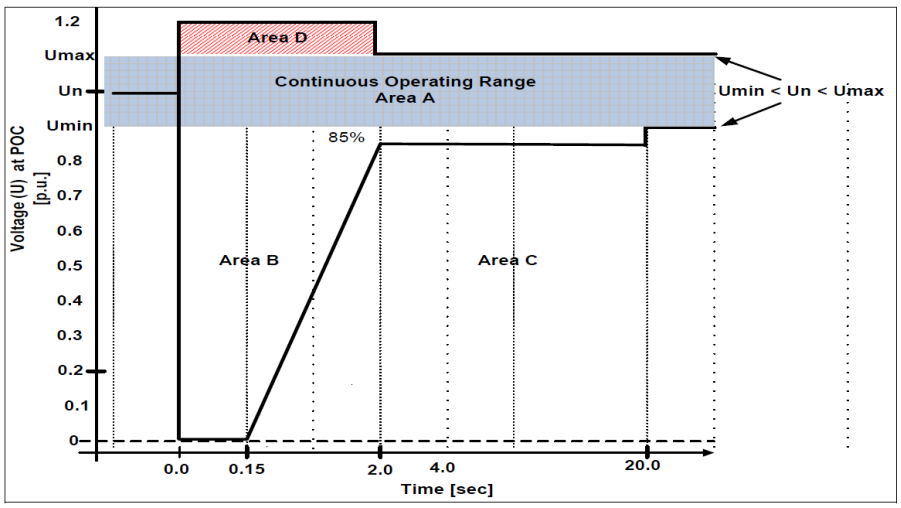

Figure 13 – RSA Renewable Grid Code Voltage Ride Through Capability requirement [37]

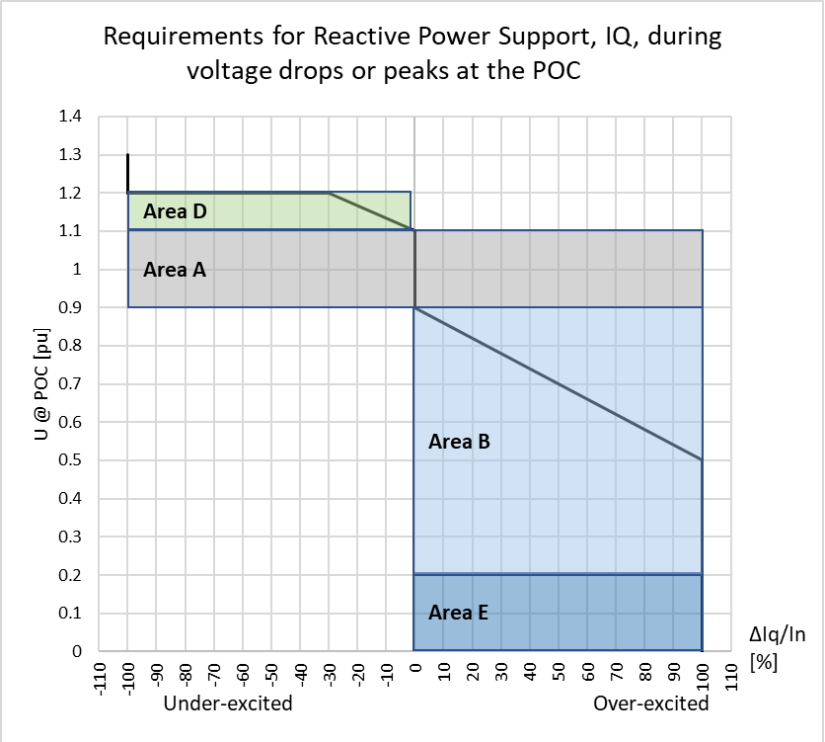

Figure 14 – SAGCRPP requirements for reactive-current export ΔIq/In, during low-voltage and high-voltage events at the POC [37]

The above reactive-power requirement is critical to the change in active-power export during a grid fault because of the restriction of the IBT RES current rating (In). The formula for the gradient of the reactive-current injection versus the change in voltage at the POC is defined as the constant k and can be calculated as

$$k = \frac{Change\ in\ \frac{I_q}{I_n}\ at\ POC}{Change\ in\ voltage\ at\ POC} \qquad (2\text{-}8)$$

Using the values in Figure 14 $k = \frac{100\% - 0\%}{50\% - 10\%} = 2{,}5$

Figure 14 only defines the reactive-power export with no definition of the active-power export for a drop of voltage >10% and <50%. For example, a voltage drop of 11%, could result in a 100% active-power export reduction (an extreme scenario) or it could be a change proportional to the amount of current committed to reactive-power export (a more likely scenario). This key parameter is not defined in this Grid Code. This Grid

Code does however define the active-power export ramp up following fault clearance as follows: Upon clearance of a fault each Renewable Power Plant (RPP) shall restore active-power production to at least 90% of the level available immediately prior to the fault within one second, illustrated in Figure 15.

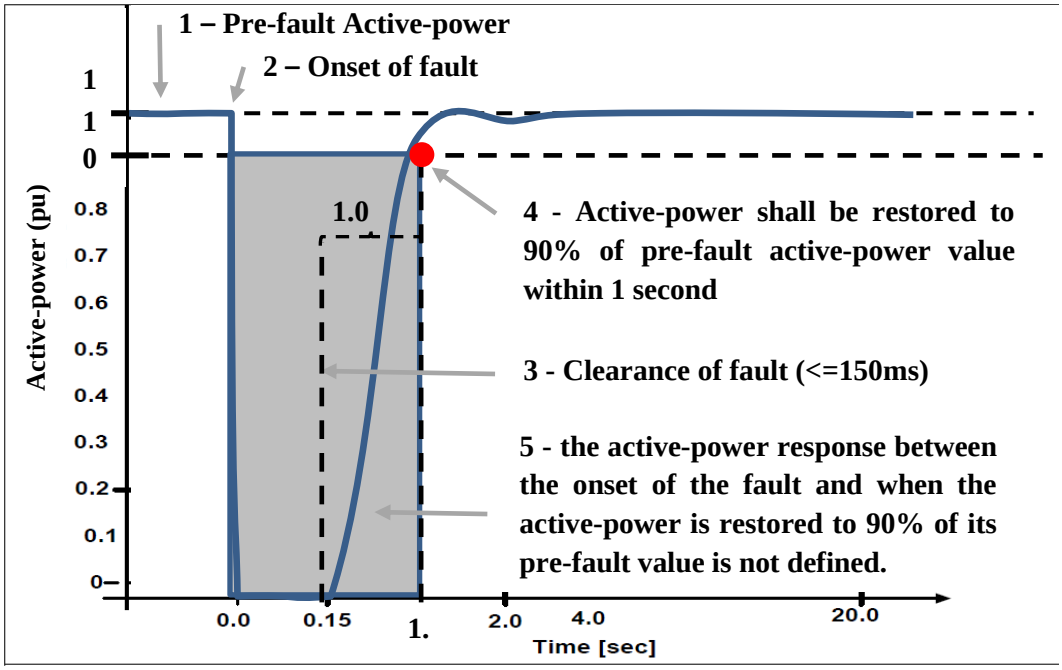

Figure 15 – Post-fault active-power ramp up

2.3 IBT RES Models

International best-practice modeling for steady-state and dynamic models are reviewed in this section. The models considered are power flow – simple single-generator and dynamic – 2nd generation models.

2.3.1 Power flow – simple single-generator model

The single-generator equivalent power flow representation is well established for modelling IBT RES and described in many reports, papers, and presentations [5, 28, 38-40]. The model consists of five elements: namely, IBT RES generation, pad-

mounted transformer, collector system, plant level reactive-power compensation and the substation transformer. The elements are aggregated into a simplified model. The collector system and reactive-power compensation are often unknown and not included. Models of the collector system and reactive-power compensation do not affect the dynamic simulations as the equivalent model must comply with the Grid Code dynamic requirements and hence how this is achieved is not necessary to know. The single-generator equivalent power flow representation obtained from [28] is illustrated in Figure 16.

The equivalent generator at bus 5 is the sum of all the IBT RES individual wind or PV in the generation plant. The pad-mounted transformer between bus 4-5 is the sum of the MVA of all the transformers and the parallel equivalent impedance. The collector system is the equivalent, however, if unknown, is sometimes not included.

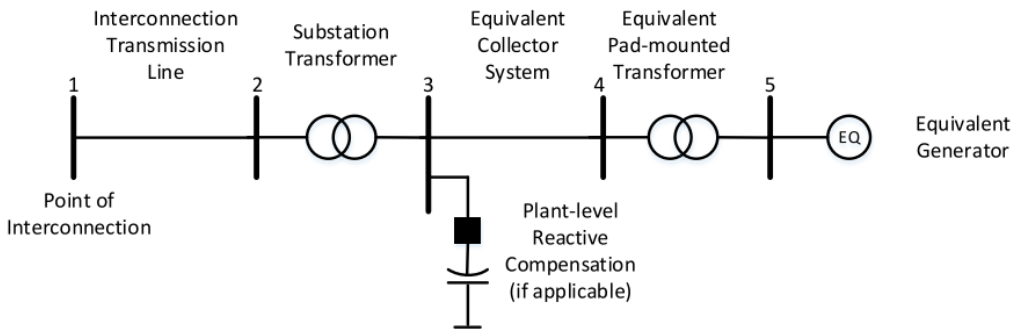

Figure 16 – Typical Single-Generator Equivalent Power Flow Representation [28]

2.3.2 Dynamic – 2nd RE generation models

The two dominant generic models for dynamic simulation of IBT RES are the Western Electricity Coordinating Council (WECC) model and the International Electrotechnical Commission (IEC) model. The dynamic model evolution is illustrated in Figure 17

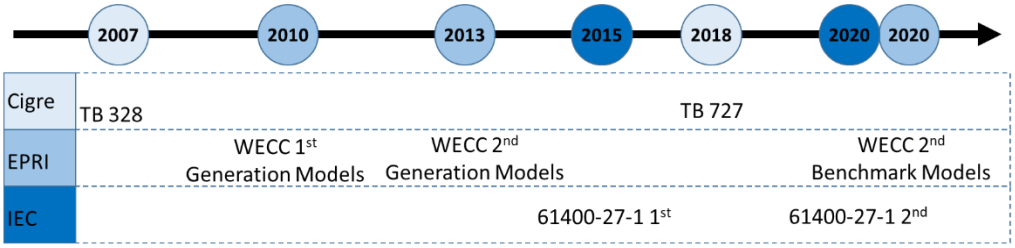

Figure 17 - Dynamic Model Evolution

After initial Cigre work on the dynamic models, described in TB 328 [41] and TB 727 [40], two major industry groups, Western Electricity Coordinating Council (WECC) Renewable Energy Modeling Task Force (REMTF) and International Electrotechnical Commission (IEC) Technical Committee (TC) 88, Working Group (WG) 27 continued developing IBT RES generic models for use in power system simulations. WECC 2nd Benchmark Models (2020) and the IEC 61400-27-1 2nd edition (2020)[42] models where released. The WECC models have found their way into several of the major commercial software platforms, namely, Siemens PTI PSS®E, GE PSLF, PowerWorld Simulator, DIgSILENT and PowerTech Labs TSAT™ and will be used in this study.

2.4 The limitation of classical P-V steady-state voltage stability analysis

Classical voltage stability analysis uses P-V curves produced in steady-state load flow simulations. Dynamic behaviour such as IBT RES active-power export reduction and IBT RES active-power export restoration resulting from the IBT RES response to LVRT events is not included. The IBT RES response to a grid fault is different from the conventional synchronous generator response to a grid fault. During a three-phase grid fault, such as one occurring at the local generator bus, the active-power from the synchronous generator cannot be injected into the grid. This is often compared with the IBT RES reduction in active-power export during an LVRT event. However, the synchronous generator shaft power during the fault is conserved in the acceleration of the rotor. The grid voltage is also supported with reactive-power and once the grid voltage recovers, the previous shaft power stored as excess kinetic energy in the rotor acceleration is released back into the grid. The synchronous generator can supply up to six times its rated active-power during the transient event. The increase in rotor angle

results in the increased active-power export into the grid following the transient event. The traditional concern is to ensure that rotor angle stability is maintained.

However, this is not applicable to IBT RES. In the case of a system low-voltage event caused by a system fault, the active-power export restoration is limited by the IBT RES current rating. The active-power export is gradually ramped up over time, which usually takes around one second. All IBT RES affected by a voltage reduction will reduce the active-power export in compliance with the Grid Code. However, the impact of this reduction and the methodology to study this risk are not defined. With increased IBT RES, the potential location and exposure of low voltage events resulting in cumulative active-power export reduction are also unclear.

Significant research has been published on LVRT for individual IBT RES. However, there is limited published research available on the impact (temporary reduction of multiple IBT RES active-power export during an LVRT event) on classical P-V steady-state analysis. This research investigates whether the individual IBT RES reduction in active-power export during LVRT events presents a cumulative system risk and what the impact is on classical P-V steady-state analysis.

.

Chapter 3: Task 1: IBT RES active-power export response for a 400 kV Tx voltage depression

This chapter investigates the relationship between a 400 kV Tx (where the fault occurs)(Figure 19) voltage depression and the IBT RES active-power export reduction (the IBT RES is typically located at a lower voltage level). Voltage stability is sensitive to any change in active-power export and any change in reactive-power export. The IBT RES response for a 400 kV Tx voltage depression was simulated with a single-machine equivalent [5, 28, 38-40] WECC dynamic IBT RES model [28, 38-40, 43-45] subjected to the simulated IBT RES voltage reduction at its POC.

3.1 LVRT response test system and system condition

The voltage depression dynamic response was examined with a single-machine infinite-bus IBT RES [5, 28, 38-40] connected to an external grid model. The single IBT RES model used a single-machine equivalent model [40, 43] and WECC dynamic models which are well documented by CIGRE, NERC, ESIG, EPRI, WECC and others [28, 38-40, 43-45].

The model allowed examination of the response of an IBT RES connected to the Tx substation which can be represented in three ways: schematic, zonal, and model representation which are illustrated in Figure 18.

In Figure 18A the IBT RES was connected to the 132 kV satellite and collector network which was connected to the Tx (400 kV) network through transformers. The location of the collector and satellite substations is some distance from the Tx substation. The various distances from the Tx substation can be considered as zones represented in Figure 18B. A fault on the 400 kV Tx busbar causes a voltage depression seen by each of the IBT RES within the 132 kV network. Depending on the distance away, the voltage will differ because of the different impedance to the IBT RES. The single-line model representation used for simulation modelling is represented in Figure 18C.

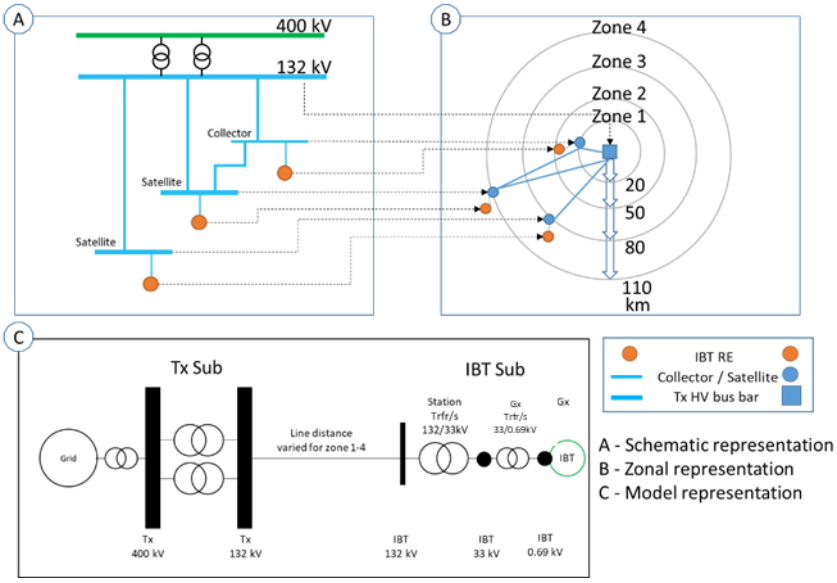

Figure 18 – Simulation model

3.2 System conditions impacting LVRT

Various factors impact the relationship between the 400 kV Tx voltage depression, the IBT RES active-power export reduction and the IBT RES reactive-power export increase:

- 400 kV Tx fault admittance – impacting the voltage dip depth.
- Distance of the IBT RES from the 400 kV Tx substation (where the 400 kV Tx voltage is measured) – represented by line length which impacts the POC voltage seen by the IBT RES.
- IBT RES initial active-power export and subsequent reactive-power export – limited by the IBT RES current rating.
- System strength (short circuit ratio (SCR)) at the 132 Tx busbar (Figure 19) – impacts the 132 kV IBT RES POC (Figure 19) voltage dip depth during the 400 kV Tx (Figure 19) voltage depression.

The network variables impacting the 132 kV IBT RES POC voltage dip are listed in Table I.

Table I– Network variables impacting the 132 kV POC voltage dip depth seen by the IBT RES

Variable	Number of variables	Description
400 kV Tx busbar voltage depression	9	Voltage (pu) at 400 kV Tx busbar where the fault is. The fault admittance is selected to produce the required 400 kV Tx voltage depression.
Distance from the 400 kV / 132 kV Tx substation to the 132 kV IBT RES POC	4	132 kV line lengths (20, 50, 80 and 110 km)
Initial IBT RES active-power export	2	IBT RES active-power export (pu)
Initial IBT RES reactive-power export	3	Power factor at the 132 kV IBT RES POC. No reactive-power export (pf=1), exporting (pf=0.95 leading) and importing (pf=0.95 lagging)
System strength at the 132 kV Tx busbar (Figure 19)	3	Low SCR, medium SCR and high SCR (the Short Circuit Ratio(SCR)) is the three-phase fault level (MVA) divided by the total IBT RES apparent-power rating (MVA)).

Simulations were performed with the various system conditions to evaluate the IBT RES active-power export reduction due to the 400 kV Tx fault. The varied system conditions and monitored values are illustrated in Figure 19

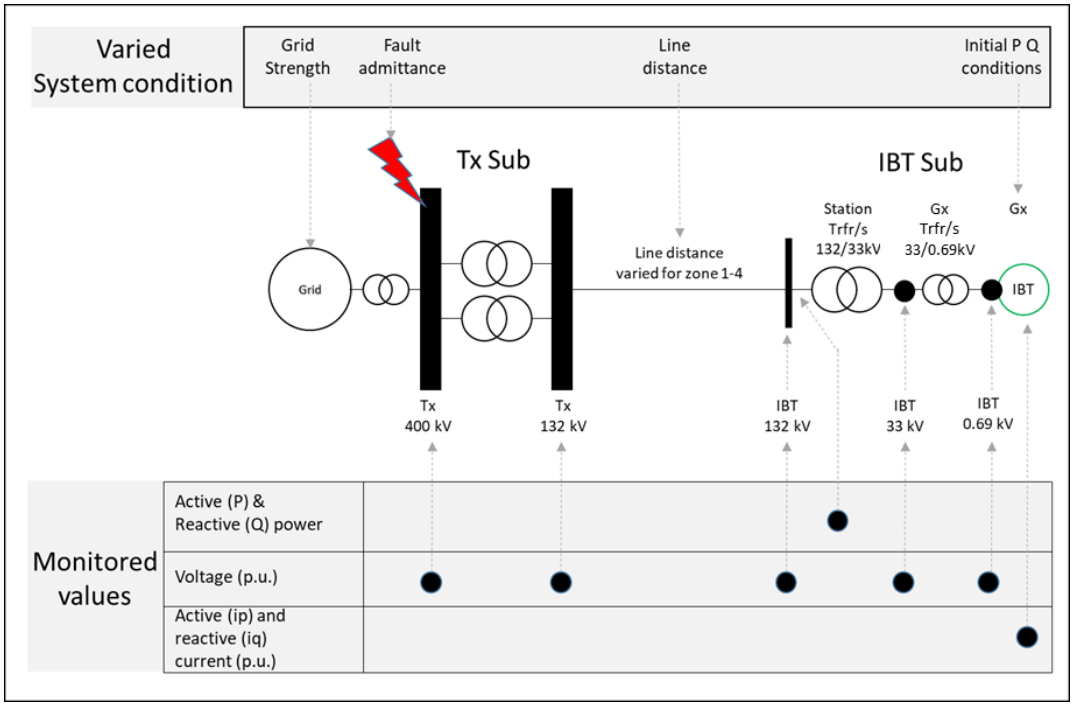

Figure 19 – System conditions that were varied and the variables that were monitored

3.3 System strength (Short Circuit Ratio (SCR))

The SCRs for low, medium and high system strengths at the 132 kV Tx busbar were calculated to be 4.4, 6.4 and 13.9. For these values the SCR at the 132 kV IBT RES busbar varied with the different line lengths simulated. The 132 kV Tx SCR remained constant and hence is used as the reference for the low, medium and high system strengths. The SCRs at the 132 kV Tx busbar and the 132 kV IBT RES busbar for the variation of line 1-4 are shown in Table II

Table II – SCRs at the 132 kV Tx busbar and at the 132 kV IBT RES busbar

	SCR at 132kV Tx busbar	4.4	6.4	13.9
		SCR at 132 kV IBT RES busbar		
Line	**km**	**Low**	**Medium**	**High**
Line1	**20**	3.9	5.2	8.7
Line2	**50**	3.3	4.1	5.8
Line3	**80**	2.9	3.5	4.4
Line4	**110**	2.6	3.0	3.6

The simulations initially considered a low SCR at the 132kV Tx busbar. Nine faults were applied on the 400 kV Tx busbar with varying fault admittances producing a range of voltage dip depths: 100%, 82%, 68%, 57%, 39%, 30%, 23%, 13% and 4%. Faults were applied for two initial active-power exports of 1pu and 0.5pu and three initial reactive-power exports of zero (pf=1), reactive-power export (pf=0.95 leading) and reactive-power import (pf= 0.95 lagging) and four line lengths of 20 km, 50 km, 80 km and 110 km.

3.4 Simulation scenarios

The process followed in the study is illustrated in Figure 20. Step 1 developed the network variables impacting the voltage depressions and the simulation model for steady-state and dynamic modelling. The details covered in this section have the same titles. Step 2 developed the model based on the IBT RES model and the Grid Code requirements. Step 3 ran the various simulations under the defined initial conditions. Step 4 was the predicted response based on the Grid Code requirements. The Grid Code defines the response of the IBT RES for a voltage at the IBT RES and not for a voltage depression at the Tx busbar. The next step refined the model to predict the active-power export reduction of the IBT RES for a Tx voltage reduction.

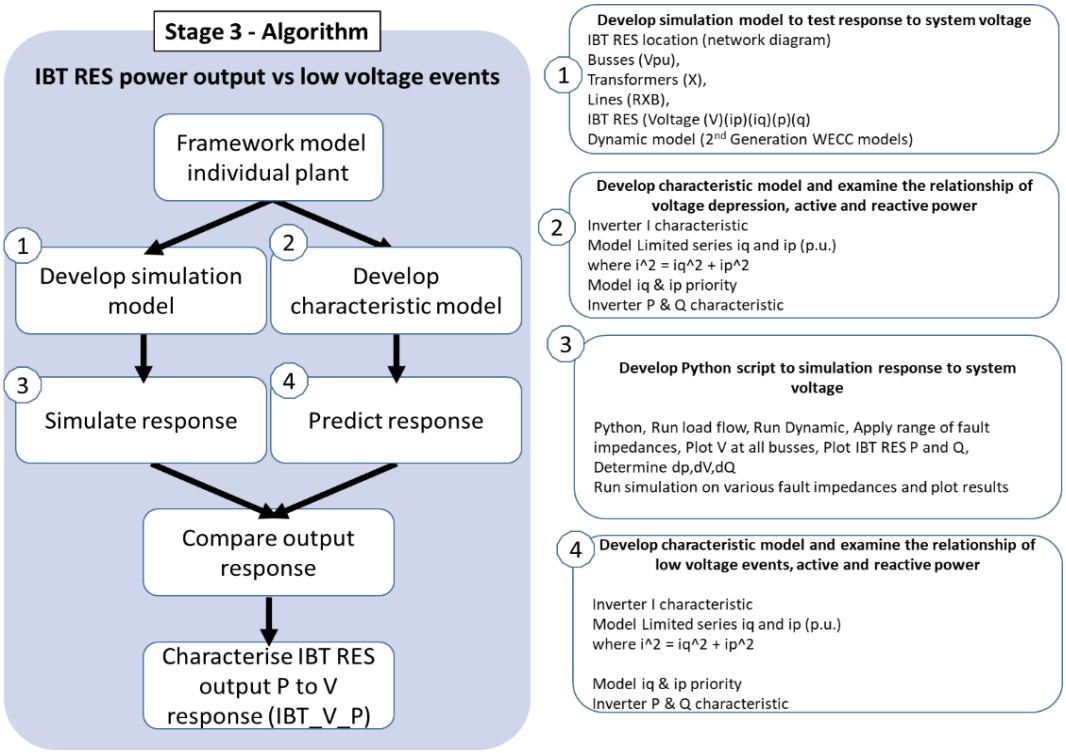

Figure 20 – IBT RES active-power vs LVRT procedure

3.5 Network variables impacting voltage depressions

Simulation scenarios were derived from the parameter combinations indicated in Table III. This resulted in 216 dynamic simulations for each system SCR.

The simulations were repeated for medium and high SCRs. This resulted in 3 × 216 = 648 dynamic simulations. The scenarios and monitored responses are shown in Table III

Table III– Network variables impacting by the voltage depressions

SCR	Active-power	Power Factor	Distance and fault admittance	IBT response	400kV Tx voltage	Voltage profile
Low	1.0 p.u.	1.0	Line (4) x voltage dip (9)	V,P,Q,iq,ip	V	V at all busses
		0.9lead	Line (4) x voltage dip (9)	V,P,Q,iq,ip	V	V at all busses
		0.9lag	Line (4) x voltage dip (9)	V,P,Q,iq,ip	V	V at all busses
Med	1.0 p.u.	1.0	Line (4) x voltage dip (9)	V,P,Q,iq,ip	V	V at all busses
		0.9lead	Line (4) x voltage dip (9)	V,P,Q,iq,ip	V	V at all busses
		0.9lag	Line (4) x voltage dip (9)	V,P,Q,iq,ip	V	V at all busses
High	1.0 p.u.	1.0	Line (4) x voltage dip (9)	V,P,Q,iq,ip	V	V at all busses
		0.9lead	Line (4) x voltage dip (9)	V,P,Q,iq,ip	V	V at all busses
		0.9lag	Line (4) x voltage dip (9)	V,P,Q,iq,ip	V	V at all busses
Low	0.5 p.u.	1.0	Line (4) x voltage dip (9)	V,P,Q,iq,ip	V	V at all busses
		0.9lead	Line (4) x voltage dip (9)	V,P,Q,iq,ip	V	V at all busses
		0.9lag	Line (4) x voltage dip (9)	V,P,Q,iq,ip	V	V at all busses
Med	0.5 p.u.	1.0	Line (4) x voltage dip (9)	V,P,Q,iq,ip	V	V at all busses
		0.9lead	Line (4) x voltage dip (9)	V,P,Q,iq,ip	V	V at all busses
		0.9lag	Line (4) x voltage dip (9)	V,P,Q,iq,ip	V	V at all busses
High	0.5 p.u.	1.0	Line (4) x voltage dip (9)	V,P,Q,iq,ip	V	V at all busses
		0.9lead	Line (4) x voltage dip (9)	V,P,Q,iq,ip	V	V at all busses
		0.9lag	Line (4) x voltage dip (9)	V,P,Q,iq,ip	V	V at all busses

3.6 Steady-state model

Load flow and dynamic models were created in PSSE. The model represented the busbars (Vpu), Transformers (X), Lines (RXB), IBT RES (Voltage (V)(ip)(iq)(p)(q) and Dynamic model (2nd Generation WECC models). The PSSE single-line diagram (SLD) is shown in Figure 21.

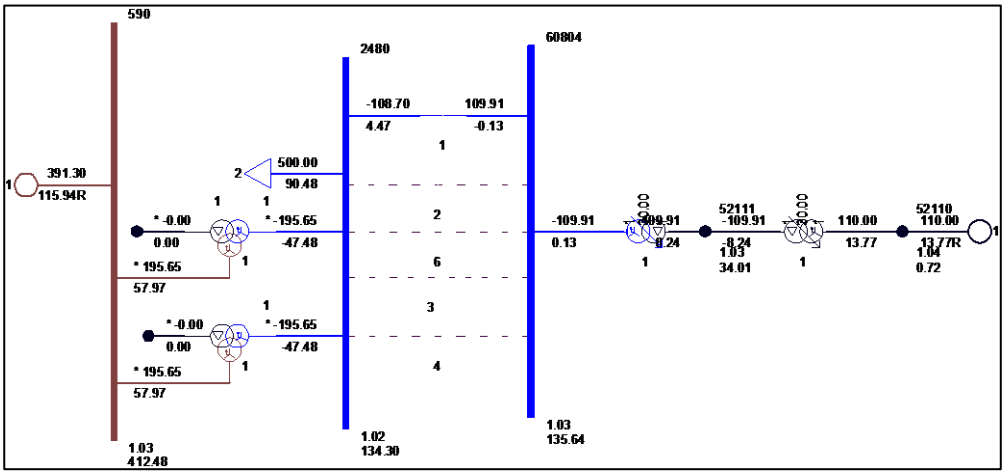

Figure 21 – PSSE Model

The model represented the Tx substation as having 400 kV busbars and 132 kV busbars with two transformers coupled to an external 400 kV grid. The external grid source impedance was varied for the different SCR scenarios. The Tx substation supplied a 132 kV (bus 2480) load and four lines connected to the point of 132kV IBT RES busbar (bus 60804). The lines represent the four distances studied from the Tx substation to the IBT RES busbar. Only one line is connected per study. The IBT RES identified in the literature review was used with an active-power output of 110 MW. The per unit base used in PSSE is 100 MVA. The model equivalences the station and generation transformers (the internal line cable connected are not considered).

3.7 Dynamic models

The IBT RES was modelled with the WECC 2nd generation models [38, 44].
The rate at which the active- power returns after a voltage dip is an important setting. The rate of active-power return affects the system voltage and dynamics. This study used the South African Grid Code requirement for active-power return post fault clearance namely 0.9pu/s.

3.7.1 Inverter model

Generic renewable energy system models are well documented by CIGRE, NERC, ESIG, EPRI, WECC and others [28, 38-40, 43-45]. The IBT RES power generation (positive active-current, ip) current characteristic illustrated in Figure 22. Current priority for active-current, ip, and reactive-current, iq, must respect these limits of IBT maximum current (imax) at all times in equation (3-1)

$$imax^2 = iq^2 + ip^2 \quad \textbf{(3-1)}$$

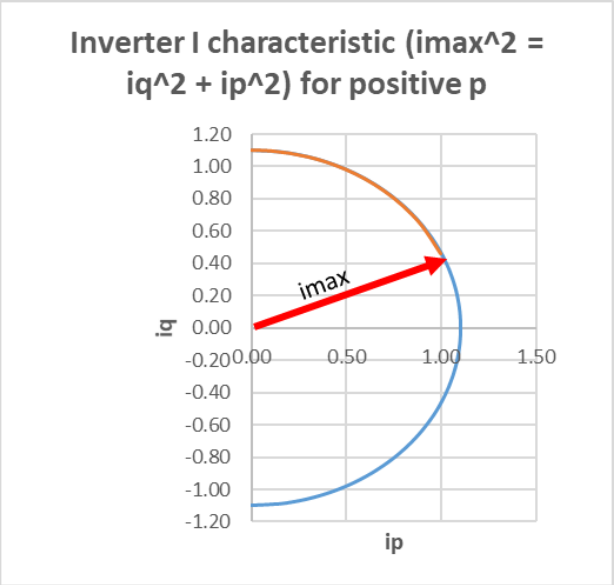

Figure 22 - Inverter Current (I) characteristic (active and reactive current)

The rate of active-power export recovery affects the system voltage and dynamics. This study uses the SAGCRPP requirement for active-power export recovery after fault clearance: Upon clearance of fault each RPP shall restore active-power production to at least 90% of the level available immediately prior to the fault within one second. Thus, the minimum active-power export ramp rate after the 400 kV Tx fault is cleared is 0.9(pu/s). This delayed recovery in active-power export after the Tx fault is cleared is included in the IBT RES model used in this study as it temporarily increases the active-power that must be transferred through the Tx-corridor immediately after the 400 kV Tx fault is cleared – which is the major concern in this study. The Grid Code requirement is that the inverter shall supply 1pu active-power at 0.95 pf (leading or lagging) within the normal operating voltage (+/- 5%), hence the minimum rated current is

$$\begin{aligned} &Minimum\ current\ limit \\ &= \frac{active\ power\ requirement\ (p.u)}{required\ power\ factor(pf)\ \times lower\ operating\ limit(p.u.)} \\ &= \frac{1}{0.95\ \times 0.95} \\ &= 1.1(\text{p.u.}) \end{aligned} \qquad \textbf{(3-2)}$$

'REGCCU' model - parameter (J+10) Imax – maximum current limit (pu) is set to 1.1. The dynamic models details are indicated Annexure: WECC 2nd Generation - PSSE Dynamics Data. The model is a voltage source model and is numerically stable for zero voltage fault conditions.

The IBT RES iq-priority determined by the Grid Code requirement is shown in Figure 23(left). The active-current or active-power export for 0.9pu voltage to 0.5pu voltage is not defined and is assumed to utilise the remaining available inverter current rating. The active-power and reactive-power are calculated by multiplying the current order (iq and ip) by the simulated terminal voltage as well as the square root of three. The ip and iq priority and associated P and Q characteristic are illustrated in Figure 23 and were implemented in the WECC IBT model.

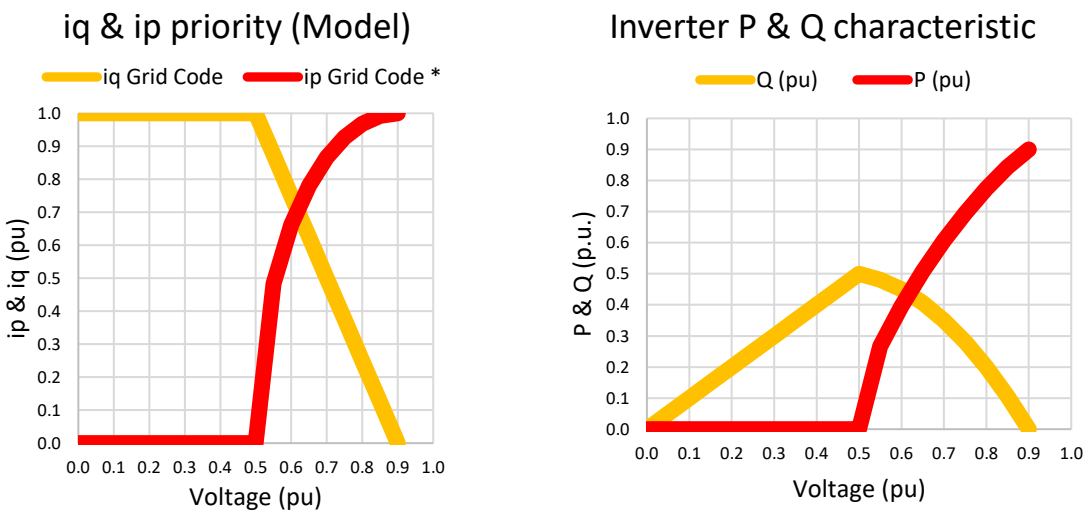

Figure 23 - IBT RES active current (ip) and reactive current (iq) priority (left) and active-power export (P) and reactive-power export (Q) as a function of the voltage at the IBT RES POC (assuming inverter initially exporting zero reactive-power and initially exporting maximum active-power)

The above inverter responses were implemented in the WECC dynamic model. The WECC dynamic model has only four points on the piece-wise-linear iq and ip curves. The iq can be modelled precisely. This is shown in Figure 24 by the iq Grid Code inverter response (thick yellow line) and the solid black overlapping WECC dynamic model line. However, the non-linear ip response was approximated as indicated in Figure 24 by the dashed black line due to the restricted number of points in the WECC model. The thick red line indicates the ip required response and the dotted black line the dynamic model response.

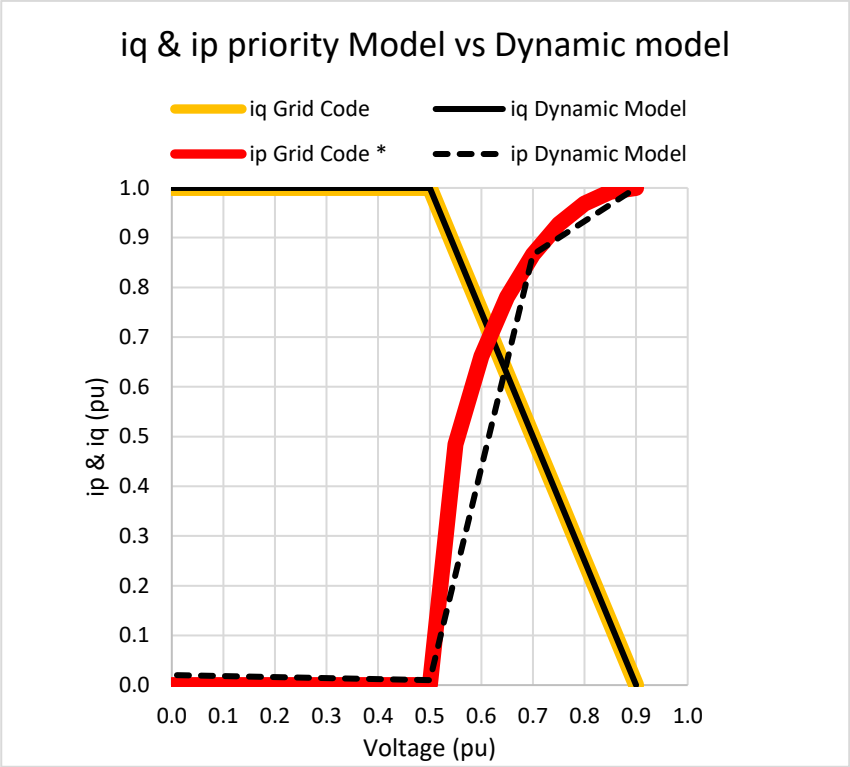

Figure 24 – iq and ip Grid Code requirement versus WECC dynamic model (assuming inverter initially exporting zero reactive current and exporting maximum active current)

3.8 Simulation results

This section provides the results of the RMS time response simulations for the previous scenarios. The results are structured as follows.

IBT RES response for:

- single fault at the 132 kV Tx busbar
- multiple fault admittance at the 132 kV Tx busbar with defined initial condition
- multiple fault admittance at 132 kV Tx busbar with multiple initial conditions
- system strength impact
    - multiple fault admittance at 132 kV Tx busbar with multiple initial conditions
    - initial power factor (pf) – 132 kV Tx voltage vs active-power
    - initial power factor (pf) – 132 kV Tx fault admittance vs active-power

3.8.1 Simulation Results - IBT RES responses

The IBT RES responses are presented in a series of three graphs for each fault applied. The 132 kV IBT RES busbar voltage (POC bus 60804), active-power and reactive-power are plotted as a function of time. For each run, nine faults with different per initial fault admittance values causing different Tx busbar voltage dip depths are applied for each of the four-line lengths. This results in 36 × 3 = 108 graphs for each of the 18 runs.

3.8.2 IBT RES responses for a fault at the Tx busbar

A fault response for one of the nine faults is illustrated in Figure 25. The voltage responses for all nine faults are shown in Figure 26. The dotted lines in Figure 25 indicate the Grid Code compliance limits and the solid line the output response. The minimum voltage and power responses are tracked to determine the voltage versus active-power export characteristics.

In all cases the reactive-power export to support the voltage was observed. In some cases, the post-fault voltage exceeded the limits. However, this does not influence the voltage depression active-power export so it was not investigated further. The first set of graphs for medium SCR, active-power 1pu, pf=1 and line 1 are illustrated in Figure 25 and Figure 26

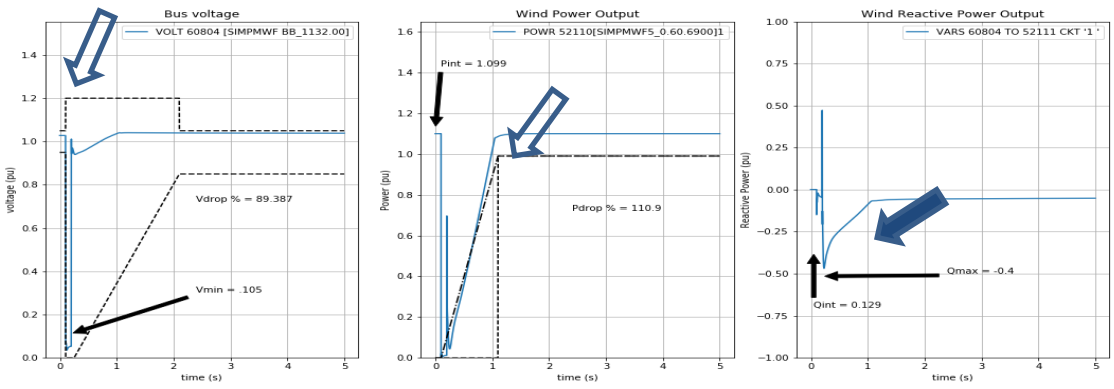

Figure 25 - IBT RES response for fault initial conditions

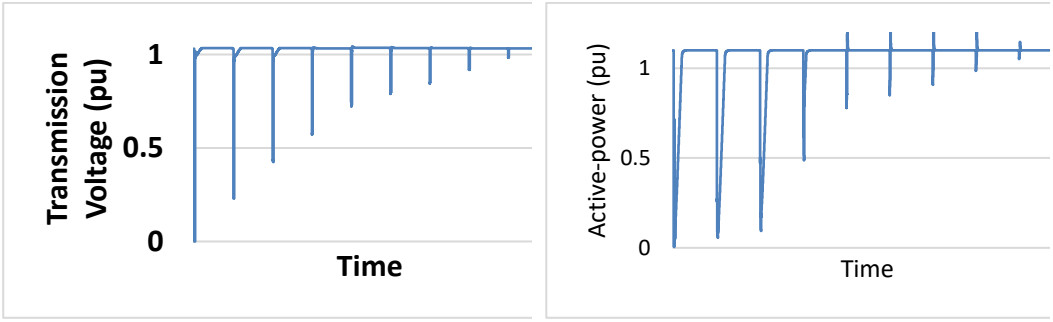

Figure 26 - Nine faults with different fault admittance values causing different Tx busbar voltage dip depths (left) and different IBT RES active-power exports (right)

The three high, medium and low system strengths, as described in section 0, are applied to each initial condition scenario with the same admittance fault applied to the transmission bus. A single initial condition with full active-power export (P100), no reactive-power import or export (pf=1) for the three system strength conditions is illustrated in Figure 27.

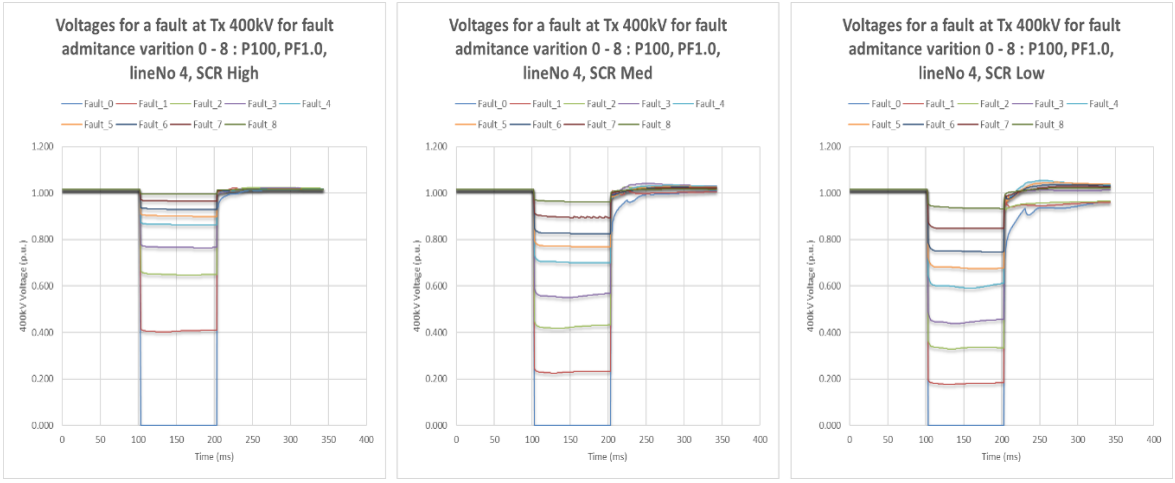

Figure 27 – Transmission voltage depression for high, medium and low system strength

It can be observed that an increased spread of voltage response for the same fault admittance occurs. This can be seen by the voltage plot clustering for high system strength (left) to a great spread (far right). The high source impedance from the low system strength causes a greater voltage depression for the same fault condition. The decreasing system strength hence makes the system less “stiff” to maintain the voltage

at the Tx busbar and which impacts the active-power reduction from all IBT RES that are impacted by the reduction of voltage.

3.8.3 System strength - Tx fault admittance versus active-power export.

The output plots examining the impact of active-power export reduction of the IBT RES for a Tx fault of varying fault admittance is described in this section. The results are plotted in Figure 28. Each plot provides the high, medium, and low system strength results for 100% power output. The columns provide the results for varying initial conditions of reactive-power export. The first column is zero injection (pf=1), the second column is exporting reactive-power (pf=0.95 leading) and the third column importing reactive-power (pf=0.95 lagging). The first row of three graphs illustrates the result for IBT RES integration at various line lengths from the Tx substation for each system strength. The second row indicates the average value of the various line lengths for each system strength.

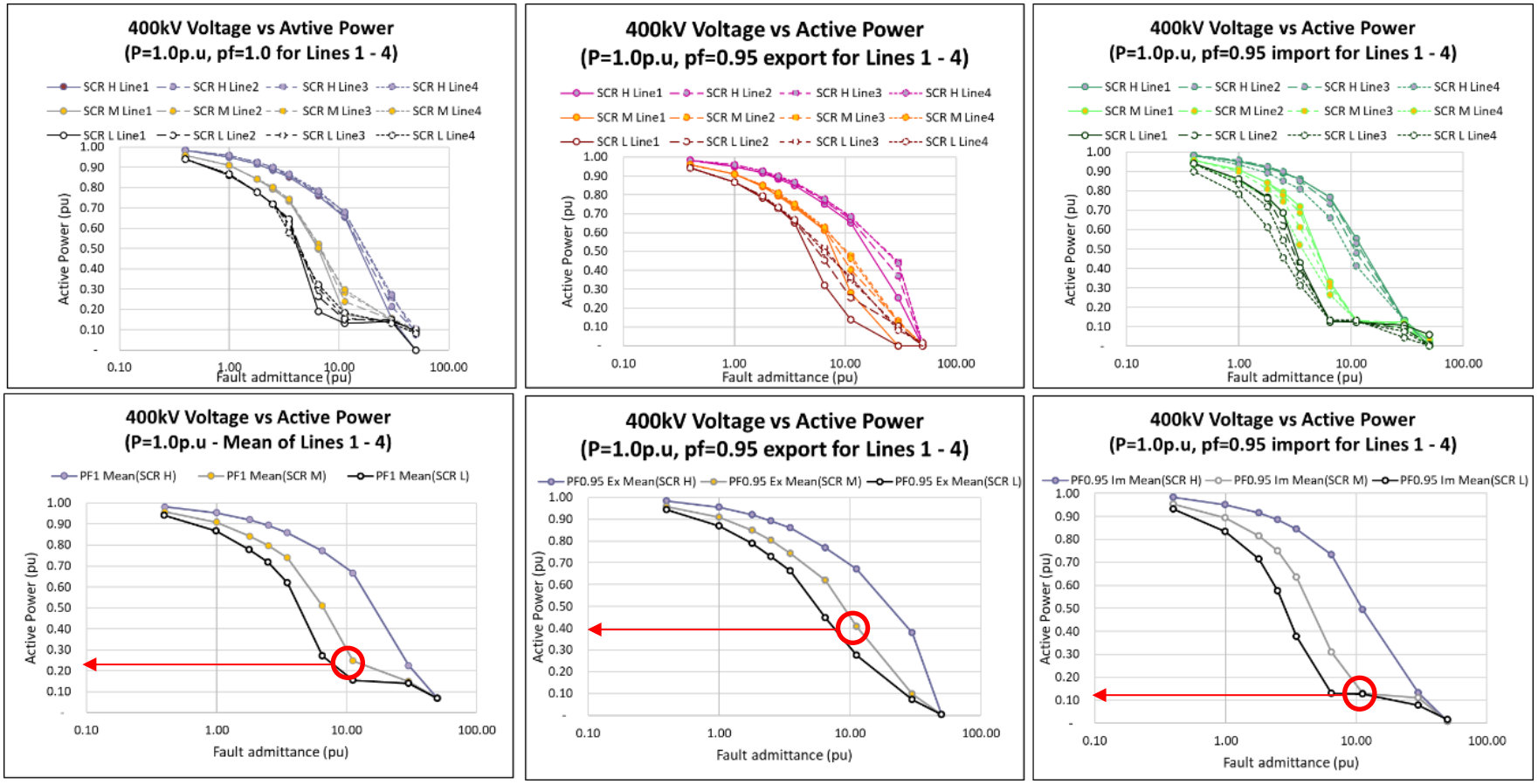

Figure 28 – Active-power export reduction for varied fault admittances for high, medium and low system strengths for various initial conditions of active-power and reactive-power.

The initial reactive-power has an impact on the voltage support and hence the reduction of active-power export. This is illustrated by the red circle indicated in the second row of graphs in Figure 28. All the circles are for the same fault admittance on the medium system strength curves. The first graph (in row 2) with no reactive-power contribution (pf=1) will experience an active-power export reduction to 25%. for a medium system strength (SCR=M). The second graph initial condition with exporting reactive-power (pf=0.95 leading) will experience an active-power export reduction to 40% of initial active-power export. The third graph initial condition with importing reactive-power (pf=0.95 lagging) will experience an active-power export reduction to 10%. Therefore, the range of initial reactive-powers between zero (pf=1) and exporting (pf=0.95 leading) is more favourable to reduce the impact of active-power export reduction during system fault conditions.

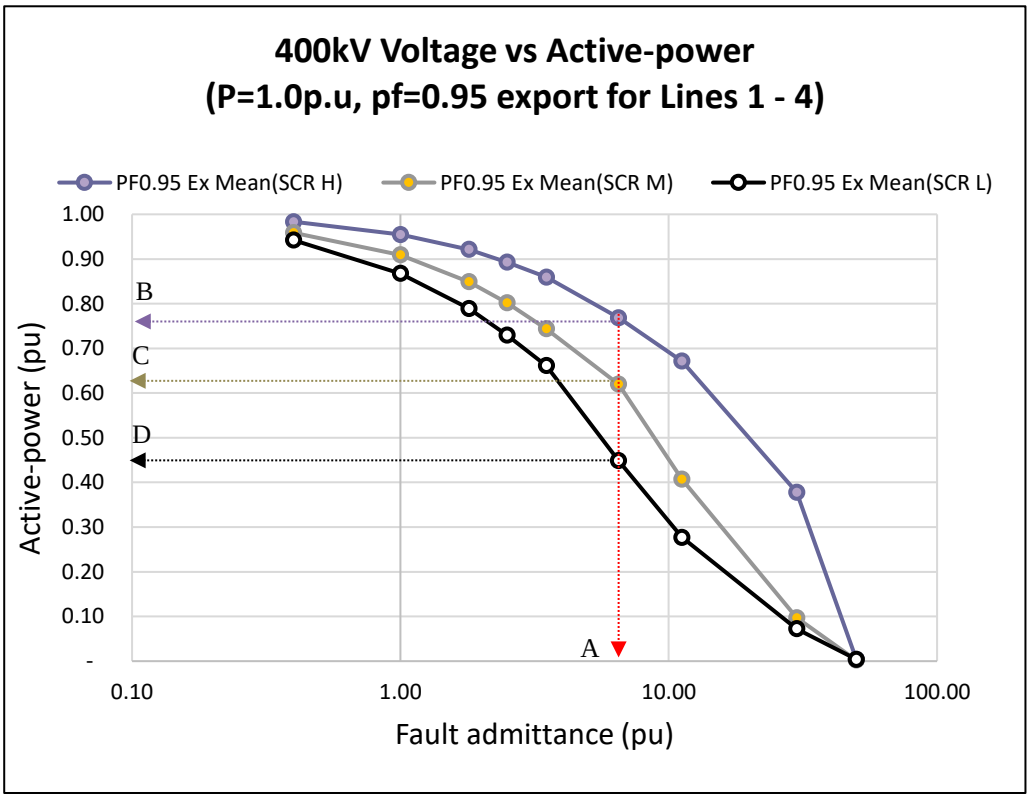

Figure 29 – Impact of active-power export reduction for varied fault admittance for high, medium and low system strengths for various initial conditions of active-power and reactive-power

System strength - Transmission fault admittance versus active-power.

The graph above indicates the impact of a weaker system on the reduction of active-power export for the same fault admittance (A) applied on the 400 kV Tx bus. For the same fault admittance indicated at A, a strong system (SCR=H) would see an active-power export reduction to point B. Whereas a weak system (SCR=L) active-power export reduction would be to point D. The higher the fault admittance the higher the active-power export reduction. The lower source impedance of a strong system reduces the system voltage drop under a fault condition. The lower reduction in voltage in turn results in a lower reduction of active-power export. In an integrated network the lower Tx voltage reflects to adjacent Tx busbars resulting in a greater potential of cumulative active-power export reduction in a high penetration network of IBT RES.

Key observations

- The reactive-power initial condition has a significant impact on the active-power export reduction
- Importing reactive-power should be avoided because of a significantly poorer performance
- System strength impacts the active-power export reduction for the same fault admittance applied to the Tx bus.
- The active-power export reduction increases more than 200% for a low system strength compared to a high system strength.
- No significant impact was observed for various IBT RES distances from the Tx busbar. Thus an average value can be used to represents the active-power export reduction.

Tx voltage vs active-power export reduction for same system strength with varying PF

This section examines active-power export reduction for voltage changes on the Tx busbar for different initial reactive-power export conditions with the same system strength (SCR). Three initial reactive-power are considered, no reactive-power (pf=1), reactive-power exporting (pf=0.95 leading) and reactive-power importing (pf=0.95 lagging). The system strength is held constraint for each

reactive-power condition and repeated for four different distances (line impedances) from the Tx grid to represent the potential of different locations. The average of the four line lengths is plotted in Figure 30. The three initial reactive-powers are shown as power factors pf=1 (A -solid line), pf=0.95 leading (B - dashed line) and pf=0.95 lagging (C- double dashed line). The first graph is for high system strength, the second graph for medium system strength and the third graph for low system strength.

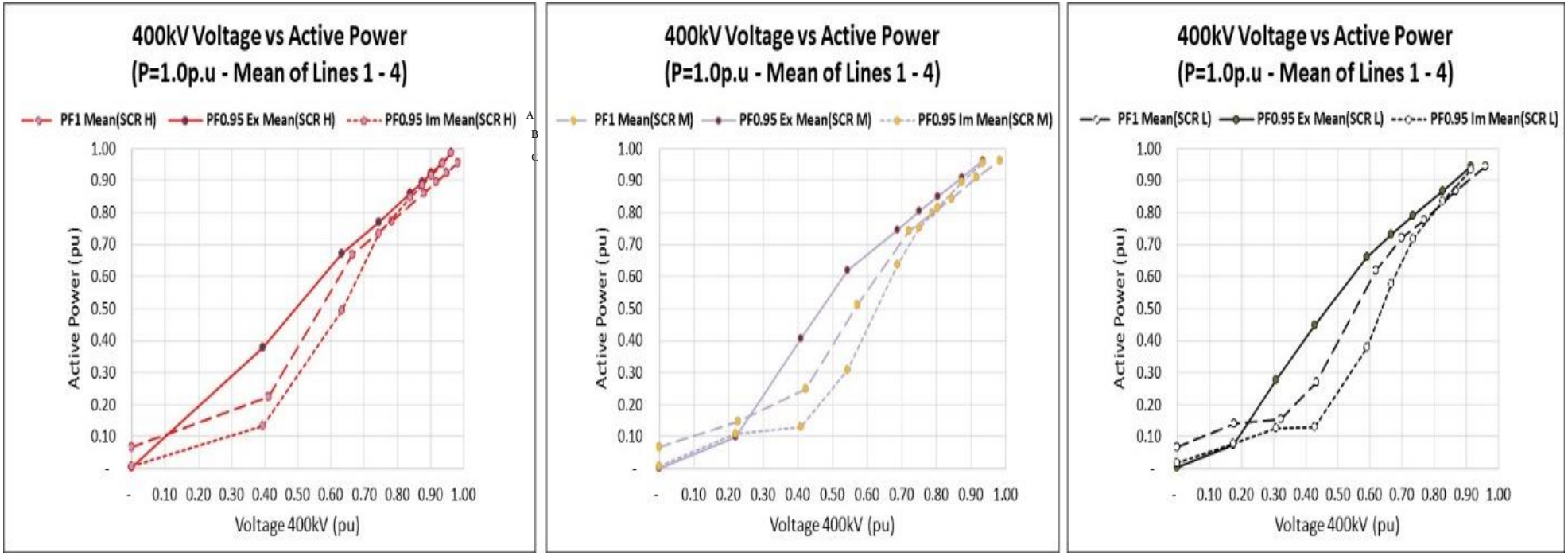

Figure 30 – Active-power export reduction for varied fault admittances for high, medium and low system strengths for various initial conditions.

Key observations

- A linear response between the voltage reduction and active-power export reduction is observed for all reactive-power conditions and system strengths for voltage variation between 1pu – 0.7pu
- Voltage support reducing the active-power export reduction for reactive-power for a pf=0.95 leading (see point A) between voltage 0.7pu – 0.2pu is observed when compared with reactive-power importing pf (point C).
- The most onerous active-power export reduction results from importing reactive-power for all system strength conditions. Therefore, importing reactive-power is not a preferred operating mode for IBT RES.
- Initial conditions between unity power factor and exporting reactive-power are a more prudent initial state to consider.

Tx voltage versus active-power export reduction for same pf with varying system strengths

This section examines active-power export reduction for voltage changes on the Tx busbar for different initial system strengths (SCRs) and with the same initial reactive-power export conditions. Three initial system strengths of high, medium and low are considered for three fixed initial reactive-power export conditions: no reactive-power flow (pf=1), reactive-power exporting (pf=0.95 leading) and reactive-power importing (pf=0.95 lagging). The reactive-power is held constant for the different system strengths and repeated for four different distances (line impedances) from the Tx grid to represent the potential of different IBT RES locations, see Figure 31 row 1 graphs. The average of the four-line lengths for each system strength condition is shown in row 2. The three initial system strength states are shown as SCR=H, SCR=M and SCR=L for an initial no reactive-power flow (pf=1) row 2 graph 1, for pf=0.95 leading row 2 graph 2 and pf=0.95 lagging row 2 graph 3.

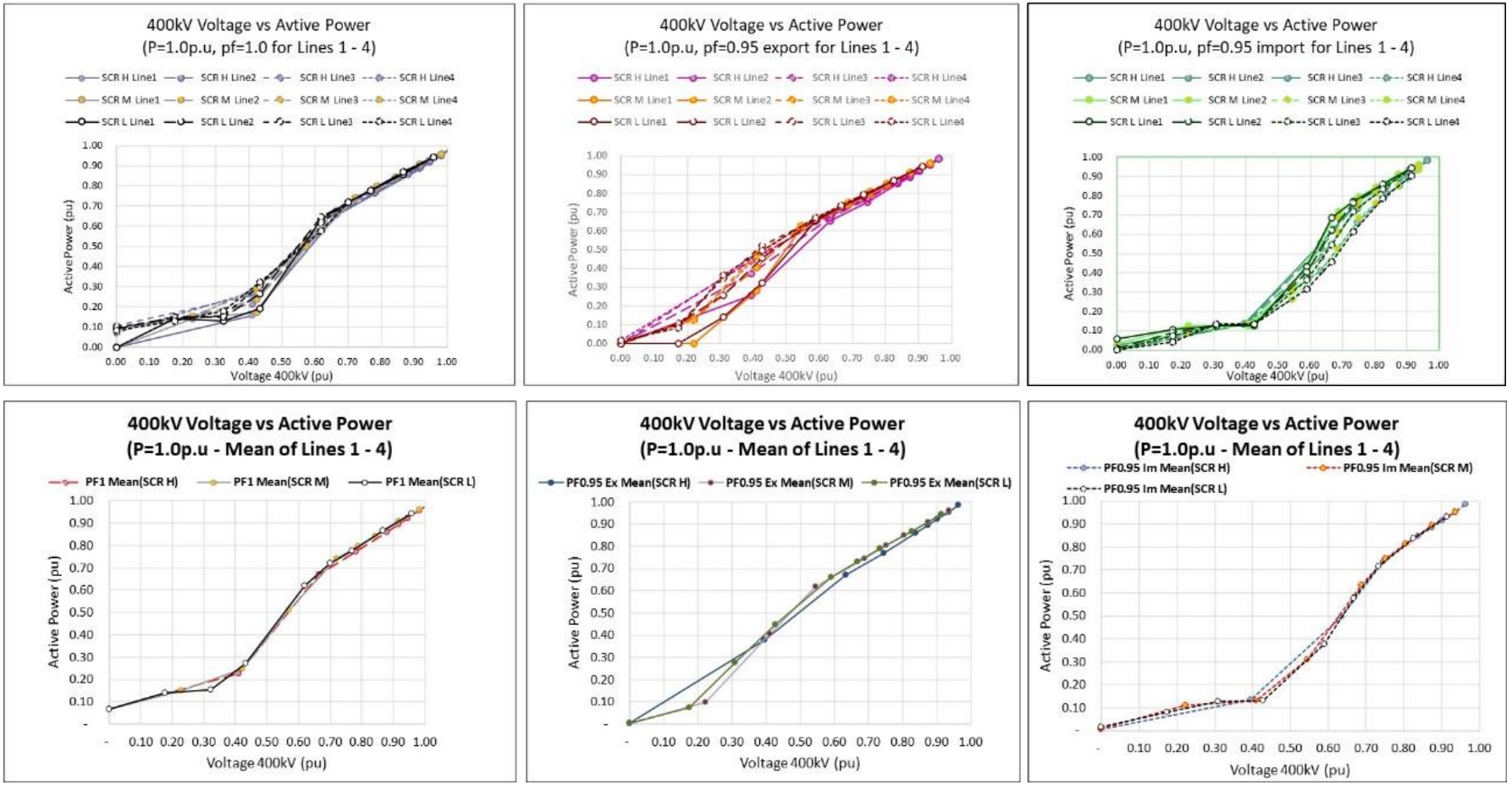

Figure 31 – Active-power export reduction for varied system strengths: high, medium and low for various fixed reactive-power initial conditions.

The distance the IBT RES is from the 132 kV Tx busbar, represented by the four lines, introduces a marginal variation on active-power export reduction. The average value of the four lines retains the shape and provides a very good representation of the IBT RES active-power export reduction response.

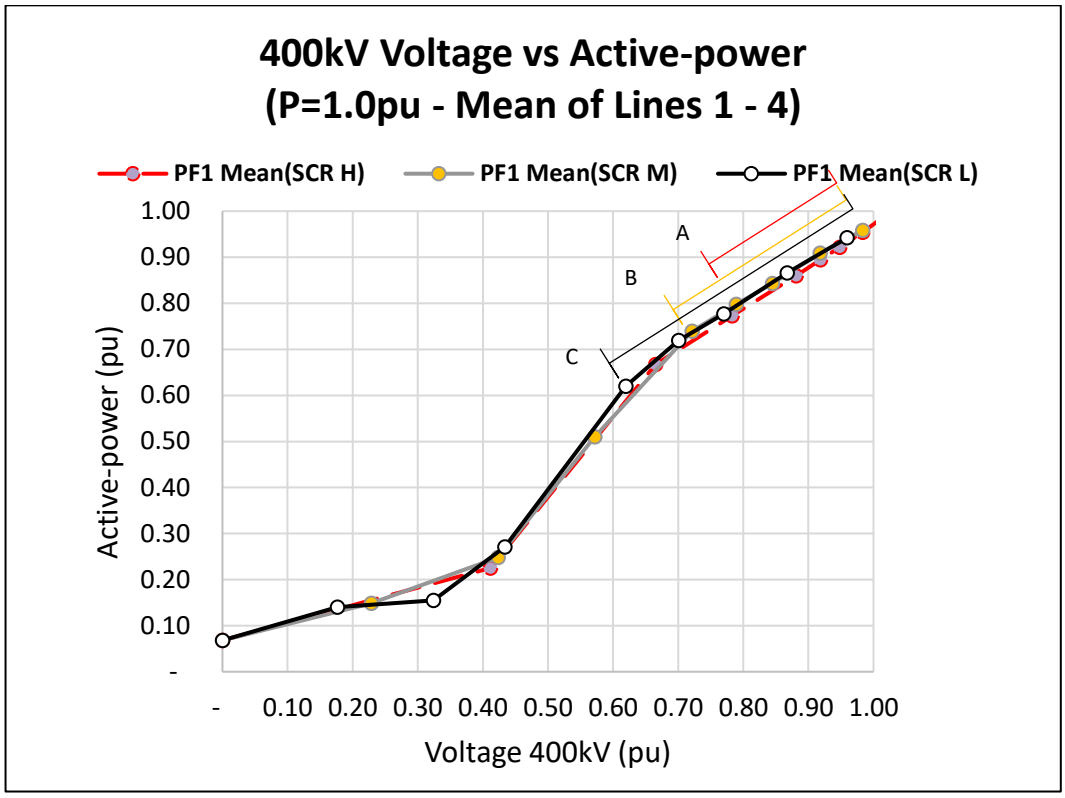

Figure 32 – Tx voltage vs active-power export reduction for the same pf with varying system strengths.

Figure 32 plots the 400 kV Tx voltage depression versus IBT RES active-power export reduction for the same IBT RES power factor of unity with varying 132 kV Tx busbar SCRs. The 400 kV Tx voltage depression versus IBT RES active-power export reduction is similar for varying 132 kV Tx busbar SCRs for a constant IBT RES power factor of unity. The 132 kV Tx busbar SCR impacts the depth of the 400 kV Tx voltage depression for the same fault admittance. This can be seen by comparing a cluster of faults. Considering the first five faults (five different fault admittances are kept constant for all three SCRs) The five cluster faults (the first five dots from top right) for three high SCR (SCR=H), medium SCR (SCR=M) and low SCR (SCR= L) are indicated by cluster A, B and C respectively (on the right). As the SCR reduces the cluster stretchers, indicating an increased voltage drop.

Key observations

- The reactive-power import initial condition results in the highest active-power export reduction. This initial state is not preferred and is not considered in further discussions.
- The shape of the active-power export reduction response curve remains constant for a constant initial power factor
- A linear response is observed for voltage variation on the Tx busbar up to 1pu - 0.6pu voltage reduction.
- A high system strength results in clustering in the upper region of the linear part of the curve. This has the effect that for the same fault admittance applied to the Tx busbar a lower voltage reduction occurs and an associated lower active-power export reduction response result.
- A low system strength results in "stretching" of the clustering. Effectively distributing the response over the entire linear part of the curve. This has the effect that for the same fault admittance applied to the Tx busbar a higher voltage reduction occurs and an associated higher IBT RES active-power export reduction.
- The response curve seen from the Tx voltage is not the same shape as the Grid Code requirement. The Grid Code requirements are specified at the IBT RES POC. The impedance (Tx transformer, line impedance, etc) between the Tx busbar and the IBT RES impact the active-power export reduction response.
- There is no zero active-power export from the IBT RES even for a zero voltage at the Tx bus.
- The response of the IBT RES for a Tx busbar voltage differs from the Grid Code compliance requirements because of the different impedances between the voltage depression location. To predict IBT RES active-power export reduction for Tx faults the Tx busbar voltage vs active-power reduction curve provides a more accurate response.

3.9 Developing a robust Tx voltage versus active-power export reduction model

A lagging power factor has significantly increased the active-power export reduction for the same voltage depression. This is an undesirable operating condition. Therefore,

the development of the 400 kV voltage versus active-power export reduction considers the range between pf=0.9 leading and pf=1.

Firstly, the results for the previous section consider that an IBT RES active-power output of 1pu is consolidated into a Tx busbar voltage vs active-power export reduction model. It was determined that the two most favourable initial conditions for reactive-power output are no reactive-power contribution (pf=1) and reactive-power exporting (pf=0.95 leading). The IBT RES is thus likely to operate between these two boundary conditions. To minimise the operation condition error the characteristic model is obtained by taking the average curve between these boundary conditions, see Figure 33.

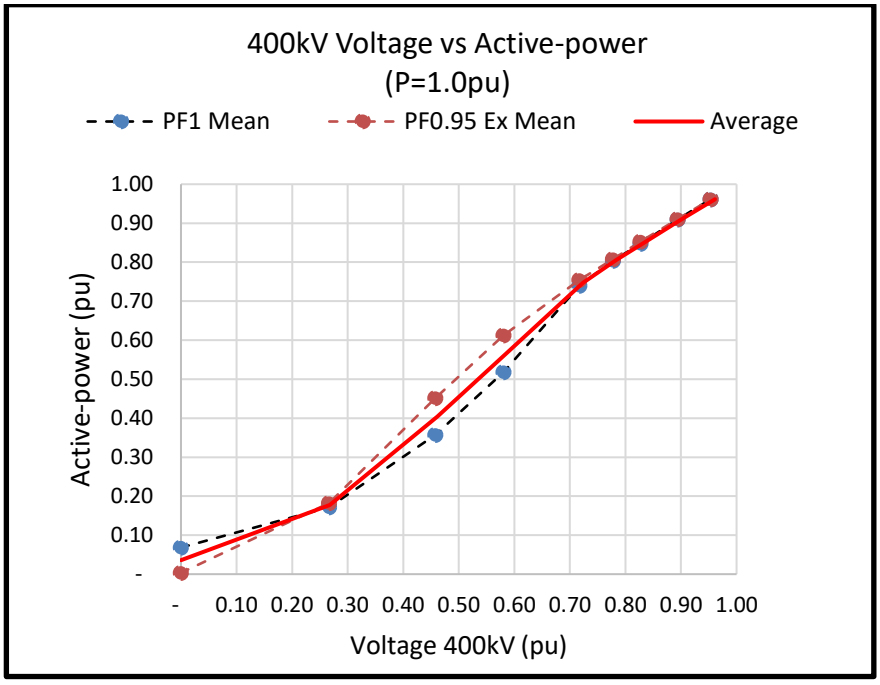

Figure 33 – Average Tx busbar voltage vs active-power export reduction for active-power output 1p.u.

However, in order to determine a robust model, additional initial conditions for active-power output of the IBT RES are required. The process to determine the model, described in the previous section, is repeated with the IBT RES initial active-power output of 0.5pu. The two most favourable initial condition for reactive-power output namely, no reactive-power flow (pf=1) and reactive-power exporting (pf=0.95 leading) are plotted and the average curve between these boundary condition, are shown in Figure 34.

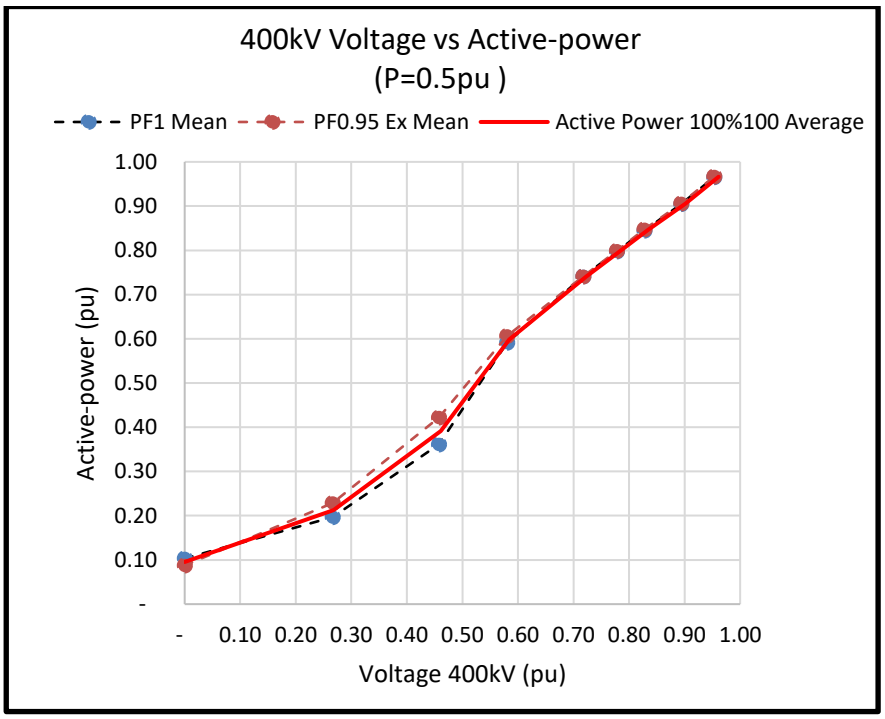

Figure 34 – Average Tx voltage versus active-power export reduction for initial active-power export of 0.5pu

The average voltage versus active-power export reduction for these conditions with an initial IBT RES active-power output of 1pu in Figure 33A and initial IBT RES active-power output of 0.5pu are shown in Figure 34.

The lower initial active-power export allows greater reactive-power export for supporting the voltage during a voltage depression. This has the effect that the linear region (the upper right part of the curve) is extended and reduces the variance of the response.

The average curve for the 1pu (black line) and 0.5pu (green line) active-powers are plotted together in the top Figure 35. The average of these two curves is used to determine the characteristic model. The characteristic model and equation are shown in the bottom graph with the characteristic equation.

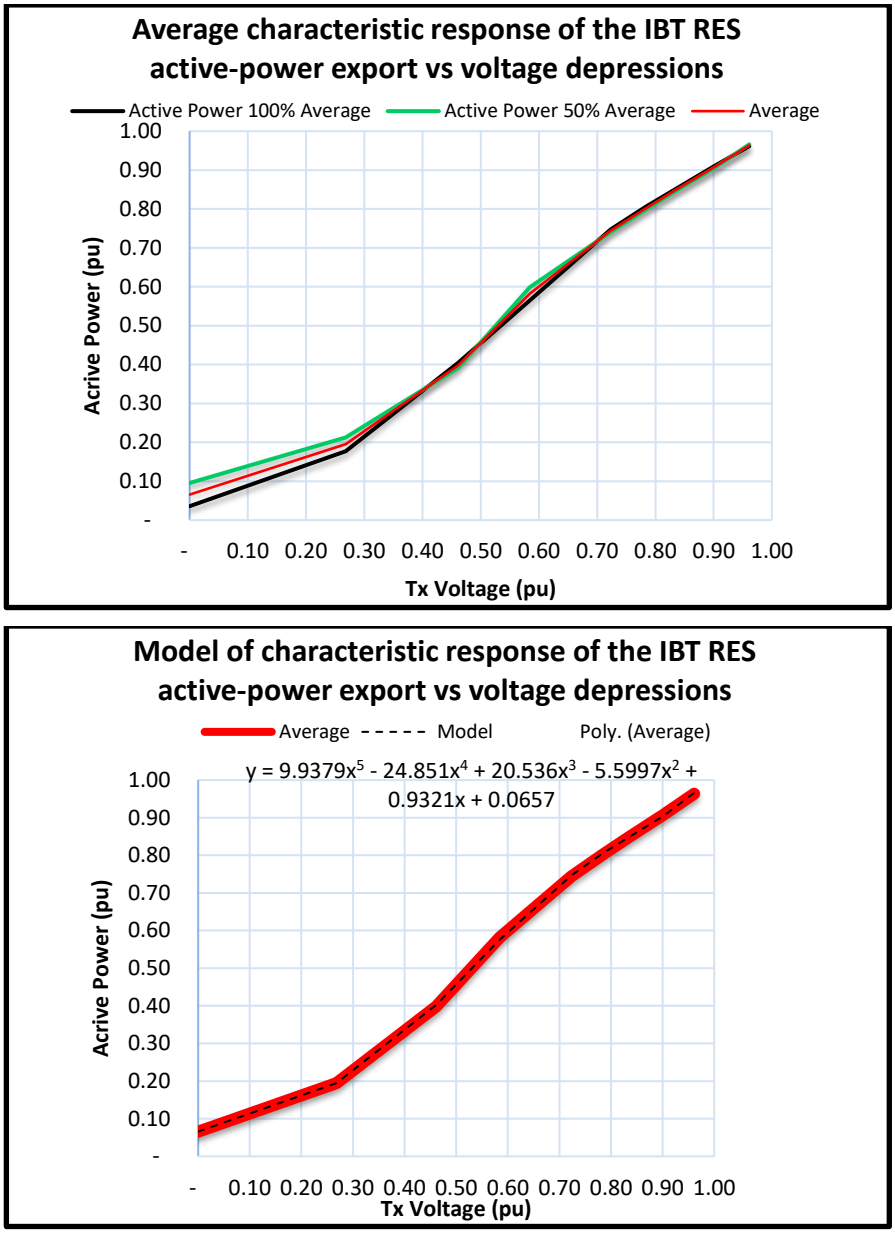

Figure 35 - Average characteristic response of 1pu and 0.5pu initial IBT RES active-power export curves to determine the Tx voltage vs active-power export characteristic model

The average voltage versus active-power export reduction characteristic for initial active-power export of 1pu and 0.5pu allows determination of the real power and reactive-power response to voltage dip depth. The average characteristic response for the IBT RE can be formulated by averaging these responses. The averaging and formulation of the model for the characteristic response is in the right graph. The red line indicates the average response and the dashed black line the curve for the model.

The model allows the establishment of a lookup table based on the observed response to determine the associated delta change in IBT RES active-power export. This enables the prediction of the impact of loss of active-power export from IBT from a Tx voltage depression

Impact of the collector network

The model of the characteristic response was tested in the collector network (see Figure 18) representing a high penetration meshed grid to test the robustness of the model to predict reduction in active-power export for reduction of voltage on the Tx busbar in a high penetration collector network. The results of the prediction of the active-power export reduction within a collector network are shown in Figure 36. The solid black line in Figure 36 is the dynamic response of the collector network summated active-power export response to voltage dips. The results compared to the characteristic model (dashed bold black line) and average (red line) indicates an error within 0.05pu (dotted grey lines). The individual variation is less the 4% for a voltage of 0.5pu. For low active-power output (for example less than 0.2pu) the error is 12% on the small base, resulting in a marginal error.

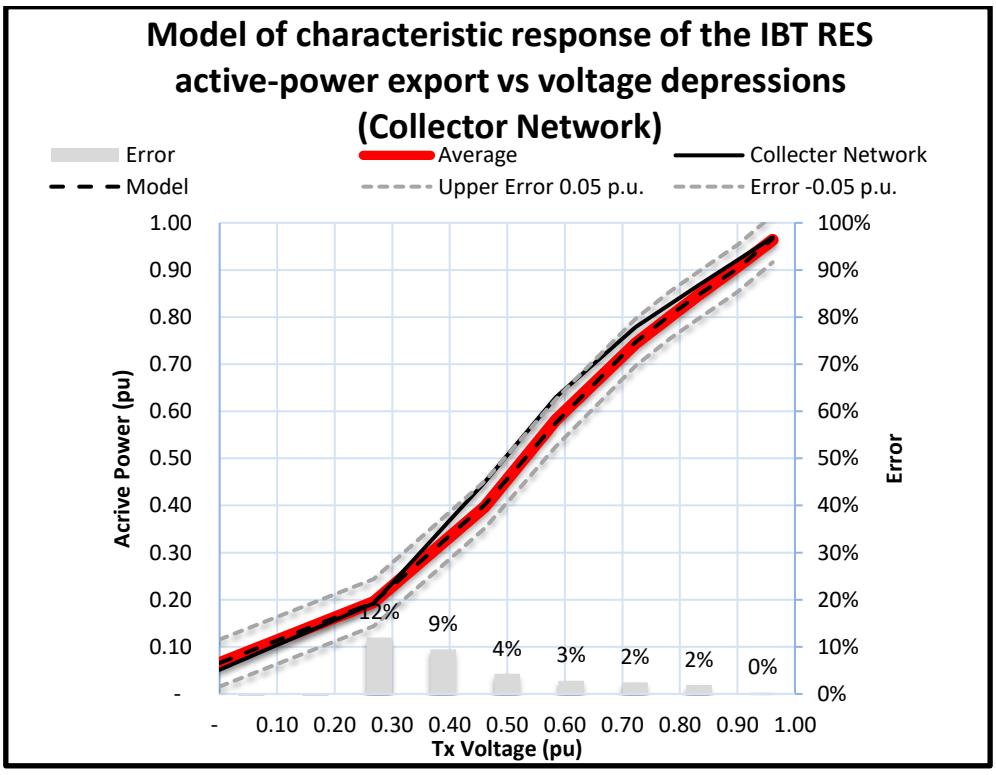

Figure 36 – Characteristic model versus collector network response

Chapter 4: Task 2: Classical P-V steady-state analysis with and without IBT RES present (no Tx fault and hence no IBT RES LVRT response) for the Cigre Nordic voltage collapse test network

This chapter investigates P-V steady-state analysis on the Cigre Nordic test network for both the synchronous scenario and for the IBT RES scenario. The network, initial conditions, and contingencies are identical for both cases. P-V curves are generated, considering voltage collapse, reactive-power margins and safe operating limits. The Cigre Nordic test network, initially comprising only synchronous generators, is modified in the IBT RES scenario by substituting synchronous generators with the equivalent IBT RES. The synchronous scenario and the IBT RES scenario are analysed separately. In the next chapter, the P-V steady-state network limits obtained in this chapter will be subjected to Tx fault conditions to establish if these limits remain valid for increased IBT RES integration.

4.1 Cigre Nordic Test Network

The Cigre Nordic test network was selected because it was one of the original models used to investigate voltage stability [46]. The steady-state and dynamic models are well documented [46-48]. Network topology and maps are also readily available. Figure 37A shows the spatial overlay of the network, Figure 37B shows the network topology. The base Nordic network contains only synchronous generators. The demand (load) in the south is indicated by the green-shaded area and is the study area for voltage collapse. This study area is supplied by the Tx-corridor and four local synchronous generators. In the IBT RES scenario, three of the synchronous generators are replaced with IBT RES and are indicated in Figure 37B by the hollow green circles. The yellow dots are not relevant to this study as they indicate the current location of IBT RES.

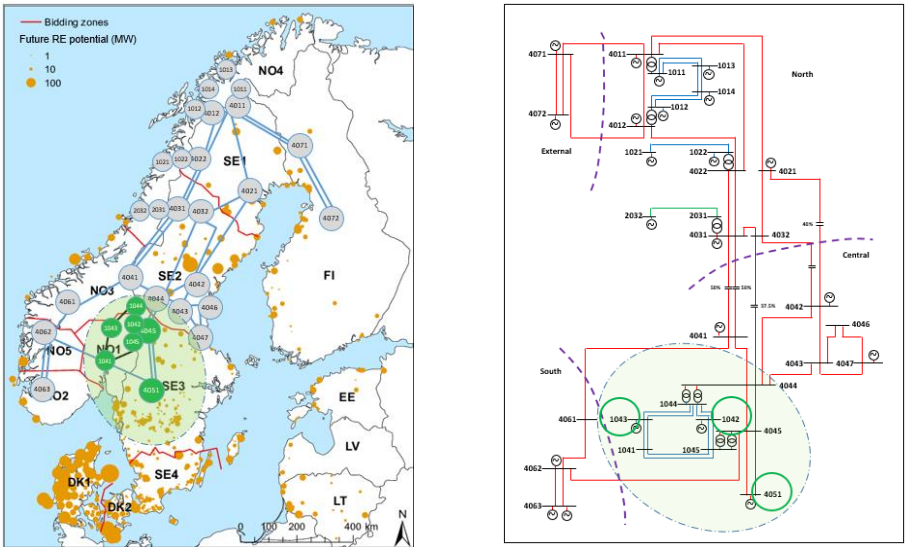

A B

Figure 37 – Cigre Nordic voltage collapse test network

Five transmission lines, indicated by the red dots in Figure 38, supply the power from the north to the voltage collapse study area in the south.

P-V steady-state analysis is performed using PSSE for the base network and for each contingency.

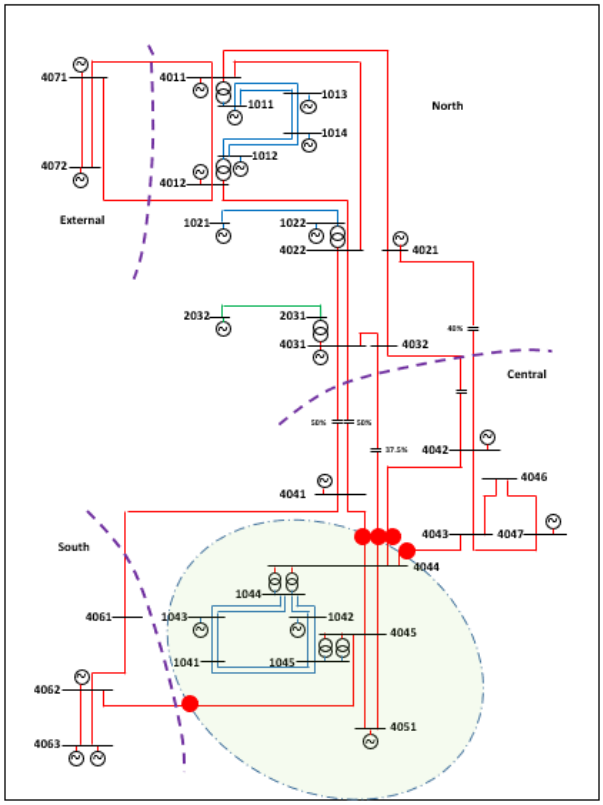

Tx-corridor lines indicated by red dots

Figure 38 – Tx-Corridor (for contingency analysis)

P-V steady-state analysis is performed by increasing the demand (load) in the study area in incremental steps and monitoring all busbar voltages. Reactive-power from local synchronous generators is also monitored. P-V curves are plotted for each contingency and the voltage collapse point is determined. A 5% margin from the limit of reactive-power support is adopted. The Tx-corridor active-power transfer limit (for the limiting contingency) also adopts a 5% margin from the knee point. The lowest transfer capacity of these two margins is the final Tx-corridor capacity. Active-power transfer on the Tx-corridor is the sum of all the active-power flowing along the five Tx lines (Tx-corridor) feeding the voltage collapse study area. The difference between the local load active-power plus active-power loss and the local active-power generation is fed along this Tx-corridor.

CON#	LABEL	Max MW	DESCRIPTION
	BASE CASE	848.75	BASE CASE
1	4031_4041_1_LINE	583.125	OPEN LINE FROM BUS 4031 [BUS4031 400.00] TO BUS 4041 [BUS4041 400.00] CKT 1
2	4041_4044_1_LINE	581.25	OPEN LINE FROM BUS 4041 [BUS4041 400.00] TO BUS 4044 [BUS4044 400.00] CKT 1
3	4032_4044_1_LINE	548.125	OPEN LINE FROM BUS 4032 [BUS4032 400.00] TO BUS 4044 [BUS4044 400.00] CKT 1
4	4042_4044_1_LINE	738.75	OPEN LINE FROM BUS 4042 [BUS4042 400.00] TO BUS 4044 [BUS4044 400.00] CKT 1
5	4032_4042_1_LINE	626.25	OPEN LINE FROM BUS 4032 [BUS4032 400.00] TO BUS 4042 [BUS4042 400.00] CKT 1

4.2 Synchronous scenario: P-V steady-state curve analysis

The base Nordic network was used for this scenario which contains only synchronous generators. The study-area load was 3383 MW and the local synchronous active-power generation was 1620 MW. The remaining system is shown in Table IV below.

Table IV– Synchronous scenario: initial conditions

Area	Synchronous Gx (MW)	IBT RES Gx (MW)	Load (MW)
Study-area	1620	0	3383
External	9481	0	7503
Total	**11255**	**0**	**10886**

The demand (load) location is shown in Figure 39A and synchronous generation in MW in Figure 39B below. The generation number (in red) provides the dispatched generation / installed generation at each busbar.

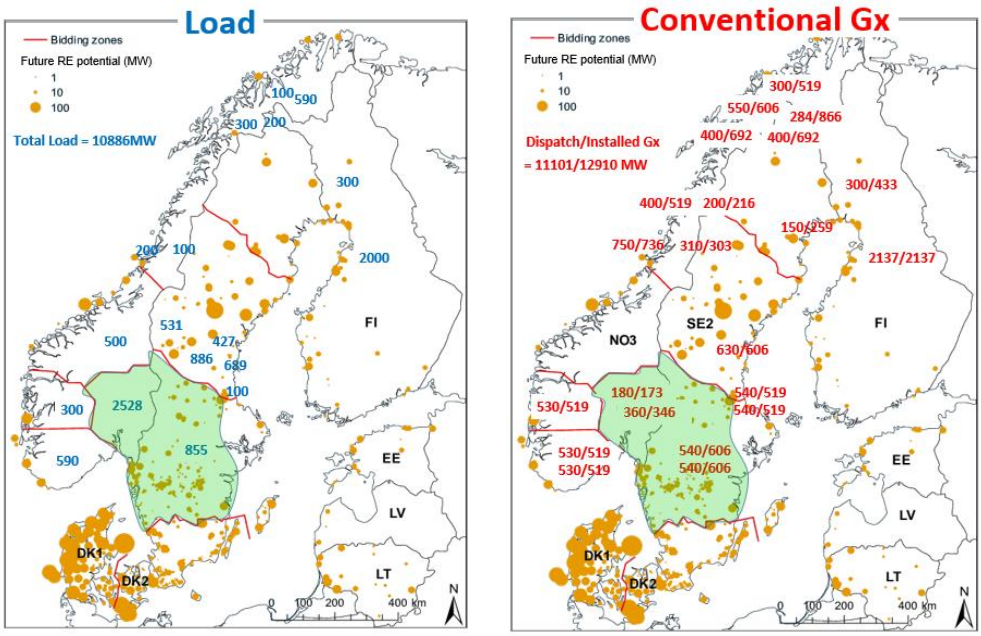

A B

Figure 39 – Synchronous scenario: Load (MW) and generation (MW) location

4.2.1 Synchronous scenario: P-V steady-state analysis results

The synchronous system base case and contingency P-V analysis results are shown in Table V below and the P-V curves in Figure 40 below. The P-V curve for the base case (N network) is indicated in the bold black curve, while the P-V curves for the contingencies are indicated by the dashed curves in grey and red. The network contingency that provides the lowest Tx-corridor active-power transfer limit (referred to as the limiting network contingency) is shown as a bold red dashed curve.

Table V– Synchronous scenario: P-V steady-state analysis results

No	Contingency	Initial Load (MW)	Maximum Additional Load (MW)	Voltage Collapse Load (MW)	With 5% margin from collapse (MW)
	BASE CASE	**3383**	**911**	**4294**	**4079**
1	4045_4062_1_LINE	3383	737	4120	3914
2	4041_4044_1_LINE	3383	667	4050	3848
3	**4032_4044_1_LINE**	**3383**	**601**	**3984**	**3785**
4	4042_4044_1_LINE	3383	808	4191	3981
5	4043_4044_1_LINE	3383	845	4228	4017

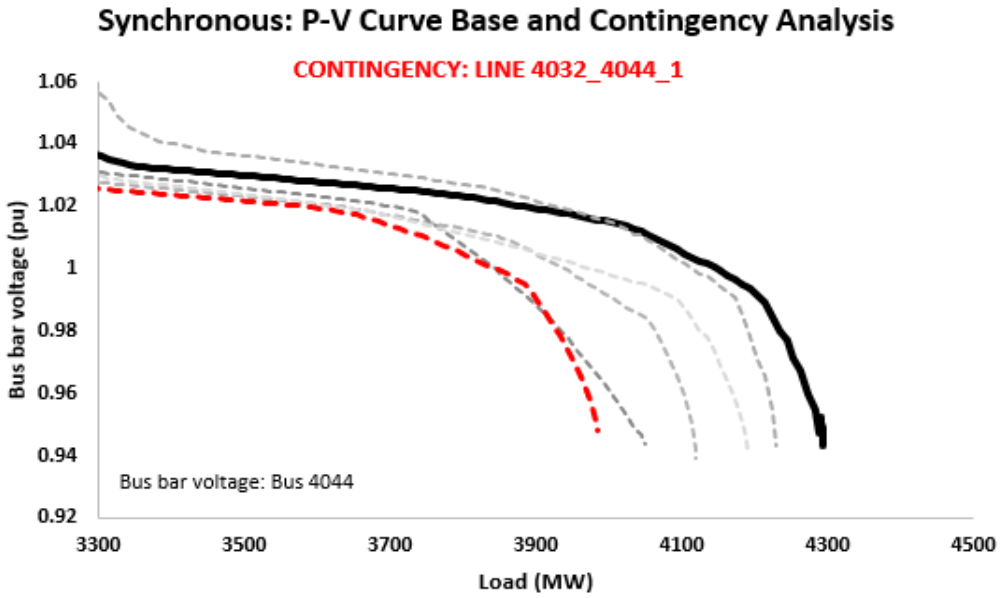

Figure 40 – Synchronous scenario: P-V steady-state analysis for base and contingencies

The grey line in Figure 41 below indicates the increase in reactive-power as the system demand (load) increases (dashed red line). The reactive-power operating margin is set at 5% from the limit of reactive capacity of the synchronous generators. The reactive-power limit is indicated in Figure 41 at point 1 and the 5% margin at point 2. The load points are 3984 MW and 3963 MW at point 2, which is the reactive-power loading limit of the network.

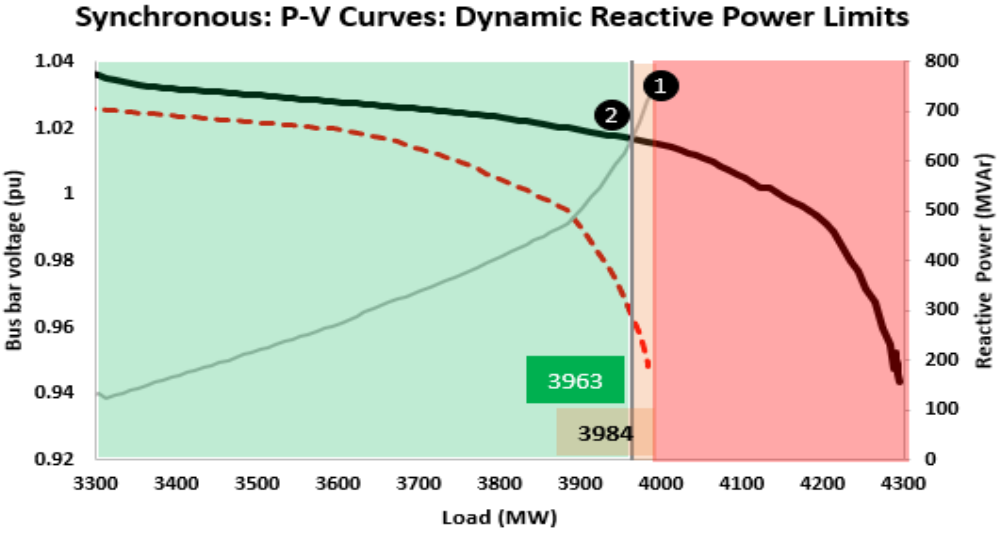

Figure 41 – Synchronous scenario: P-V steady-state analysis with 5% reactive-power safety margin and limit

The red area in Figure 42 below indicates the voltage collapse region. The collapse point is indicated on the bold red dashed curve at a load of 3984 MW. The margin for safe operating is indicated by the orange area which is 5% back from the collapse point at 3785 MW. This means that from point 1 on the bold black line (System healthy), if a contingency occurs, the active-power transfer capacity would move from the bold black curve to point 1 in the bold dashed red curve (limiting network contingency).

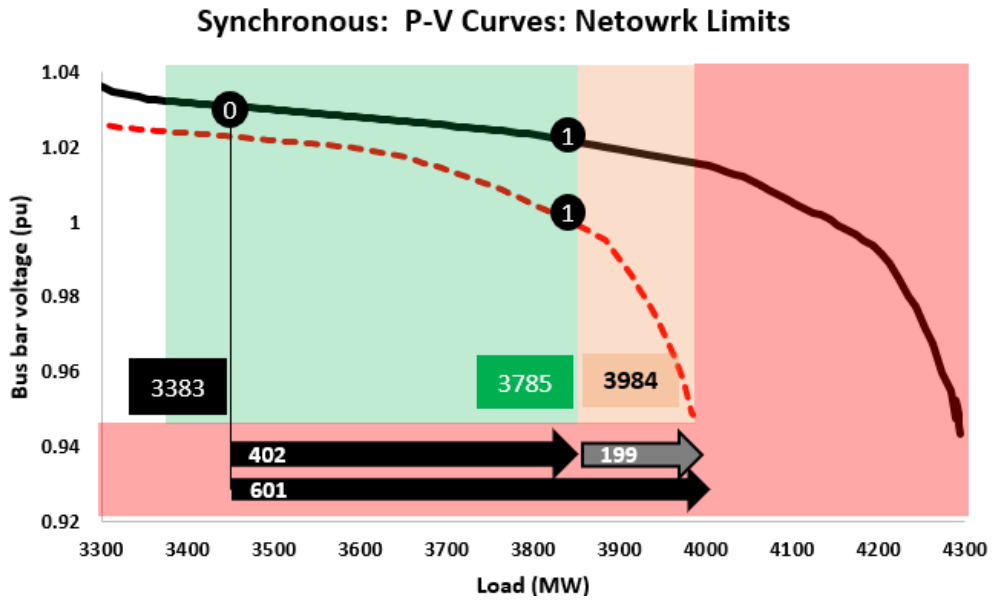

Figure 42 – Synchronous scenario: P-V steady-state analysis for Tx margin (still safe for limiting network contingency) and network limit (voltage collapse for worst network contingencies)

This does not consider the dynamics of the system during the fault and hence the margin in orange. The initial condition of the test network is at point 0. This means there is 601 MW (3984 MW – 3383 MW) ascribed to voltage collapse. The system can add 402 MW to the safe operating point. The margin is 199 MW before the voltage collapse condition. The network limit of 3785 MW is lower than the 3963 MW limit associated with reaching the reactive-power limit. Therefore the lower of the two, that is the network limit 3785 MW is considered the active-power transfer limit. The Tx-corridor capacity is the active-power at the point of collapse by the P-V curve loading and is indicated in indicated in Figure 43 below.

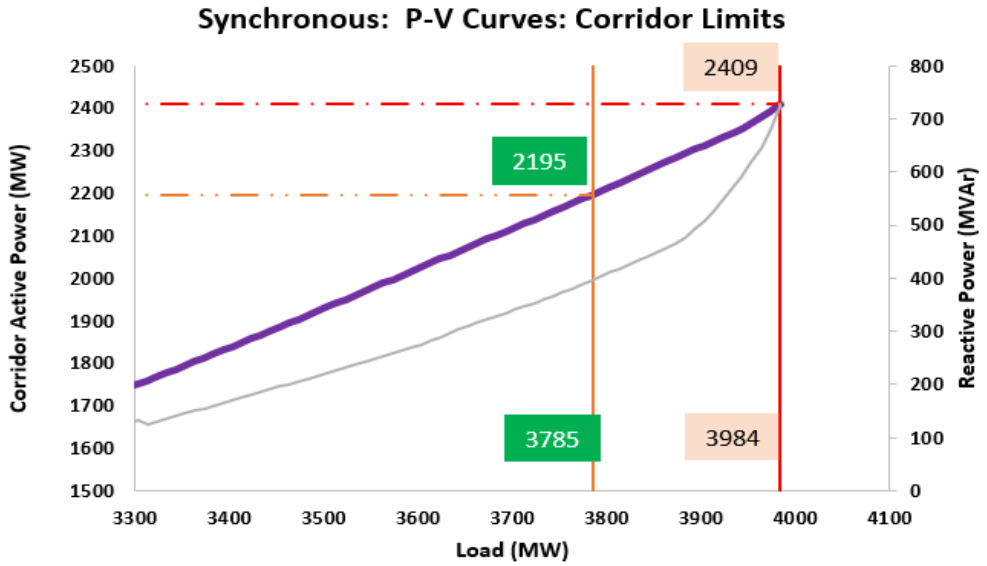

Figure 43 – Synchronous scenario: P-V steady-state analysis Tx-corridor margin and limit

The previously determined Tx-corridor active-power limit and collapse point are shown on the x axis, as 3785 MW and 3984 MW respectively. The corresponding Tx-corridor active-power limits are shown on the left Y axis, 2195 MW and 2409 MW. The grey line is the reactive-power support in the supply area shown on the right Y axis. The Tx-corridor active-power flow increases the demand for reactive-power as it approaches voltage collapse.

4.3 IBT RES scenario: P-V steady-state analysis

The base Nordic network was also used for this scenario. The study-area load was 3383 MW and the local active-power generation was 1620 MW. However, 1080 MW of the synchronous generation was replaced with IBT RES. The remaining system is set up as indicated in Table VI below.

Table VI– IBT RES scenario: initial conditions

Area	Synchronous Gx (MW)	IBT RES Gx (MW)	Load (MW)
Study-area	540	1080	3383
External	9481	0	7503
Total	**11255**	**0**	**10886**

The demand (load) location remained unchanged in both the synchronous scenario and the IBT RES scenario, as shown in Figure 39A below. The synchronous generators and IBT RES are shown in Figure 44 in the shaded green area which indicates the generation dispatched generation / installed generation at each busbar.

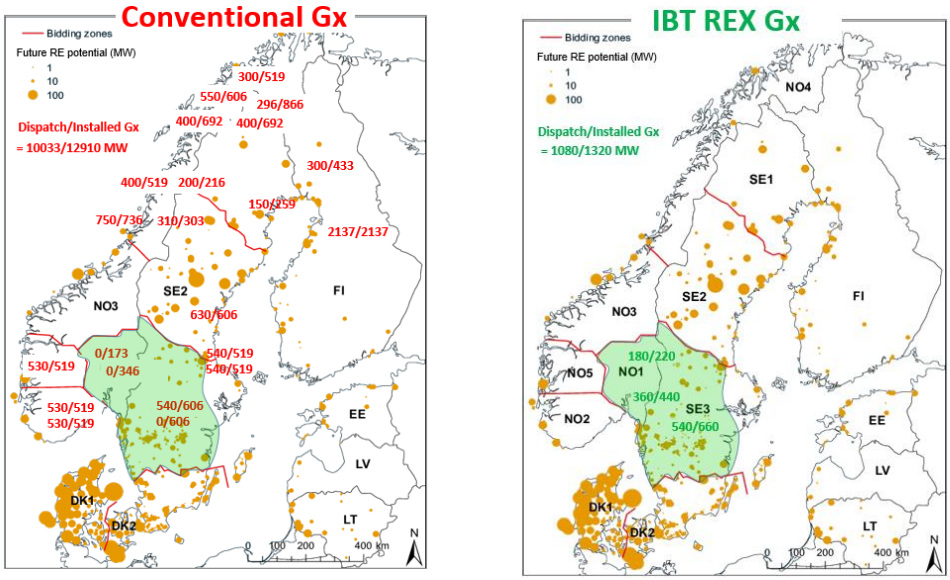

A B

Figure 44 – IBT RES scenario: Synchronous (MW) and IBT RES (MW) location

4.3.1 IBT RES scenario: P-V steady-state analysis results

The IBT RES system base case and network contingency P-V analysis results are shown in Table VII below and the P-V curves in Figure 45 below. The P-V curve for the base (N network) is indicated in the bold black curve, while the P-V curves for the contingencies are indicated by the dashed curves in grey and red. The network contingency that provides the lowest Tx-corridor active-power transfer limit (referred to as the limiting network constraint) is shown as a bold red dashed curve.

Table VII– IBT RES scenario: P-V steady-state analysis results

No	Contingency	Initial Load (MW)	Maximum Additional Load (MW)	Voltage Collapse Load (MW)	With 5% margin from collapse (MW)
	BASE CASE	**3383**	**849**	**4232**	**4020**
1	4045_4062_1_LINE	3383	647	4030	3829
2	4041_4044_1_LINE	3383	582	3965	3767
3	**4032_4044_1_LINE**	**3383**	**549**	**3932**	**3735**
4	4042_4044_1_LINE	3383	739	4122	3916
5	4043_4044_1_LINE	3383	763	4146	3939

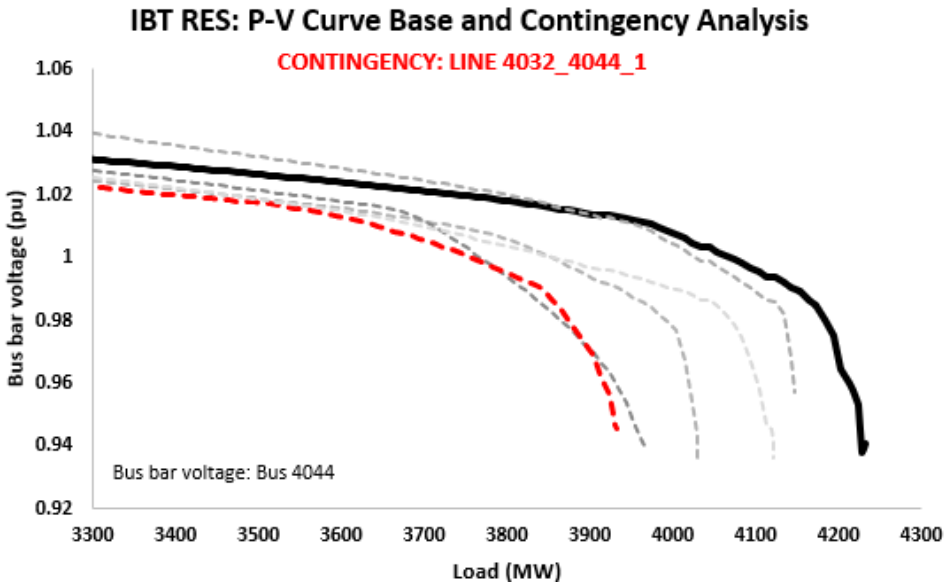

Figure 45 – IBT RES scenario: P-V steady-state analysis for base and contingencies

The grey line in Figure 46 below indicates the increase in reactive-power as the study-area demand (load) increases (dashed red line). The reactive-power operating margin is set at 5% from the limit of the reactive-power capacity for the local synchronous generators. The reactive-power limit is indicated in Figure 46 below at point 1 and the 5% margin at point 2. The load at point 1 is 3932 MW and at point 2 the load is 3883 MW, which is the reactive-power loading limit of the network.

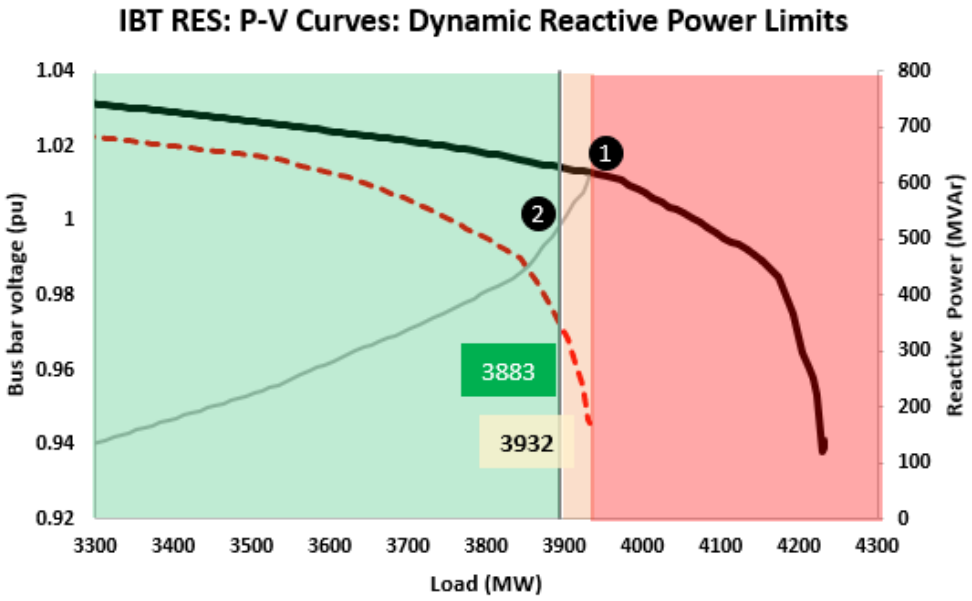

Figure 46 – IBT RES scenario: P-V steady-state analysis with 5% reactive-power safety margin and limit

The red area in Figure 47 below indicates the voltage collapse region. The collapse point is indicated on the bold red dashed curve at a load of 3932 MW. The margin for safe operating is indicated by the orange area which is 5% back from the collapse point at 3735 MW. This means that from point 1 on the bold black line(system healthy), if a network contingency occurs, the active-power transfer capacity would move from the bold black curve to the bold dashed red curve (limiting network contingency). This does not consider the system dynamics during the fault and hence the margin in orange. The initial condition of the network is at point 0. This means there is 549 MW ascribed to voltage collapse. The system can add 352 MW to the safe operating point. The margin is 197 MW before the voltage collapse condition.

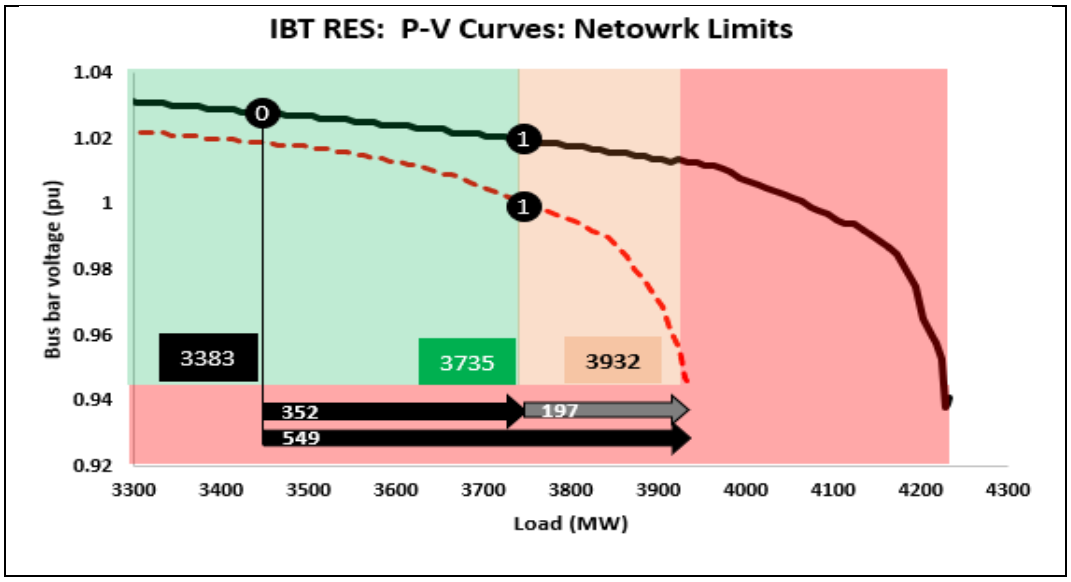

Figure 47 – IBT RES scenario: P-V steady-state analysis for Tx margin (still safe for limiting network contingency) and network limit (voltage collapse for worst network contingencies)

The network limit, 3735 MW, is lower than the 3883 MW limit associated with the reactive-power limit. Therefore the lower of the two, that is the network limit of 3735 MW is considered the active-power transfer limit.

The Tx-corridor capacity is the active-power flow at the point of collapse determined by the P-V curve loading and is indicated in Figure 48 below.

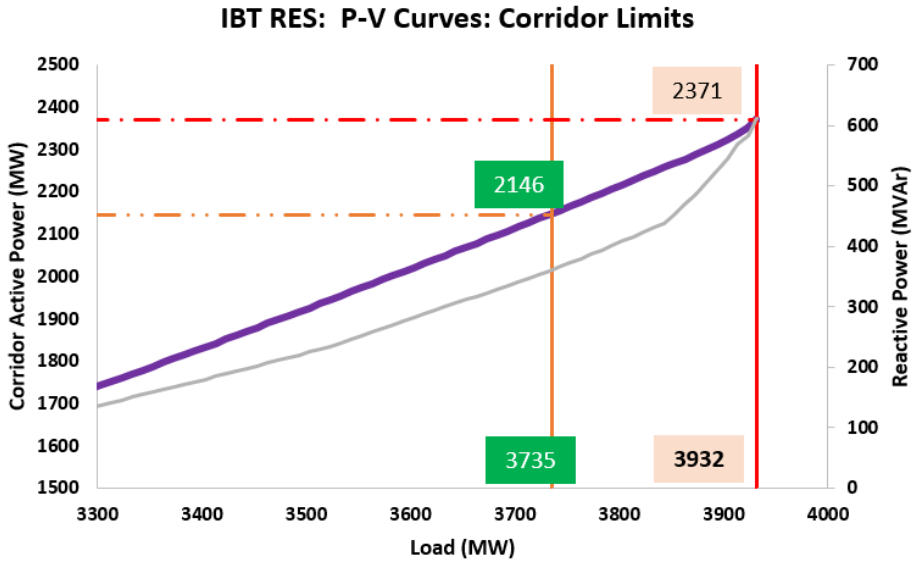

Figure 48 – IBT RES scenario: P-V steady-state analysis Tx-corridor margin and limit

The previously determined Tx-corridor active-power limit and collapse point are shown on the x axis, as 3735 MW and 3932 MW respectively. The corresponding Tx-corridor active-power limits are shown on the left Y axis, 2146 MW and 2371 MW. The grey line is the reactive-power support in the supply area shown on the right Y axis. The Tx-corridor increases the demand for reactive-power as it approaches voltage collapse.

4.4 Comparison between the synchronous scenario and the IBT RES scenario P-V steady-state results

The P-V steady-state results of the synchronous scenario and the IBT RES scenario analysis are compared in Table VIII. Both studies started from the same initial conditions (3383 MW study-area demand (load)). Voltage collapse loading (for the limiting network contingency) for the synchronous scenario compared to the IBT RES scenario is marginally more (by 52 MW) and the Tx-corridor active-power limit (adequate safety margin for the limiting network contingency) for the synchronous scenario compared to the IBT RES scenario is marginally more (by 50 MW). The Tx-corridor can accommodate an increased loading from initial condition of 402 MW for the synchronous scenario and 352 MW for the IBT RES scenario. In both cases the active-power limit was determined by the limiting network contingency and not by the reactive-power limit.

Table VIII– Comparison of P-V steady-state results for the synchronous scenario and for the IBT RES scenario

	Initial load (MW)	**Collapse point (for the limiting contingency) (MW)**	**Grid limit (5% safety margin for the limiting contingency) (MW)**	**Increase from the initial load to the Grid limit (5% safety margin for the limiting network contingency) (MW)**	**Margin between the collapse point and the grid limit (MW)**	**Increase from the initial load to the collapse point (MW)**
Synchronous scenario	3383	3984	3785	402	199	601
IBT RES scenario	3383	3932	3735	352	197	549
Difference	**0**	**52**	**50**	**50**	**2**	**52**

The comparison is provided in Figure 49 below which plots the P-V steady-state curve of the synchronous scenario (blue) and of the IBT RES scenario (green). The base network (solid lines) and limiting network contingency (dashed lines) shows the difference between these two scenarios.

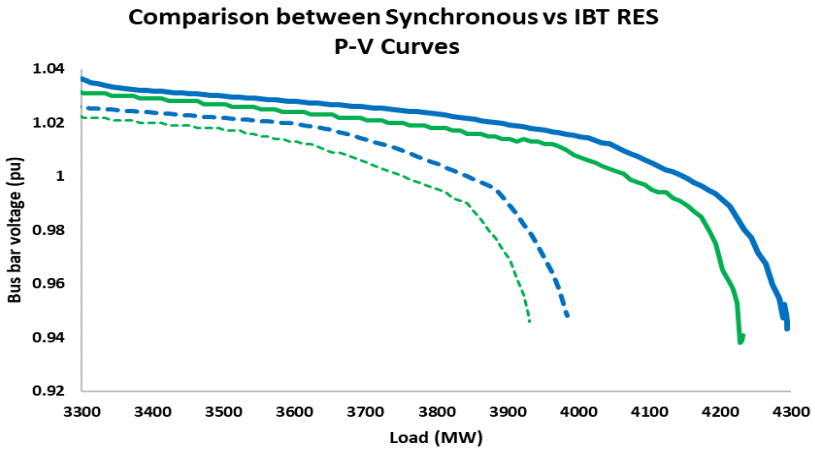

Figure 49 - P-V curve comparison of the synchronous scenario (blue) and of the IBT RES scenario (green) for the base network (solid lines) and worst contingency (dashed lines)

Figure 50 compares the reactive-power in the voltage collapse study area as the Tx-corridor active-power flow approaches voltage collapse for the limiting network contingency. The sum of all reactive-power available from the local generation is the same. However, at the contingency voltage collapse the system absorbs 727 MVAr in the synchronous scenario and 612 MVAr in the IBT RES scenario.

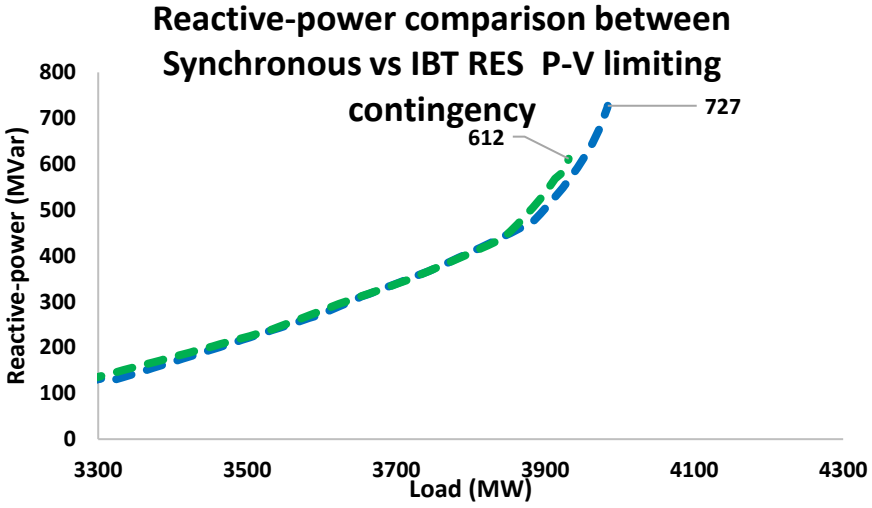

Figure 50 – Reactive-power comparison of the synchronous scenario (blue) and of the IBT RES scenario (green) for the limiting network contingency (dashed lines)

The higher the 132 Tx fault level, the greater the Tx-corridor active-power transfer capability. Hence, the fault level at four buses were compared (Figure 51 below) for the two scenarios. It can be observed that the fault level reduces at all buses between 8% and 50%. This is attributed to the substitution of synchronous generators with current-limited IBT RES resulting in the reduction in the Tx-corridor active-power transfer limits in the voltage collapse scenarios.

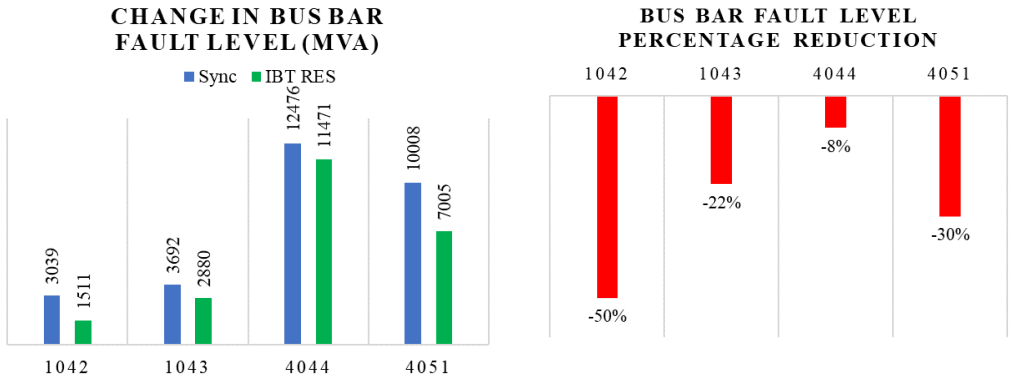

Figure 51 – Fault level comparison for the synchronous scenario and for the IBT RES scenario

The P-V steady-state voltage collapse analysis on the Cigre Nordic test network was for both the synchronous scenario and for the IBT RES scenario. The analysis concluded that increased IBT RES has a marginal reduction in the P-V steady-state analysis voltage collapse points, marginal reduction in the Tx-corridor active-power transfer limits (for the limiting network contingency) and marginal reduction in the reactive-power support. The reduction in Tx-corridor active-power transfer limits (for the limiting network contingency) is due to the reduction of SCR with fewer synchronous generators present. The IBT RES scenario may not have sufficient reactive-power capacity to replace that provided by the substituted synchronous generators and this will result in reduced reactive-power support. Lower SCRs result in more severe voltage dips, which in turn, increases the IBT RES active-power export reduction during 400 kV Tx faults. This impact of the IBT RES LVRT response is not accounted for in the classical P-V steady-state voltage collapse analysis.

Chapter 5: Task 3: Effect of the IBT RES LVRT response during a 400 kV Tx fault on the Tx-corridor active-power transfer.

The simulations were conducted for the synchronous scenario and for the IBT RES scenario. The task was divided into two phases. The first phase involved examining the network behaviour under conditions where voltage collapse during a 400 kV Tx fault does not occur. The second phase incremented the load to the P-V steady-state voltage stability limits to investigate the impact of the IBT RES active-power export reduction on network voltage collapse. The study also analysed the factors that influence the increase of active-power flow along the Tx-corridor. The analyses also examined the impact of the IBT RES LVRT response on the P-V collapse margin, posing a risk of voltage collapse.

5.1 Phase 1 of task 3: a 400 kV Tx fault does not cause voltage collapse

The network was set to the initial conditions described in the P-V steady-state voltage collapse analysis conducted in a previous chapter to investigate the response of the synchronous scenario and the IBT RES scenario when a 400 kV Tx fault occurs. This enables investigation into the active-power response, reactive-power response, Tx-corridor active-power transfer and prediction of the IBT RES active-power export reduction. Further, it is investigated whether the post-fault IBT RES active-power export can be predicted. The prediction is calculated using the approximate IBT RES characteristic response model developed in chapter 3. The input for this approximated IBT RES characteristic response model is the simulated 400 kV Tx bus voltages for the accurate network model.

5.1.1 Network initial conditions

The study-area initial steady-state conditions and Tx-corridor active-power transfer limits (for the limiting network contingency) are given in Table IX. The remaining system conditions are described in section 4.2. The study-area load-flow results are shown in Figure 52 for the synchronous scenario and Figure 53 for the IBT RES scenario. The numbers in the figure relate to the following.

1. Bus 4044 is the location of the 400 kV three-phase fault and the main Tx-corridor infeed.
2. Bus 4051 is the second 400 kV Tx-corridor infeed.
3. The bus where the local synchronous generation is monitored.
4. The 400 kV Tx-corridor consisting of five lines. The line clearing the fault is between bus 4044 and bus 4032.
5. The IBT RES integration

Table IX– Initial steady-state conditions and limits

	Synchronous scenario (MW)	IBT RES scenario (MW)
Study-area demand (load) (Table VI)	3383	3383
Study-area synchronous generation	1680	1080
Study-area IBT RES generation	0	600
Tx-corridor active-power flow	1723 (Tx-corridor flow in Figure 54)	1733 (Tx-corridor flow in Figure 55)
Maximum study-area (load) to avoid voltage collapse (5% safety margin)	3785 (limiting contingency in Table VIII)	3735 (limiting contingency in Table VIII)
Study-area demand (load) at the voltage collapse point (without 5% safety margin)	3984 (limiting contingency scenario in Table VIII)	3932 (limiting contingency in Table VIII)
Tx-corridor active-power transfer limit to avoid voltage collapse (5% safety margin)	2195 (limiting contingency in Figure 43)	2146 (limiting contingency scenario in Figure 48))
Tx-corridor active-power transfer at the voltage collapse point (without 5% safety margin)	2409 (limiting contingency in Figure 43)	2371 (limiting contingency in Figure 48)
Study-area demand (load) margin to voltage collapse	199 (= 3984 – 3785)	197 (= 3932 – 3735)
Tx-corridor active-power margin to voltage collapse	214 (= 2409 – 2195)	225 (= 2371 – 2146)

The solution converged and stable network conditions following fault clearance were observed with acceptable oscillation damping.

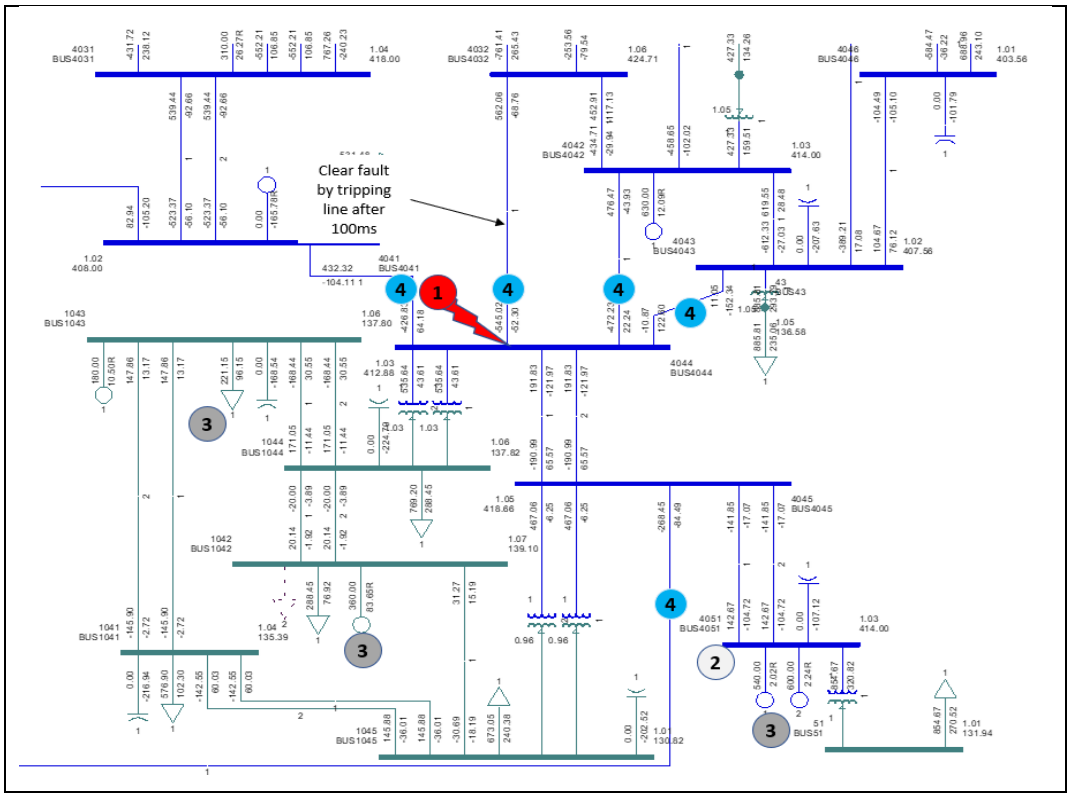

Figure 52 – Synchronous Scenario: Initial steady-state conditions and load flow results

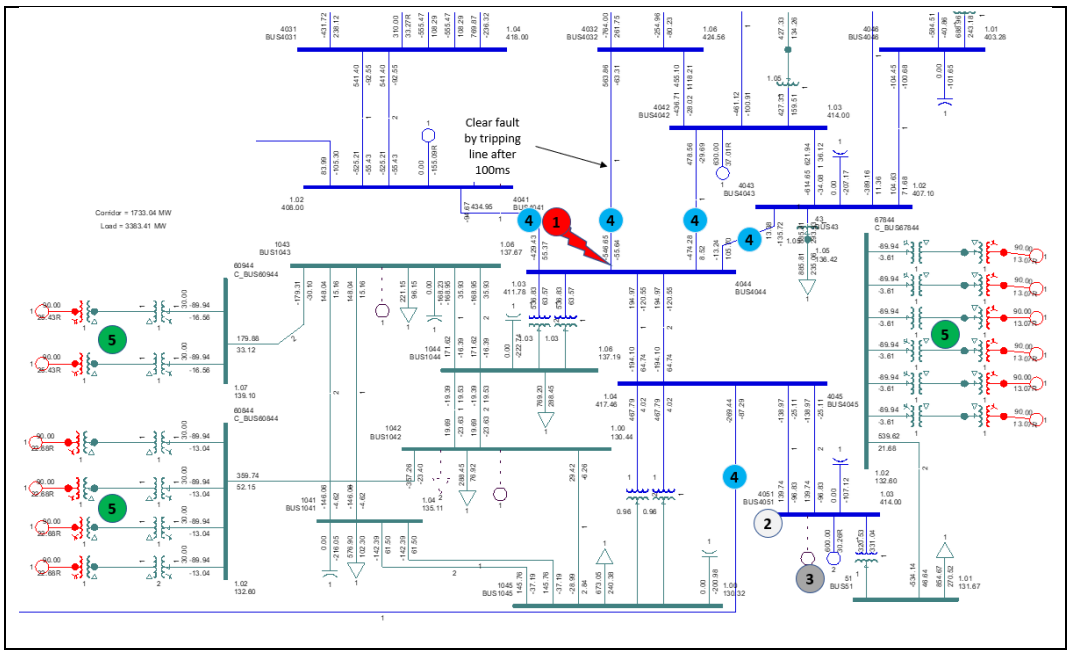

Figure 53 – IBT RES Scenario: Initial steady-state conditions and load flow results

5.1.2 Synchronous scenario

The results are plotted in Figure 54. The number on the graph relates to the load flow network locations in Figure 52 above. At the faulted bus 4044, the voltage drops to zero and can be observed in Figure 54 below top left. Top right is the voltage of the second main infeed which shows a voltage drop down to 0.59pu because of the fault at bus 4044. The middle graphs indicate the active-power (left) and reactive-power (right) responses of the local synchronous generators. The synchronous generators active-power increased beyond the steady-state initial value post voltage recovery to 1841 MW, an increase of 9.6%. The synchronous generator reactive-power, supporting the network during the fault, increases from 98 MVAr to 2315 MVAr. This is more than 3.18 times the steady-state value of 727 MVAr observed at voltage collapse.

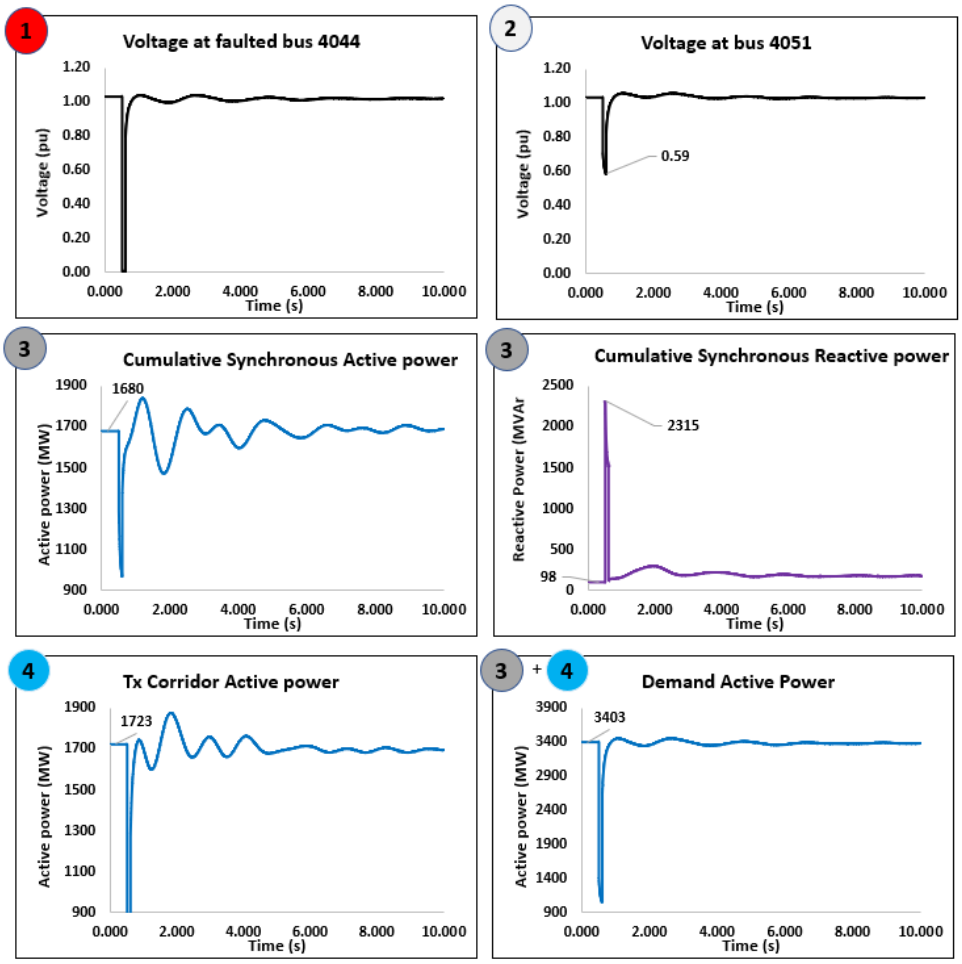

Figure 54 – Synchronous scenario

The bottom graphs indicate the Tx-corridor active-power flow (left) and load active-power including active-power losses (right). The Tx-corridor active-power flow rises to a similar value to the pre-fault condition. The active-power of the demand (load) picks up rapidly but not instantaneously. There is a slight delay in the first second of the load before pre-fault loading levels are achieved.

5.1.3 IBT RES scenario

The results are plotted in Figure 55 below and the IBT RES active-power and reactive-power are separately plotted in Figure 56 below. The number on the graph relates to the load-flow network locations in Figure 53 above. The faulted bus 4044 voltage drops to zero and can be observed in Figure 55 below top left. Figure 55 top right is the voltage of the second main infeed which shows a voltage drop down to 0.45pu as a result of the fault at bus bar 4044. The middle graphs indicate the active-power (left) and reactive-power (right) responses of the remaining local synchronous generators. The remaining local synchronous active-power export increased beyond the steady-state initial value post voltage recovery to 784 MW, an increase of 30%. The synchronous generator reactive-power supporting the network during the fault increased from 30 MVAr to 935 MVAr.

In Figure 56 below, the IBT RES active-power export reduces to 223 MW from 1080 MW and the reactive-power export increases from 220 MVAr to 623 MVAr during the 400 kV Tx fault. This total reactive-power export increases by 1558 MVAr (Total reactive-power export = cumulative synchronous generators export + cumulative IBT RES export = 935 + 623 = 1558 MVAr) which is 2.55 times the steady-state value of 623 MVAr observed at voltage collapse.

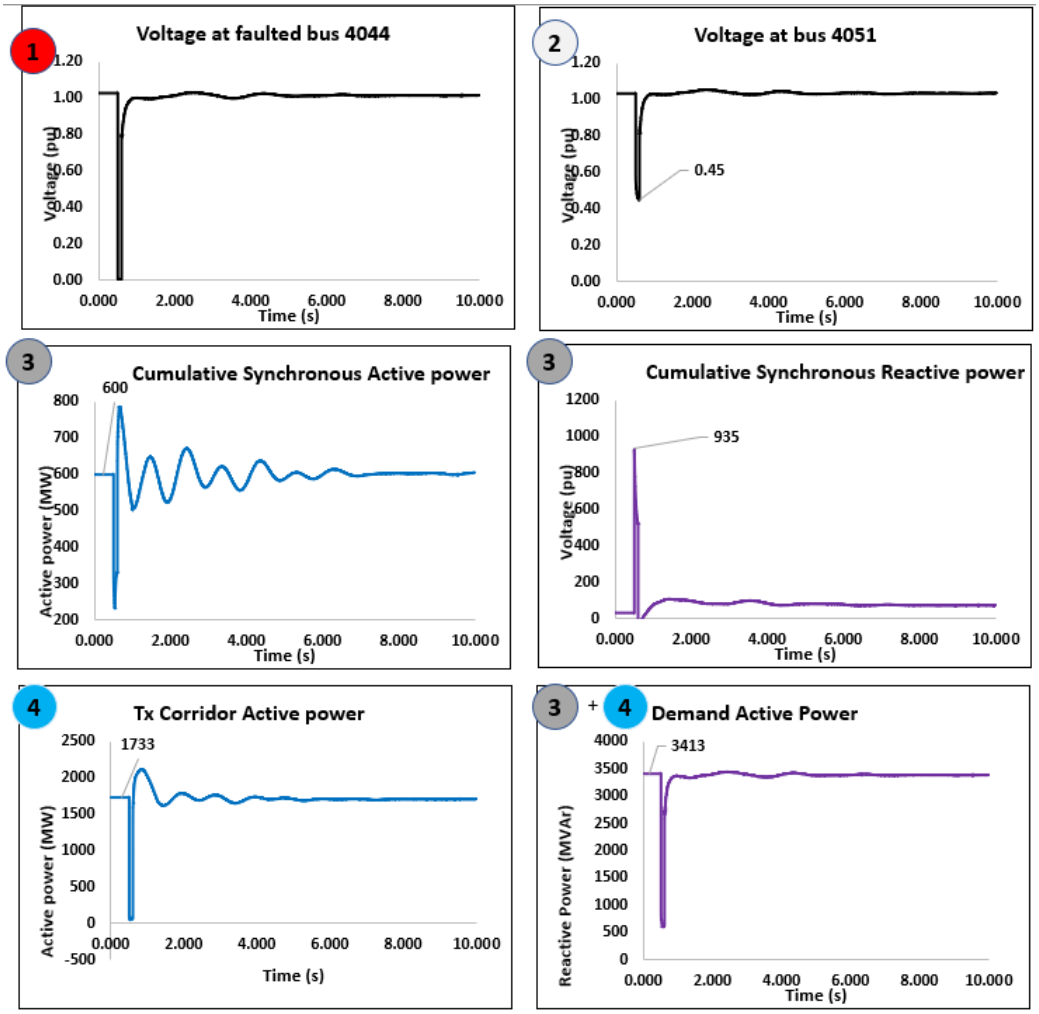

Figure 55 – IBT RES scenario

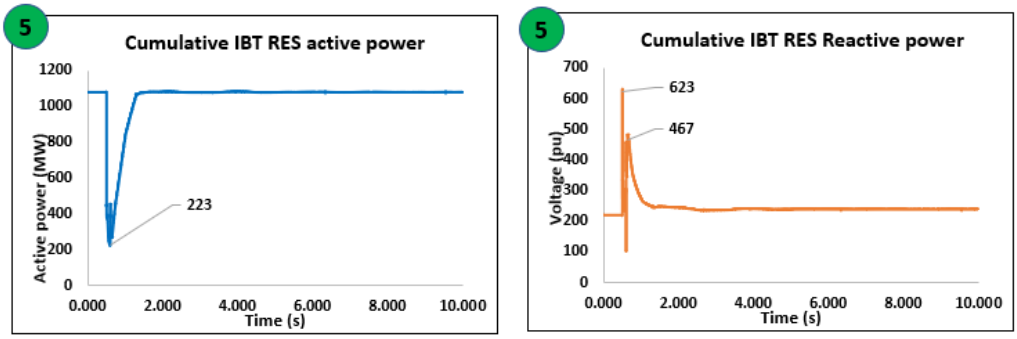

Figure 56 – IBT RES scenario cumulative active-power and reactive-power

5.1.4 Analysis of results

The active-power disturbance is the difference (Diff) between the pre-fault active-power and the post-fault active-powers. For the study-area the active-power balance and shown in Figure 57 below

$$(Sync\ Gx\ +\ IBT\ RES\ Gx\ +\ Demand\ )+\ Tx\ Corridor\ =\ 0$$

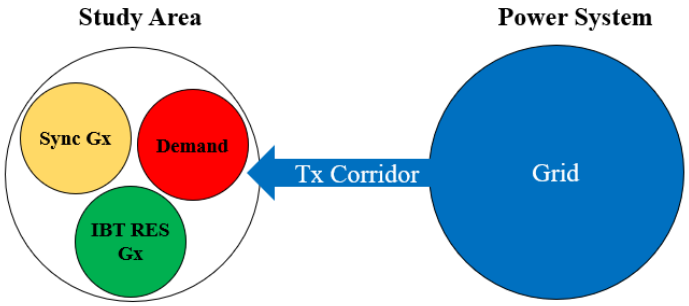

Figure 57 – Active-power balance

In terms of disturbances (differences) between pre-fault values and post-fault values the power balance equation becomes

$$Sync\ Diff\ +RE\ Diff\ +Demand\ Diff\ +Tx\ Diff\ =0$$

In the simulations, all the active-powers indicated are plotted. However, in the IBT RES scenario, there are two generator technologies (synchronous generator and IBT RES) compared to only one in the synchronous scenario (synchronous generators only). For comparison, the aggregated study area active-power generation is plotted.

5.1.5 Synchronous scenario: active-power and reactive-power response.

Active-power response for the period up to 5 s and a zoomed in view up to 2 s are shown in Figure 58A and 58B respectively.

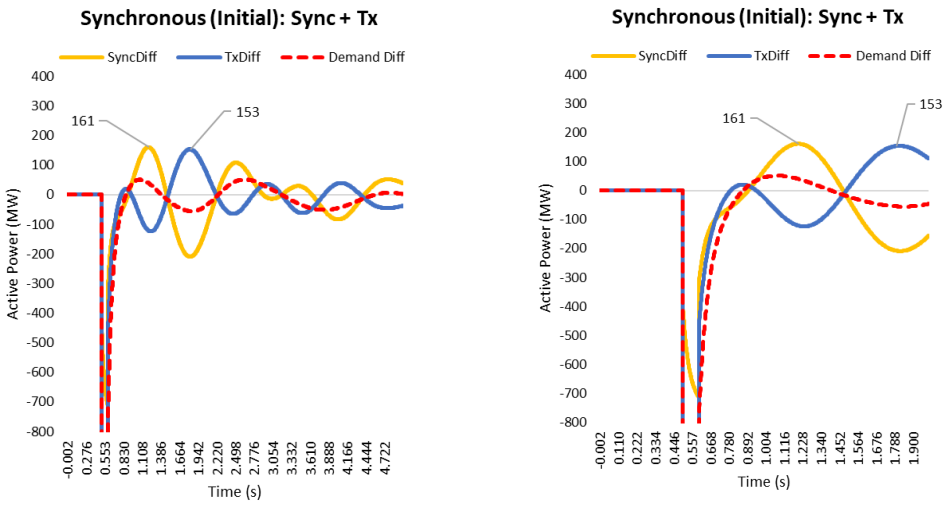

A B

Figure 58 – Synchronous scenario: active-power response

The study-area demand (load) recovery (shown by the red dashed line) delay in reaching the pre-fault levels is under 1 s.

The local synchronous generation (yellow) follows the demand (load) but overshoots (161 MW), because of the kinetic energy stored in the shaft which is now released into the grid post-fault.

The Tx-corridor active-power disturbance follows the demand (load) disturbance but reduces in response to the synchronous generator overshoot. This effectively reduces the Tx-corridor transfer (Figure 58B)

The local synchronous generation and the demand (load) disturbances are in phase and the Tx-corridor supplies the difference in active-power.

The peak active-power increase along the Tx-corridor is 153 MW.

The maximum Tx-corridor active-power transfer increase is lower than the Tx-corridor steady-state P-V margin of 214 MW.

The local synchronous generators reduce the Tx-corridor active-power transfer through the injection of post-fault active-power. The synchronous generator and demand (load) in-phase response further reduces the Tx-corridor active-power transfer.

Reactive-power response for the period up to 2s is shown in Figure 59.

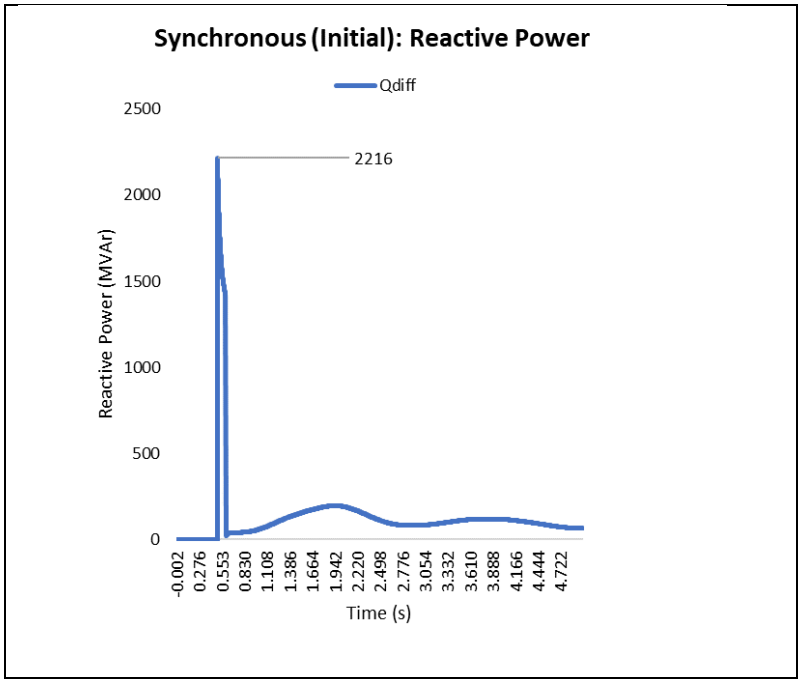

Figure 59 – Synchronous scenario: reactive-power response.

The peak change in reactive-power is 2216 MVAr which is three times the reactive-power at P-V voltage collapse.

The reactive-power increases to just below 1500 MVAr during the fault and supports post-fault voltage recovery.

The MVAr support is reduced post-fault.

5.1.6 IBT RES scenario: active-power and reactive-power response.

Active-power response for the period up to 5 s and a zoomed-in view up to 2 s are shown in Figure 60A and 60B respectively.

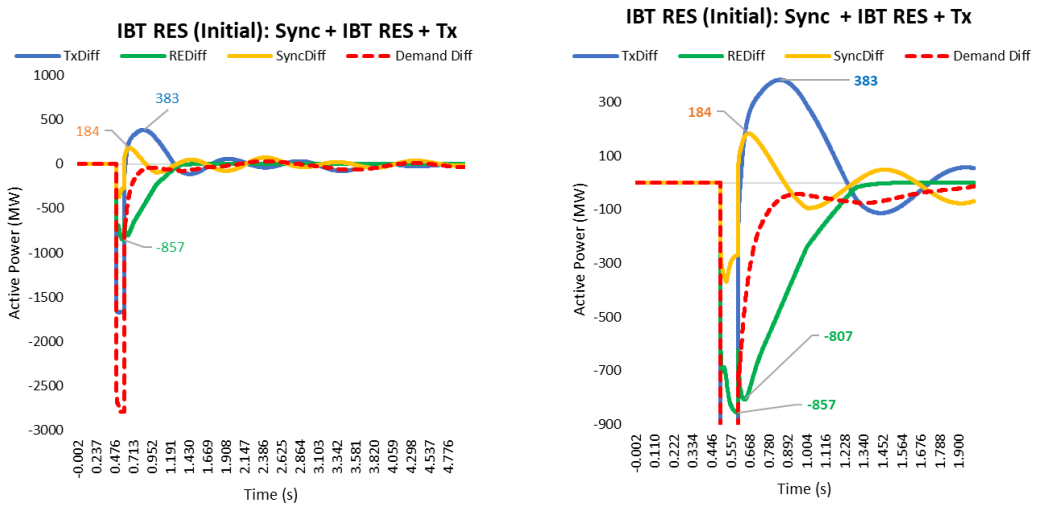

A B

Figure 60 – IBT RES scenario: active-power response

The study-area demand (load) recovery (shown by the red dashed line) delay in reaching pre-fault levels is 2 s.

The reduction in IBT RES active-power (green in Figure 60B), is 857 MW. However, the reduction at clearance of the fault is 807 MW.

The synchronous generation active-power disturbance (yellow) has a significant rate of recovery compared with the demand (load). Overshoot occurs 50 ms after fault clearance (184MW), because of the kinetic energy stored in the shaft, which is now released into the grid post-fault. The acceleration of the synchronous generators is a result of the active-power reduction from the IBT RES.

The Tx-corridor active-power disturbance (blue) follows the synchronous generators active-power profile to support the deficit of active-power in the supply area. This increases the Tx-corridor active-power transfer (Figure 60B).

The active-power transfer increase on the Tx-corridor is 383MW.

The Tx-corridor maximum active-power increase is greater than the steady-state P-V active-power Tx-corridor margin of 225 MW.

IBT RES scenario response in reactive-power is shown in Figure 61.

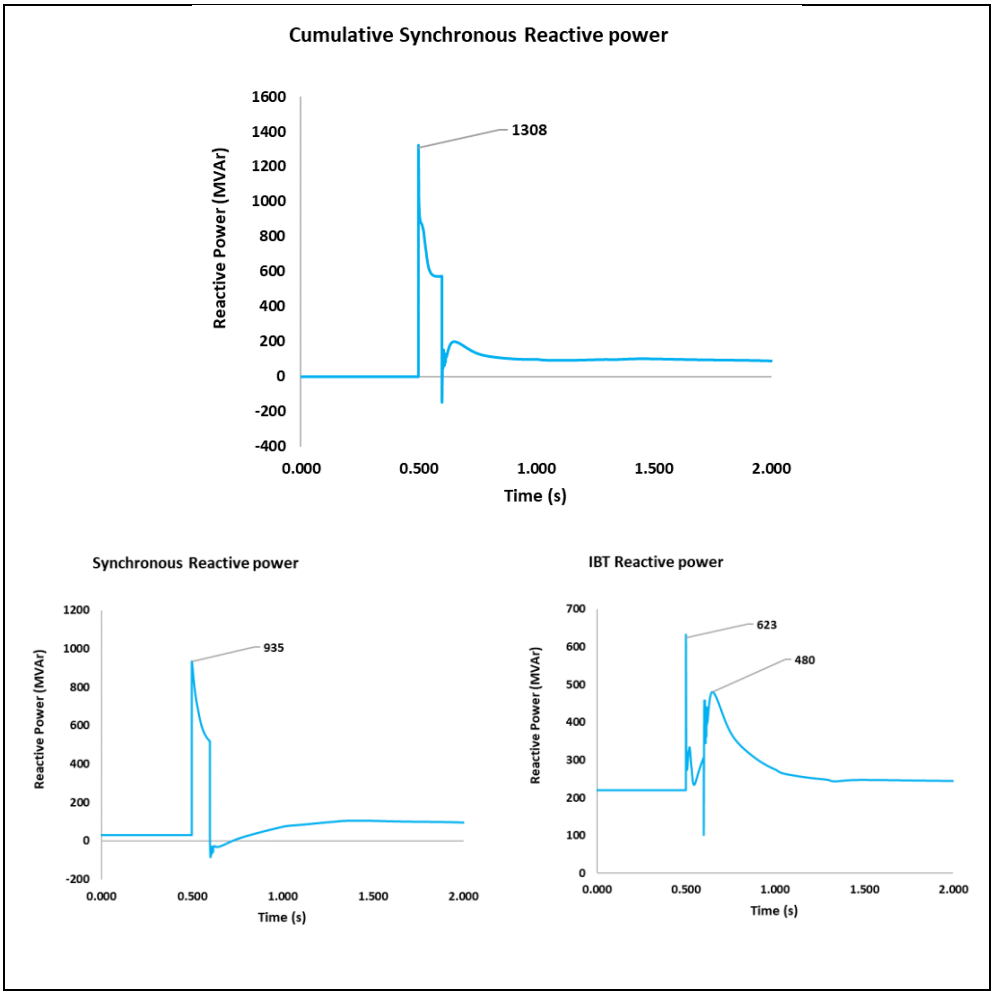

Figure 61 – IBT RES scenario: reactive-power response.

- The peak change in reactive-power is 1308 MVAr which is two times the reactive-power at P-V voltage collapse (Figure 61 top graph).
- The reactive-power support during the fault mainly comes from the synchronous generator (Figure 61 bottom left).
- The IBT RES reactive-power reduces as active-power increases (Figure 61 bottom right).

Conditions at the instant of Tx-corridor maximum active-power flow (IBT RES scenario)

The increase of active-power transfer along the Tx-corridor of 383 MW exceeds the Tx-corridor P-V steady-state margin of 225 MW. This indicates that if the initial loading conditions are set to the network limits (for the limiting network contingency) the margin is inadequate. To examine why the Tx-corridor active-power transfer has increased, the time of Tx-corridor active-power peak is plotted in Figure 62A (zoomed-in view in Figure 62B) and the system values are in Table X

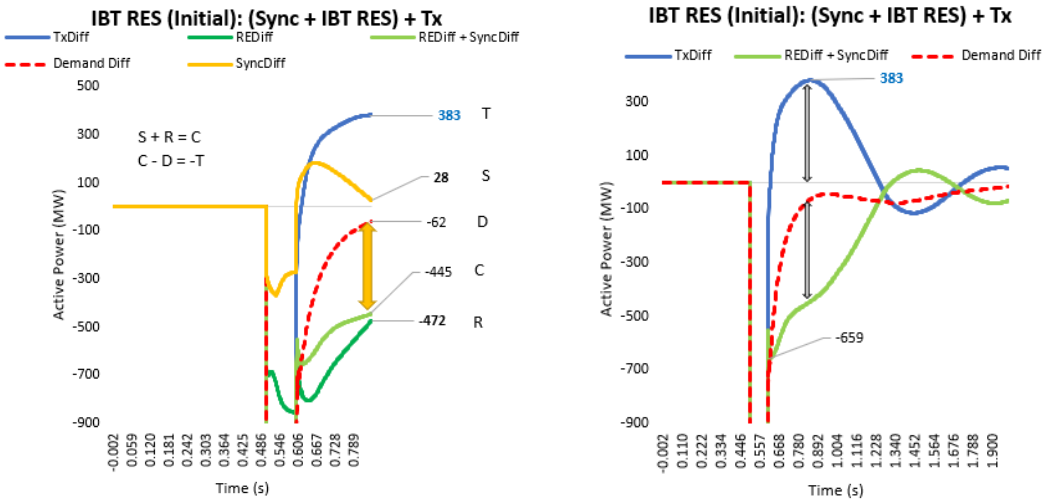

A B

Figure 62 – IBT RES scenario active-power responses (using an accurate network model)

Table X– System response at instant of Tx-corridor peak active-power transfer (using an accurate network model)(IBT RES scenario)(Figure 62A)

Description	MW
S = Local synchronous generator change (increase) in active-power export (Sync Diff)	+28
R = Local IBT RES change (reduction) in active-power export (RE Diff)	-472
C = Combined change (reduction) in locally generated active-power export (=S+R)	-445
D = Local demand change (reduction) in active-power import (Demand Diff)	-62
T = Tx-corridor change (increase) in active-power transfer (Tx Diff)	+383

The maximum active-power increase occurs at time 0.846 s. The local synchronous generator active-power (S) change is declining and is 28 MW. The IBT RES change in active-power (R) is increasing for the LVRT power reduction and is at 472 MW. The combination generation change in active-power (C) is the sum of S + R, which equals

445 MW. This indicated that the total active-power local generation has reduced by 445MW. However, the demand (load) has not fully recovered to pre-fault conditions. The demand (load) change in active-power (D) is 62 MW less than the pre-fault condition. This has the effect of reducing the need for active-power supply. The difference between the C and D (shown in Figure 62B arrow between red and green, black double arrow), is the total active-power required from the Tx-corridor. Therefore C – D = -T. The negative T value indicates transfer into the supply area and is indicated (by the black double arrow between the blue line and zero line) in Figure 62B.

5.1.7 Approximate IBT RES characteristic response model prediction

The approximate IBT RES characteristic response model developed in Chapter 3 enables the prediction of the approximate IBT RES active-power reduction for a given voltage depression on the 400 kV Tx bus. The voltages simulated at the two Tx infeeds, buses 4044 and bus 4051 are used in the approximate IBT RES characteristic response model (rather than the voltages at the IBT RES POC from the accurate network model). The dispatched IBT RES connected to the study-area (MW) is used to predict the reduction in active-power export

The results are shown in Table XI

Table XI– IBT RES scenario approximate IBT RES characteristic response model prediction

		Dispatched	Approximate IBT RES characteristic response model (input and output parameters)		
Tx bus	400 kV Tx bus voltage during fault (pu)	IBT RES connected to study-area network (MW)	400 kV Tx bus voltage during fault (pu)	Predicted active-power export (pu)	Predicted reduction of active-power export (MW)
4051	0.448910	540	0.448910	0.3854	332
4044	0.004204	360	0.004204	0.0695	335
		180	0.004204	0.0695	167
Total IBT RES		1080	Cumulative predicted reduction		834

The predicted cumulative IBT RES active-power export reduction using the approximate IBT RES characteristic response model is 834 MW and the IBT RES maximum active-power export reduction during the fault from the accurate network model is 807 MW (Figure 60 B).

	MW
IBR RES active-power export reduction during the fault using the accurate network model	807
Cumulative predicted active-power export reduction using the approximate IBT RES characteristic response model	834
Prediction error	3%

The prediction of the maximum Tx-corridor active-power transfer following fault clearance can be determined from the delay in recovery of the IBT RES active-power export, the local synchronous generator active-power overshoot in recovery and the reduction of demand (load) at the instant of the Tx-corridor peak active-power transfer. The cumulative predicted IBT RES active-power export reduction is then scaled to account for these factors.

The scaling factors at the Tx-corridor peak active-power are as follows (all from the accurate network model).

Define $IBT\ RES\ active\text{-}power\ export\ reduction\ scaling\ \ factor$

$$= \frac{IBT\ RES\ active\text{-}power\ export\ reduction\ at\ instant\ of\ Tx\ corridor\ \ peak\ active\text{-}power\ \ flow}{Maximum\ IBT\ RES\ active\text{-}power\ export\ reduction\ during\ 400\ kV\ \ fault}$$

- where the numerator is from Table X(R) and the denominator is from Figure 60

For the above example

$$IBT\ RES\ active\text{-}power\ export\ reduction\ scaling\ \ factor = \frac{472}{857} = 0{,}55$$

Also define $Tx\ corridor\ \ peak\ active\text{-}power\ flow\ change\ scaling\ \ factor$

$$= \frac{Tx\ corridor\ \ peak\ active\text{-}power\ \ flow\ change\ after\ the\ Tx\ \ fault\ is\ cleared}{IBT\ \ RES\ active\text{-}power\ export\ reduction\ at\ instant\ of\ \ Tx\ corridor\ \ peak\ active\text{-}power\ \ flow}$$

- where the numerator (T) and denominator (R) are from Table X

For the above example

$$Tx\ corridor\ \ peak\ active\text{-}power\ flow\ change\ scaling\ \ factor = \frac{383}{472} = 0{,}81$$

Therefore $Cumulative\ reduction\ of\ IBT\ \ RES\ active\text{-}power\ export\ scaling\ factor$

$$= (IBT\ \ RES\ active\text{-}power\ export\ change\ scaling\ \ factor) \times (Tx\ corridor\ \ peak\ active\text{-}power\ flow\ change\ scaling\ \ factor)$$

$$= 0{,}55 \times 0{,}81 = 0{,}66$$

Finally define the

$$Adjusted\ IBT\ \ RES\ active-power\ export\ reduction\ using\ the\ approximate\ IBT\ \ RES\ characteristic\ response\ model$$

$$= Cumulative\ reduction\ of\ IBT\ \ RES\ active\text{-}power\ export \times$$

$$Cumulative\ reduction\ of\ IBT\ \ RES\ active\text{-}power\ export\ scaling\ factor$$

$$834 \times 0{,}66 = 373\ MW$$

where the cumulative IBT RES active-power export reduction is obtained from Table XI

The adjusted cumulative IBT RES active-power export reduction is the additional active-power added to the Tx-corridor active-power transfer requirement.

This can be compared with the Tx-corridor change in active-power value from the accurate network model which is 383 MW.

5.2 Phase 2 of task 3: Set the study-area demand (load) for the Tx-corridor P-V active-power transfer limit for the limiting network contingencies in Table V and Table VII including the 5% margin

Phase 2 investigates whether the P-V voltage collapse Tx-corridor steady-state active-power limit determined in Chapter 4 both for the synchronous scenario and for the IBT RES scenarios maintain voltage stability in the presence of a Tx fault. For each scenario (synchronous and IBT RES) the study-area load is increased from the initial load to the Tx-corridor P-V active-power transfer limit (taking the limiting network contingency and the 5% margin into account).

The network is then subjected to the same Tx fault as in Phase 1. Based on the results in Phase 1, the synchronous scenario is expected to be stable (due to no IBT RES LVRT response being present) and the IBT RES is expected to be beyond the voltage stability limit (due to the IBT RES LVRT response being present). The IBT RES scenario is examined in repeated steps with increased Tx fault impedance. At each step, the approximate IBT RES characteristic response model developed in Chapter 3 is used to predict the active-power reduction and the proximity to voltage collapse.

5.2.1 Network initial conditions

The study-area demand (load) is increased above the load in Phase 1 by adding a load of 402 MW to the synchronous scenario and 352 MW to the IBT RES scenario. The Phase 2 study-area Tx-corridor active-power limits are shown in Table IX. The remaining system conditions are described in section 5.1. The load-flow results are shown in Figure 63 for synchronous scenario and Figure 64 for the IBT RES scenario. The numbers in the figures relate to the results and identify the following.

1. Bus 4044 is the location of the 400 kV three-phase fault and the main Tx-corridor infeed.
2. Bus 4051 is the second 400 kV Tx-corridor infeed.
3. The bus where the local synchronous generation is monitored.

4. The 400 kV Tx-corridor consisting of five lines. The line clearing the fault is between bus 4044 and bus 4032.
5. The IBT RES integration

Table XII– Steady-state scenario conditions and limits

	Synchronous scenario (MW)	IBT RES scenario (MW)
Study-area demand (load) (Table VI) Study-area synchronous generation Study-area IBT RES generation Tx-corridor active-power flow	3785 1680 0 2131 (corridor flow in Figure 65)	3735 1080 600 2090 (corridor flow in Figure 68)
Maximum study-area (load) to avoid voltage collapse (5% safety margin)	3785 (limiting contingency in Table VIII)	3735 (limiting contingency in Table VIII)
Study-area demand (load) at the voltage collapse point (without 5% safety margin)	3984 (limiting contingency scenario in Table VIII)	3932 (limiting contingency in Table VIII)
Tx-corridor active-power transfer limit to avoid voltage collapse (5% safety margin)	2195 (limiting contingency in Figure 43)	2146 (limiting contingency scenario in Figure 48))
Tx-corridor active-power transfer at the voltage collapse point (without 5% safety margin)	2409 (limiting contingency in Figure 43)	2371 (limiting contingency in Figure 48)
Study-area demand (load) margin to voltage collapse	199 (= 3984 – 3785)	197 (= 3932 – 3735)
Tx-corridor active-power margin to voltage collapse	214 (= 2409 – 2195)	225 (= 2371 – 2146)

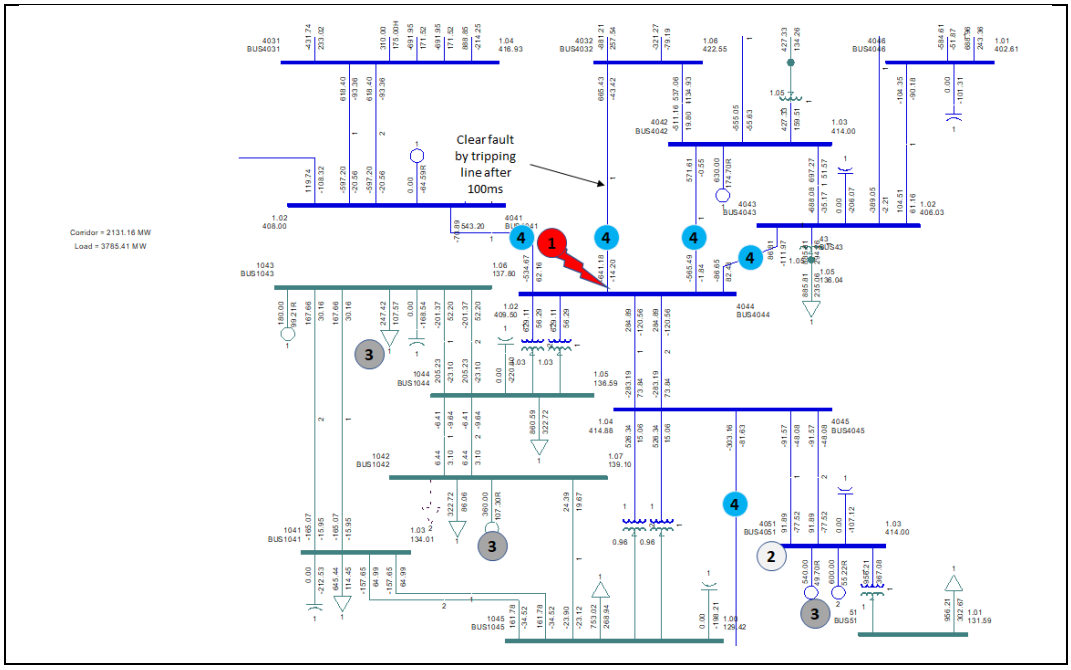

Figure 63 – Synchronous scenario: Network P-V limits condition and load flow

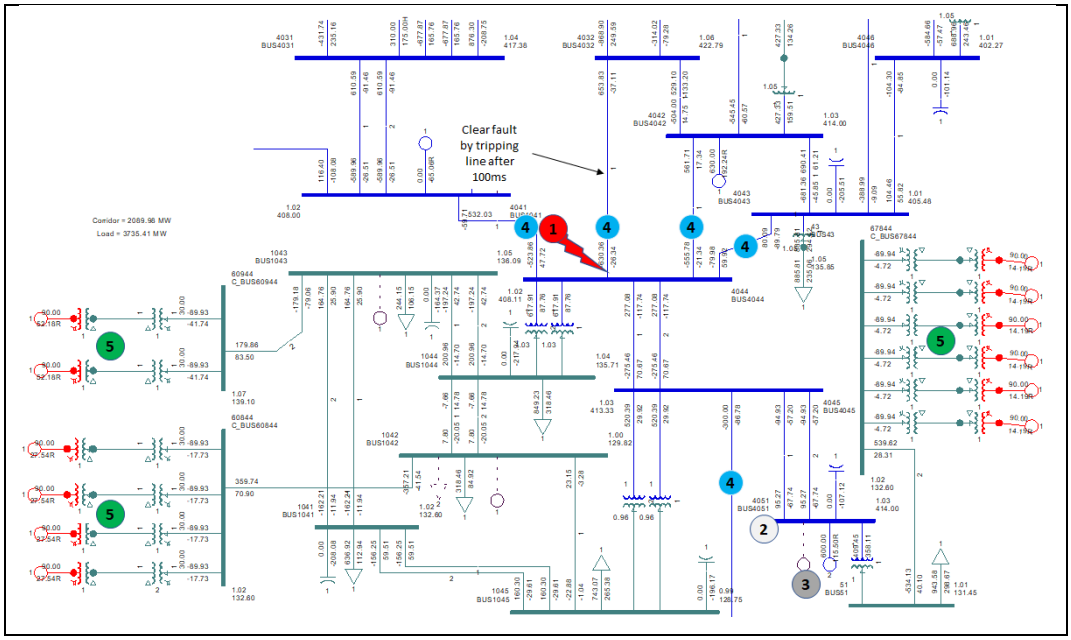

Figure 64 – IBT RES scenario: Network P-V limits and load flow

5.2.2 Results for the synchronous scenario

The load-flow solution converged and the post-fault network was stable with acceptable system oscillation damping. The results are shown in Figure 65. Figure 65, top right is the voltage of the second main Tx infeed which shows a voltage drop down to 0.59pu because of the fault at bus bar 4044. The middle graphs indicate the active-power (left) and reactive-power (right) responses of the synchronous generators. The synchronous generator active-power export increases beyond the steady-state initial value post-voltage recovery to 1841 MW, an increase of 9.6%. The synchronous generator reactive-power export supporting the network voltage during the fault increases from 311 MVAr to 2398 MVAr. This is more than 3.29 times the steady-state value of 727 MVAr observed at voltage collapse.

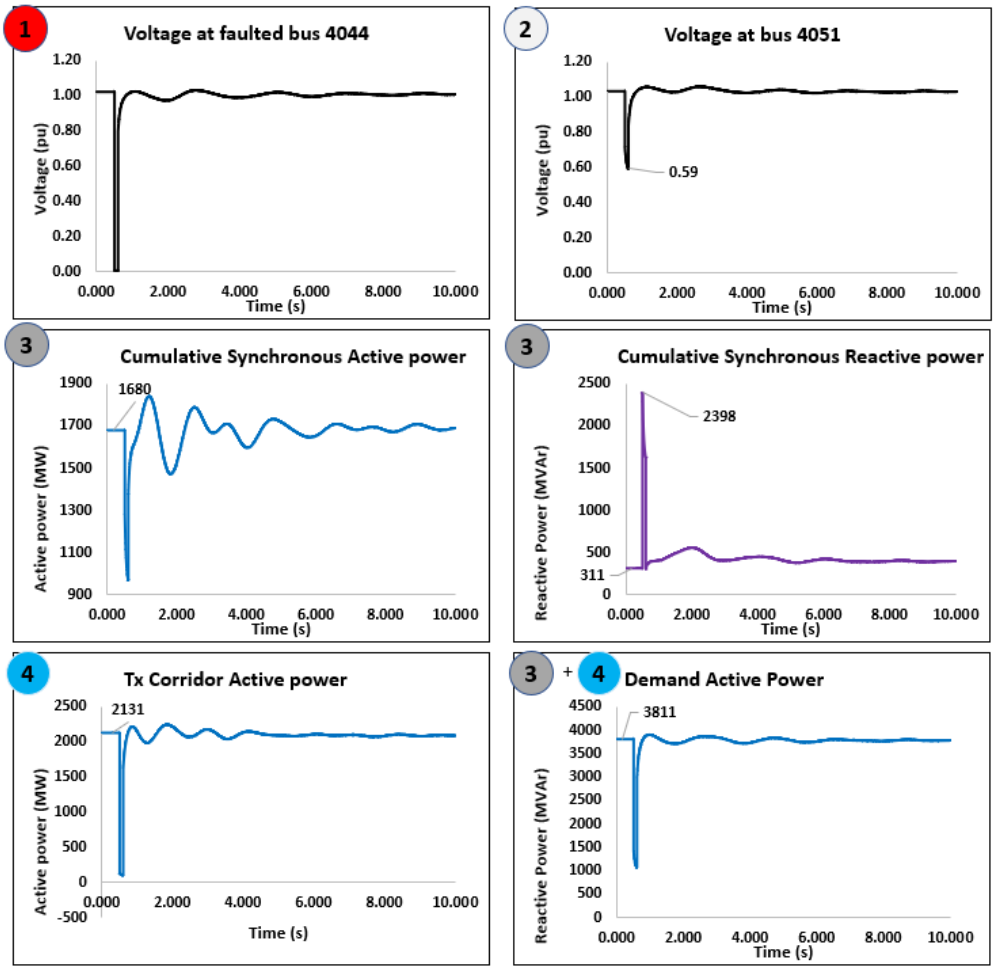

Figure 65 – Synchronous scenario: P-V network results

The bottom graphs indicate the Tx-corridor active-power transfer (left) and demand (load) including losses (right).

5.2.3 Results for the IBT RES scenario

The load-flow solution did not converge meaning that the network is either beyond the voltage stability limit or numerical instability exists. To rule out numerical instability the simulation time step was reduced from 1 ms to 1 µs. However, the load-flow solution still did not converge, this indicates voltage collapse.

The further determine the voltage collapse point the simulation was repeated varying the fault impedance. The fault impedance impacts the voltage dip which impacts the active-power export reduction of the IBT RES as determined in Chapter 3. The fault impedance was varied in five steps. The steps result in voltage reduction from nominal voltage of 18%, 55%, 72%, 92% and 100%. Simulations for each step were performed and the results are shown in Table XIII where step 1-4 load-flows converged. The step 5 load-flow failed to converge and estimated values are indicated in red.

Table XIII– Voltage collapse margin

Step	Faulted bus 4044 voltage (pu)	Simulated reduction (MW)	Adjusted reduction (MW)	Tx-corridor (MW)	Load-flow convergance	MW from Collapse
1	0.82	124	0	2090	pass	281
2	0.45	426	27	2117	pass	254
3	0.28	646	168	2258	pass	113
4	0.08	793	307	2397	Marginal	-26
5	0.00	851	401	2491	Fail	-120

The results of step 1-4 are indicated in Figure 66

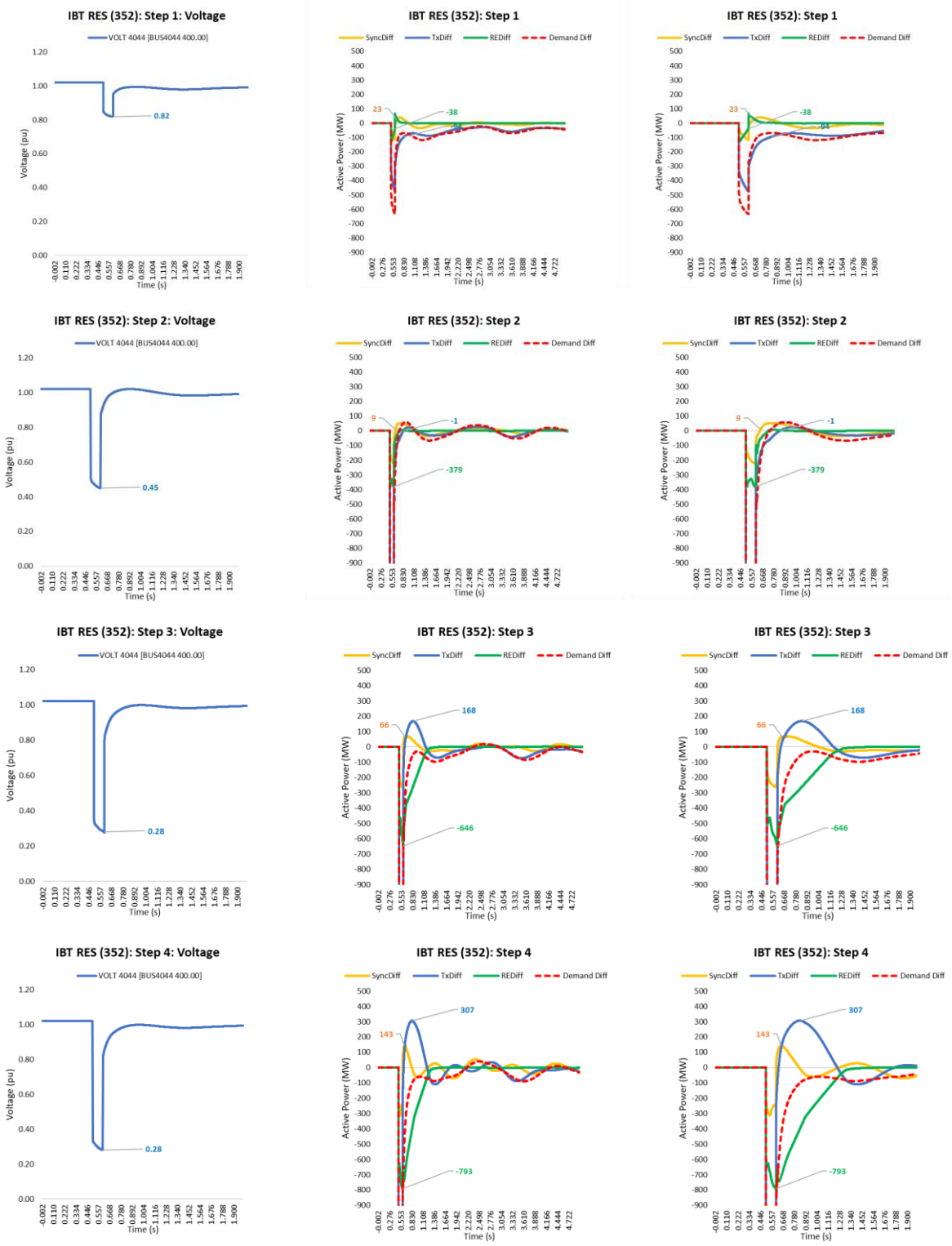

Figure 66 – Step 1-4 results

From the results in Table XIII and Figure 66 the cumulative reduction of active-power scaling factor (see Section 5.1.7) and collapse margin are shown in Figure 67

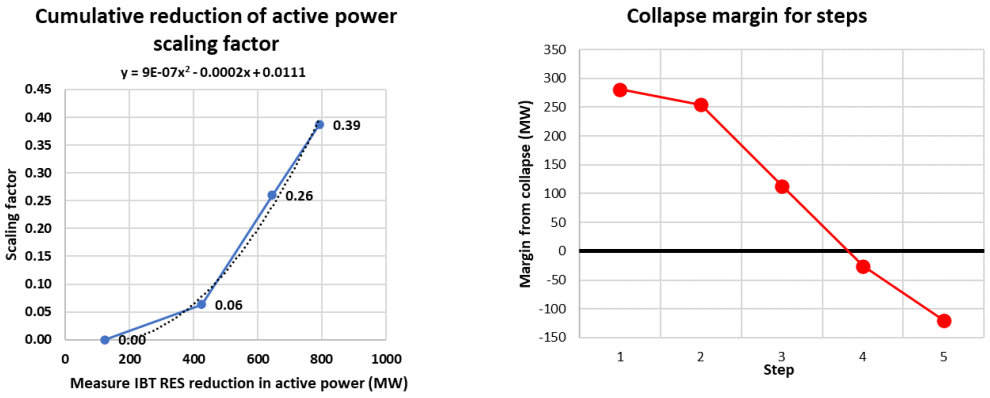

A B

Figure 67 – Cumulative reduction of active-power export scaling factor and collapse margin for steps 1-4

The cumulative reduction of IBT RES active-power export scaling factor (Figure 67 A), is the ratio of how much of the post-fault IBT RES active-power reduction needs to be supplied by the Tx-corridor. The additional active-power transfer required from the Tx-corridor reduces the margin to the voltage collapse point. This effect is not considered in the classical P-V steady-state voltage collapse analysis. The collapse margin is the difference between the Tx-corridor voltage collapse point and the initial Tx-corridor active-power plus the additional active-power.

When the margin is zero then the voltage collapse point is reached (Figure 67 B). The collapse points near zero are marginal cases. Steps 1-4 are simulated values and step 5 is an estimated value as for Step 5 no solution was found.

To predict the voltage collapse margin the cumulative reduction of active-power scaling factor is calculated using the 2nd order polynomial derived from Figure 67A. The cumulative predicted reduction of active-power is multiplied by the calculated scaling factor to calculate the adjusted reduction (Table XIV).

Table XIV– Voltage collapse margin.

Step	Faulted bus 4044 voltage (pu)	Estimated cumulative reduction of active-power (MW)r	Adjusted cumulative reduction of active-power (MW)	Tx-corridor (MW)	Load-flow convergence	MW from Collapse	Prediction % Error
1	0.82	136	0	2090	pass	281	0%
2	0.45	484	61	2151	pass	220	13%
3	0.28	653	172	2262	pass	109	4%
4	0.08	777	310	2400	Marginal	-29	14%
5	0.00	834	393	2483	Fail	-112	

5.2.4 Results for marginal stable condition (step 4)

The solution converged for the step 4 marginal case (Table XIII). Post-fault network stable conditions are observed with acceptable damping. The results are shown in Figure 68 and the IBT RES active-power export and reactive-power export are separately shown in Figure 69. The number on the graph relates to the load-flow network locations in Figure 63 and in Figure 64. Bus 4044 (with the fault) shows a voltage of 0.08pu during the fault as can be observed in Figure 68 top left. Top right is the voltage of the second main Tx infeed which shows a voltage of 0.49pu.

The voltages at both Tx buses are higher than the voltage drop in Phase 1. This reduces the impact of IBT RES active-power reduction. The middle graphs indicate the active-power (left) and reactive-power (right) responses of the local synchronous generators. The synchronous scenario active-power export increased beyond the steady-state initial value post-voltage recovery to 743 MW, an increase of 23.8%. This is lower than Phase 1 because of the local synchronous generators have less stored kinetic energy to release. The synchronous generator reactive-power export supporting the network voltage during the fault increases from 115 MVAr to 955 MVAr. The increased reactive-power export is needed to support the near voltage collapse conditions. In Figure 69 the IBT RES active-power export reduces to 287 MW from 1080 MW and the reactive-power increase from 300 MVAr to 644 MVAr. This total reactive-power

support increases by 1600 MVAr which is 2.61 times the steady-state value of 612 MVAr observed at voltage collapse.

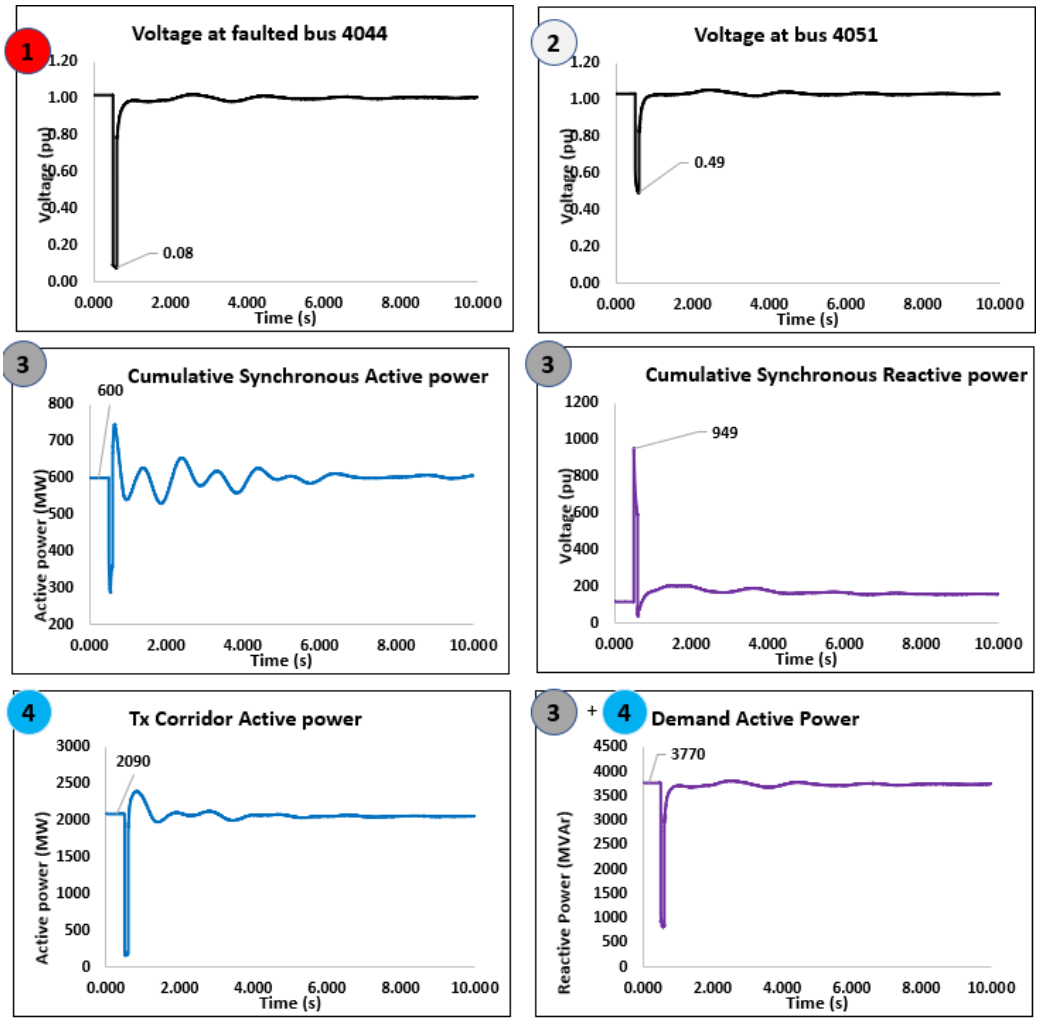

Figure 68 – IBT RES scenario: bus voltages, active-power and reactive-power

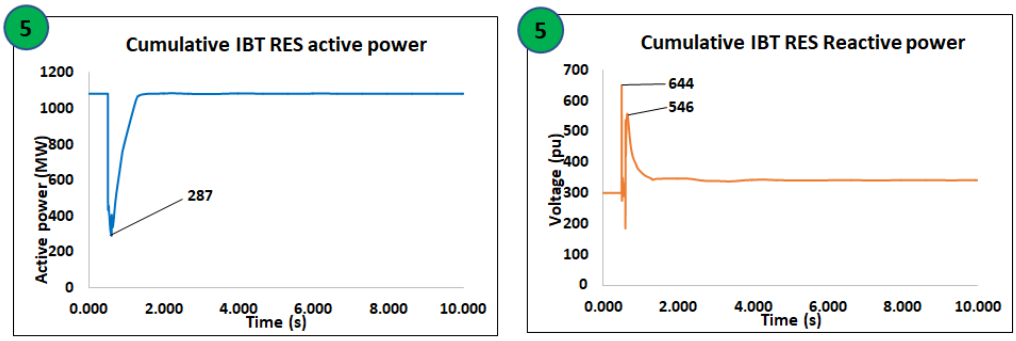

Figure 69 – IBT RES scenario: IBT RES active-power and reactive-power

5.2.5 Analysis of results

In the IBT RES scenario, there are two generator types (synchronous generators and IBT RES) compared to only one in the synchronous scenario (only synchronous generators). For comparison, the aggregated generation study area active-power is plotted. This provided an easier comparison with the synchronous scenario plots.

5.2.6 Synchronous scenario: active-power and reactive-power responses

The active-power response for the period up to 5 s and a zoomed-in view up to 2 s to is in Figure 70A and 70B respectively.

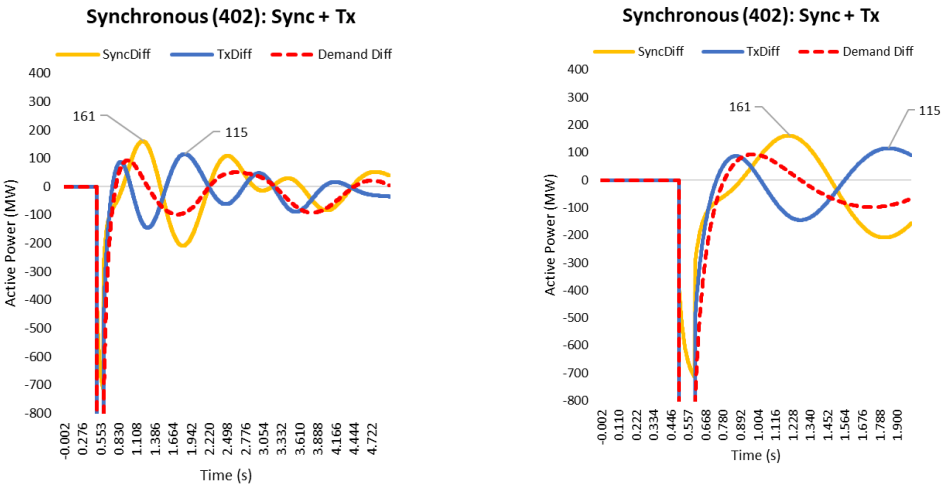

A B

Figure 70 – Synchronous scenario active-power disturbance.

The study-area demand (load) recovery has a slight delay but more accelerated than in Phase 1 with a higher overshoot. The pre-fault levels before 1sec are shown by the red dashed line. Synchronous generation (yellow) follows the demand (load) but overshoots (161 MW) because of the kinetic energy stored in the shaft which is now released into the grid after the fault is cleared. The response is in line with that of Phase 1. The Tx-corridor active-power transfer follows the study-area demand (load) curve accelerated response resulting in more power supplied along the Tx-corridor. The Tx-corridor active-power transfer reduces in response to the synchronous generator

overshoot which does not exceed the limits seen in phase 1 (Figure 70B). The synchronous generation and the study-area (load) demand are less in phase compared to phase 1 and the Tx-corridor supplies the net difference. The active-power increase on the Tx-corridor is 115 MW which is less than the 153 MW observed in phase 1. The maximum increase is lower than the steady-state Tx-corridor P-V active-power margin of 214 MW.

The local synchronous generation reduces the Tx-corridor active-power transfer through the injection of post-fault active-power observed in Phase 1. The Tx-corridor peak active-power flow respects the P-V limits.

The reactive-power response for the local synchronous generator is shown in Figure 59.

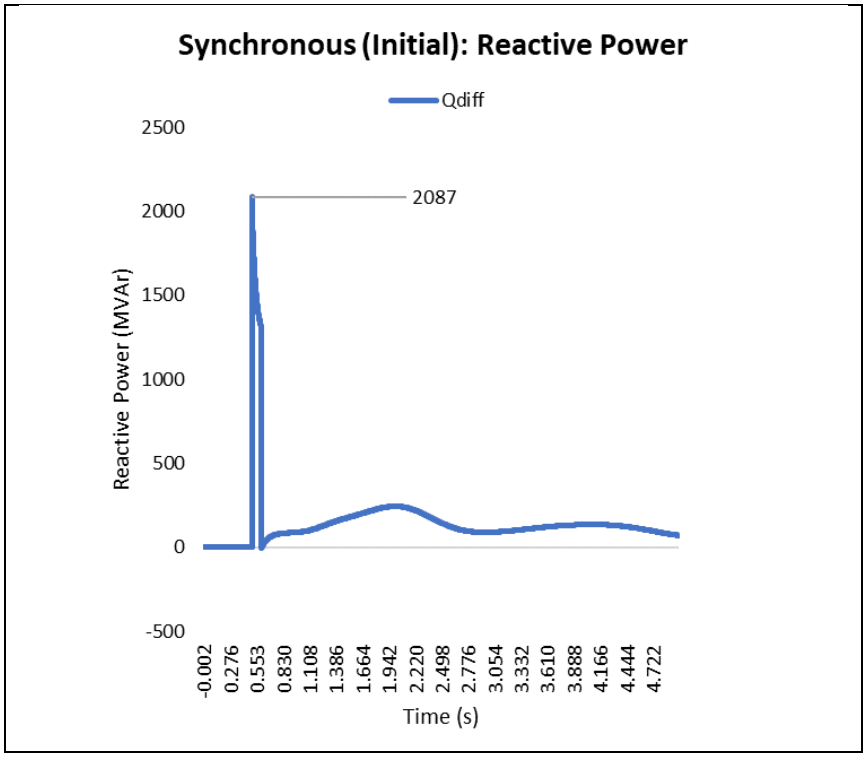

Figure 71 – Synchronous scenario reactive-power response.

The peak change in reactive-power is 2087 MVAr which is three times the reactive-power at voltage collapse. The phase 1 change is lower, but phase 2 has a higher initial reactive-power export and the overall contribution is increased. Reactive-power export is reduced to just below 1500 MVAr during the fault and supports post-fault voltage recovery

5.2.7 IBT RES scenario: active-power and reactive-power response for the marginal step case

The active-power export for the period up to 5 s is shown in Figure 72A (zoomed-in view in Figure 72B).

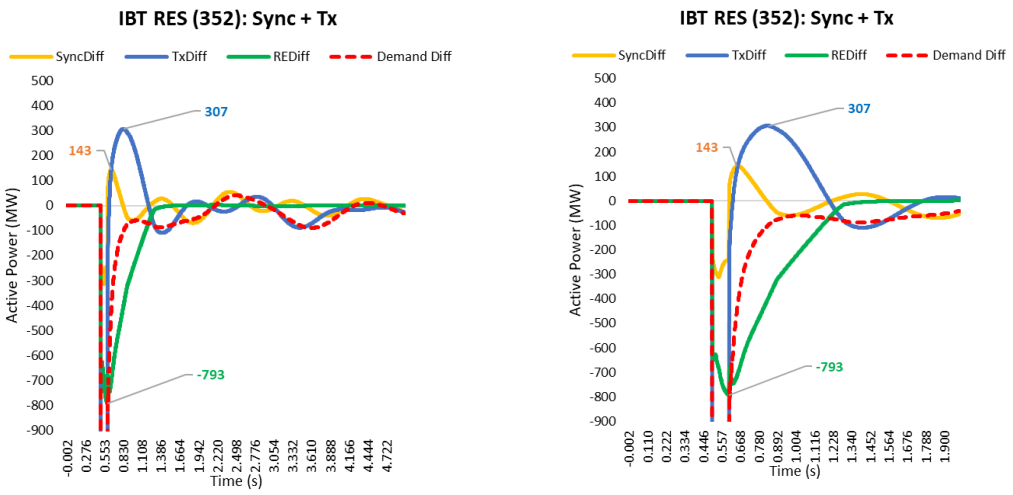

A B

Figure 72 – IBT RES scenario active-power response

The supply-area demand (load) recovery delay to reaching pre-fault levels takes 2 s, indicated by the red dashed line. The reduction in IBT RES active-power export (green)(Figure 72B) is 793 MW. The stability of this marginal case is reliant on the increased voltage at the Tx bus because of the fault impedance. The effect is to have an active-power export reduction. This reduces the risk of voltage collapse of the Tx-corridor. Synchronous generation (yellow) experiences acceleration because of the reduced electrical active-power export during the fault. Overshoot occurs 50 ms after fault clearance (143 MW), because of the kinetic energy stored in the shaft, which is now released into the grid after fault clearance. The Tx-corridor active-power change (blue) follows the synchronous active-power profile to support the deficit of active-power in the supply area. This increases the Tx-corridor active-power transfer as seen in Figure 72B. The active-power transfer along the Tx-corridor increases by 307 MW.

For the step 4 investigation the peak increase of active-power transfer along the Tx-corridor is 307 MW. The initial Tx-corridor loading is 2090 MW and when 307 MW is added, the total is 2397 MW. The Tx-corridor steady-state voltage collapse active-

power limit is 2371 MW, so the Tx-corridor active-power transfer is marginally greater than the Tx-corridor P-V steady-state margin by 26 MW (Table XIII step 4). Beyond this margin, step 5, the network was unstable.

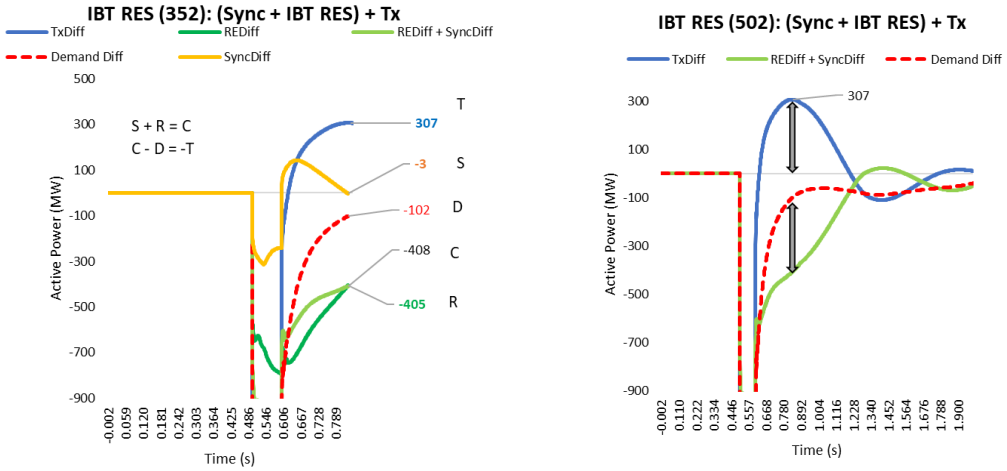

A B

Figure 73 – IBT RES active-power response

Table XV– Active-power disturbances at the time of the Tx-corridor maximum active-power flow

Description	MW
S = Local synchronous generator change (increase) in active-power export (Sync Diff)	-3
R = Local IBT RES change (reduction) in active-power export (RE Diff)	-405
C = Combined change (reduction) in locally generated active-power export (=S+R)	-408
D = Local demand change (reduction) in active-power import (Demand Diff)	-102
T = Tx-corridor change (increase) in active-power transfer (Tx Diff)	+307

The synchronous generator active-power change (S) is -3 MW. The IBT RES active-power change (R) is due to the LVRT active-power reduction of -405 MW. The combined local generation active-power change (C) is the sum of S + R, which equals -408 MW. This indicated that the total active-power generation has reduced by 408 MW. However, the study-area demand (load) has not fully recovered to pre-fault conditions. The difference between the C and D, Figure 73B arrow between red and green-black double arrow, is the total active-power transfer required from the Tx-corridor. Therefore C – D = -T. The negative T value indicates transfer into the supply

area and is indicated by the black double arrow between the blue line and zero line in Figure 73B.

The reactive-power dynamic response for the period up to 2sec is indicated in Figure 61.

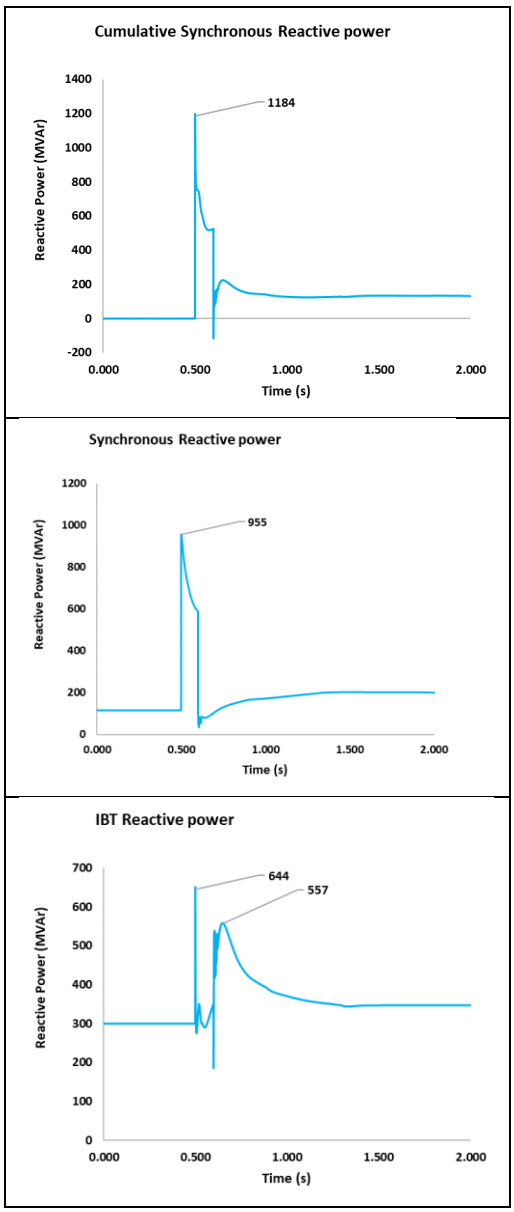

Figure 74 – IBT RES scenario reactive-power response

The peak reactive-power export is 1184 MVAr which is two times the reactive-power export at voltage collapse (Figure 74 top graph). Reactive-power supporting the fault voltage comes mainly from the local synchronous generators (Figure 74 bottom left). The IBT RES reactive-power reduces as active-power increases (Figure 74 bottom right). .

Chapter 6: Conclusions

6.1 Research conclusions

This research examined the impact of IBT RES LVRT response on classical P-V steady-state voltage collapse analysis, indicating that the IBT RES LVRT response has a large impact.

This research concluded that

- The IBT RES initial reactive-power export is an important consideration. Initial reactive-power import results in the highest active-power export reduction. This initial state is not recommended.
- Grid Codes should specify the IBT RES LVRT active-power response. The South African Grid Code and others only define the IBT RES LVRT reactive-power response. The active-power dispatch must fall within the IBT current ratings. This effectively requires the remaining current available after reactive-power prioritisation to be allocated to active-power.

The P-V voltage collapse analysis using the Cigre Nordic test network for both the synchronous scenario and the IBT RES scenarios concluded that

- Increased IBT RES reduces the system fault level and this is reflected in a marginal reduction of the Tx-corridor active-power transfer limit (for the limiting network contingency).
- Lower fault levels cause more severe voltage drops during fault conditions which in turn increases the IBT RES active-power export reduction which is not accounted for in classical P-V steady-state voltage collapse analysis.

Analysing the Tx-corridor P-V active-power transfer limits for the synchronous scenario and for the IBT RES scenario, for initial conditions that avoided voltage collapse concluded that

- The response for the synchronous scenario differs significantly from the IBT RES scenario and has a large impact on classical P-V steady-state voltage collapse limits. The post-fault response of local synchronous generators boosts active-power export and reduces the required Tx-corridor active-power

transfer. However, IBT RES has the opposite effect, increasing the required Tx-corridor active-power transfer.

- During a fault, the reactive-power export from a synchronous generator increases to over three times the steady-state value. In contrast, the reactive-power export from IBT RES is limited to its nominal reactive-power export during fault conditions.
- The approximate IBT RES characteristic response model developed, along with power scaling factors, can estimate the Tx-corridor voltage collapse active-power transfer margin. This helps determine the P-V analysis voltage collapse risk margin.

The reduction of active-power export will also impact classical frequency stability studies which only consider a trip of the largest generation unit or system infeed and not the impact of faults in the system.

6.2 Recommended for future research

It is recommended that future research investigates the impact of LVRT active-power export reduction on frequency stability studies, local area RoCoF and system RoCoF and phase jump.

MVAr planning studies for high IBT RES penetration networks with reduced synchronous plant should determine the consequences of reduced reactive-power support by IBT RES.

This research used standard load-flow software. Future studies should investigate the use of full EMT models.

Annexure: Literature platforms

Literature search performed on the following platforms but was not limited to these platforms.

- IEEE Xplore digital library - https://ieeexplore.ieee.org/Xplore/home.jsp
- Science Direct Journals - https://www.sciencedirect.com/
- Research gate - https://www.researchgate.net/
- Google Scholar - https://scholar.google.com/
- Cigre e-cigre on-line library - https://e-cigre.org/
- International Energy Agency IEA - https://webstore.iea.org/
- Electric grid test case repository - https://electricgrids.engr.tamu.edu/
- WEB search - https://www.google.com/
- Various books

Annexure: Simple Model - PSSE Load Flow Data

Lines

From Bus	From Name	To Bus	To Name	ID	R	X	B	Rate A MVA	Rate A MVA	km	R-Zero	X-Zero	B-Zero
2480	SIMPM1 132.00	60804	SIMPMWF BB_1132.00	1	0	0.0001	0	0	0	0	0	0	0
2480	SIMPM1 132.00	60804	SIMPMWF BB_1132.00	2	0.010525	0.047034	0.009911	176	238	20	0.042022	0.167435	0.007113
2480	SIMPM1 132.00	60804	SIMPMWF BB_1132.00	3	0.026311	0.117585	0.024778	176	238	50	0.105054	0.418587	0.017783
2480	SIMPM1 132.00	60804	SIMPMWF BB_1132.00	4	0.042098	0.188136	0.039645	176	238	80	0.168087	0.669739	0.028452
2480	SIMPM1 132.00	60804	SIMPMWF BB_1132.00	5	0.057885	0.258686	0.054512	176	238	110	0.23112	0.920891	0.039122

Bus

Bus Number	Bus Name	Base kV	Code
590	SIMPM4	400	3
2480	SIMPM1	132	1
52101	SIMPMWF2_33	33	4
52104	SIMPMWF2_0.6	0.7	4
52105	SIMPMWF4_33	33	4
52110	SIMPMWF5_0.6	0.7	2
52111	SIMPMWF6_33	33	1
52112	SIMPMWF7_33	33	4
52113	SIMPMWF6_0.6	0.7	4
52114	SIMPMWF7_0.6	0.7	4
60388	SIMPM	33	4
60389	SIMPM	33	4
60390	SIMPM	0.7	4

60804	SIMPMWF BB_1	132	1
Bus Number	Bus Name	Base kV	Code
92058	SIMPM22D	22	1
92060	SIMPM22E	22	1
92065	SIMPM22F	22	1
99304	SIMPM2	33	4
99305	SIMPM2	33	4
99306	SIMPM2	0.7	4

Generation

Bus Number	Bus Name	Id	Code	VSched (pu)	Remote Bus Number	In Service	PGen (MW)	PMax (MW)	PMin (MW)	QGen (Mvar)	QMax (Mvar)	QMin (Mvar)	Mbase (MVA)
590	SIMPM4 400.00	1	3	1.01	0	1	390.0979	665.1	0	-192.4535	322.1226	-322.1226	4000
52110	SIMPMWF5_0.60.6900	1	2	1	0	1	110	110	0	6.2814	53.2754	-53.2754	124
		R Source (pu)	X Source (pu)	R (pu)	Subtransient X (pu)	Transient X (pu)	Synchronous X (pu)	R-Negative (pu)	X-Negative (pu)	R-Zero (pu)	X-Zero (pu)	Machine Control Mode	Renewable Machine Power factor
		0	0.315	0	0.262	0.262	0.262	0	0.262	0	0.262	Conventional Machine	1
		0	0.8	0.8	0.8	0.8	0.8	0.01	0.8	0	0.8	Renewable: +, - Q limits based on WPF	0.9

Load

Bus Number	Bus Name	Id	Code	In Service	Scalable	Interruptible	Pload (MW)	Qload (Mvar)
2480	SIMPM1 132.00	2	1	1	1	0	500	90.4762

Annexure: WECC 2nd Generation - PSSE Dynamics Data

External Grid

590 'GENCLS' 1 3 0

Low Gain

52110 'USRMDL' 1 'REGCCU' 101 1 2 11 6 19 0 1 5.000 50.00 5.000 50.000 0.0100 60.000 1400.0 75.400 -75.400 1.00 1.1000 /

52110 'REECA1' 1 52110 0 1 0 0 0 0.9 1.1 0.02 -0.05 0.05 0.8 1 -1 0 0.1 0 0 0.02 1 -1 1.1 0 0 0.1 0 1 0 0.02 99 -99 1 0 1.2 0.04 0 1 0.5 1 0.7 0.5 0.9 0 0.02 0.01 0.5 0.01 0.7 0.5 0.9 1 /

52110 'WTDTA1' 1 4.95 0 0 1.8 1.5 /

52110 'REPCA1' 1 60804 0 0 0 0 1 0 0.02 0.5 1 0 0.2 0.7 0 0 0 99 -99 -0.01 0.01 1 -1 0.5 1 0.25 -0.0006 0.0006 99 -99 1 0 0.2 20 20 /

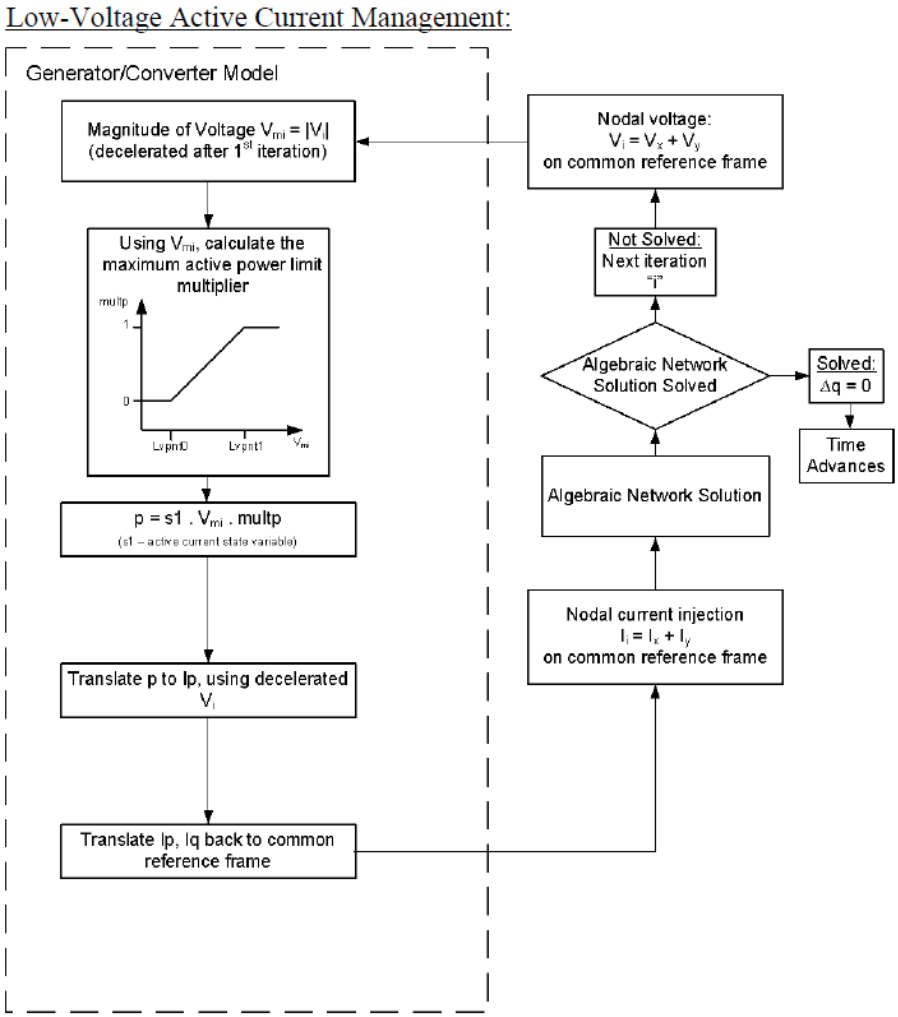

Dynamic Models – WECC 2nd Benchmark

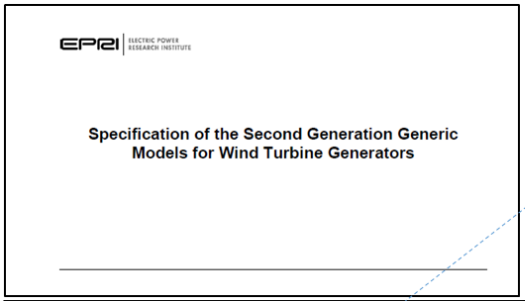

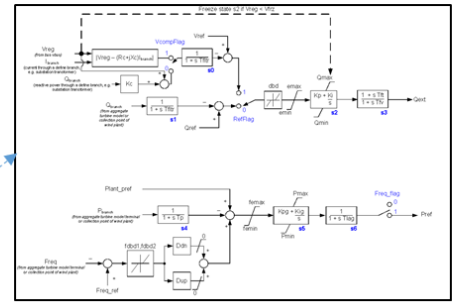

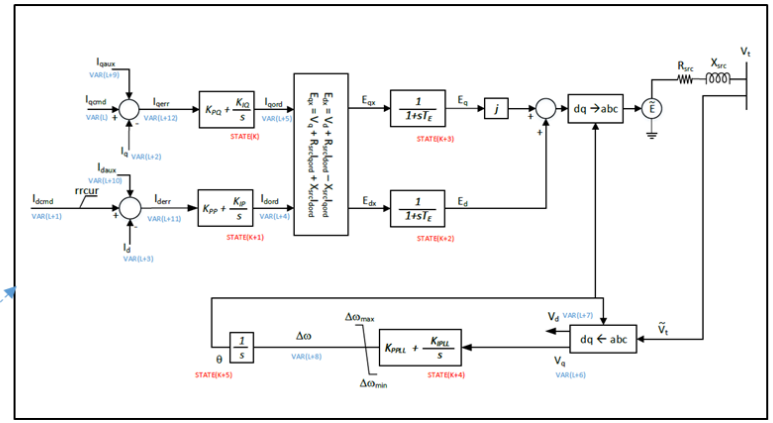

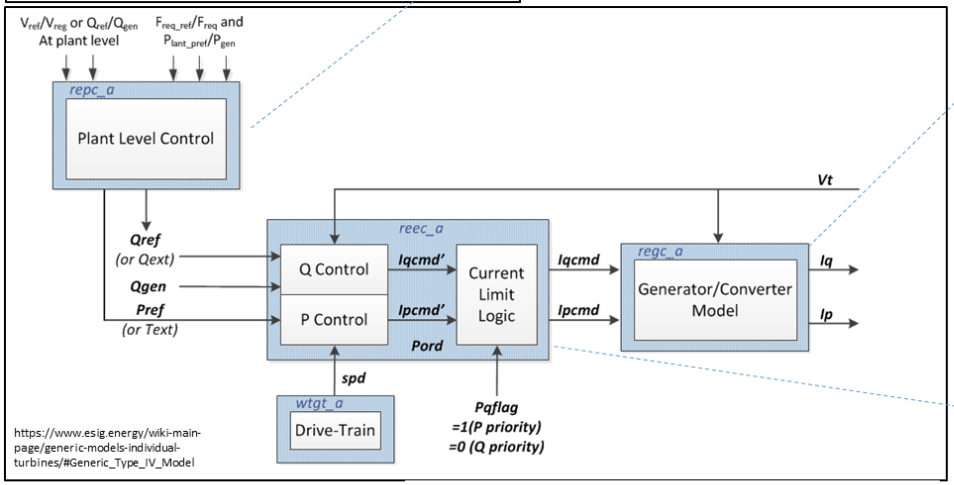

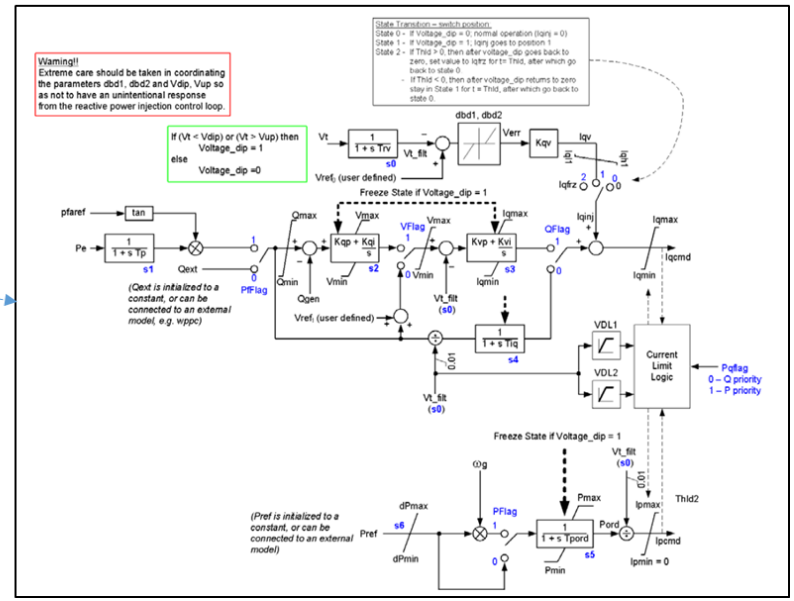

Functionality	Models Needed
Constant pf control	reec_a
Constant Q control	reec_a
Local V control only	reec_a
Local coordinated Q/V control only	reec_a
Plant level Q control	reec_a + repc_a
Plant level Vcontrol	reec_a + repc_a
Plant level V Control + coordinated local Q/V control	reec_a + repc_a
Plant level Q Control + coordinated local Q/V control	reec_a + repc_a

Dynamic control modes - Voltage control at plant level control (repc) and the electrical control (reec) constant Q control is used in this study. Below the reec constant Q indicated in red.

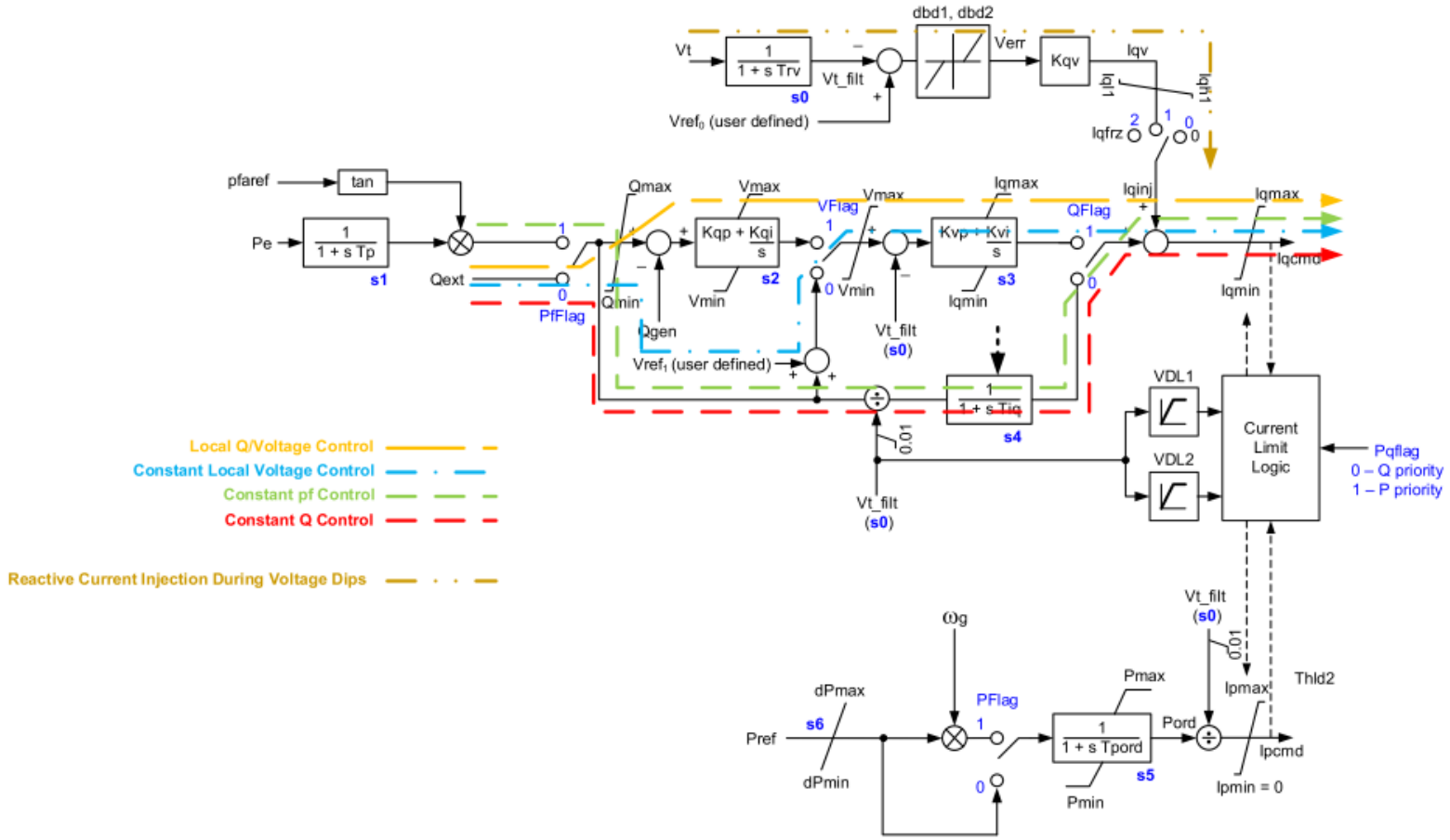

ICON	Value	Description
M	0	PQflag – current priority flag (1=Ip priority, 0=Iq priority)
M+1	1	PLLFLG – Enables/Disables PLL (1=enabled, 0=disabled)

CONs	Value	Description
J	5	K_{PQ} – Proportional gain on reactive current regulator
J+1	50	K_{IQ} – Integral gain on reactive current regulator
J+2	5	K_{PP} – Proportional gain on active current regulator
J+3	50	K_{IP} – Integral gain on active current regulator
J+4	0.01	T_E – Current delay time constant
J+5	60	K_{PPLL} – Proportional gain on PLL regulator
J+6	1400	K_{IPLL} – Integral gain on PLL regulator
J+7	75.4	Dw_{max} – Maximum angular speed limit
J+8	-75.4	Dw_{min} – Minimum angular speed limit
J+9	1	rrcur – Maximum rate of change of active current command
J+10	1.1	Imax – maximum current limit (pu)

**IBUS, 'USRMDL', ID, 'REGCCU', 101 , 1, 2, 11, 6, 19, ICON(M), ICON(M+1), CON(J) to CON(J+10) **

52110 'USRMDL' 1 'REGCCU' 101 1 2 11 6 19 0 1 5.000 50.00 5.000 50.000 0.0100 60.000 1400.0 75.400 -75.400 1.00 1.1000 /

Annexure: IBT Response – Sample for SCR Low, active-power 1.pu, pf 1 and line 1

The is a sample of the IBT response results. These set of graph relate to the dynamic run for a SCR low, Active-power 1.0 p.u., power factor 1.0 for line 1 (20km). The nine set of 6 graphs each represent the 9 faults with various admittance. The graph set are ordered from the largest admittance to the lowest. The largest admittance results in the lowest voltage reduction.

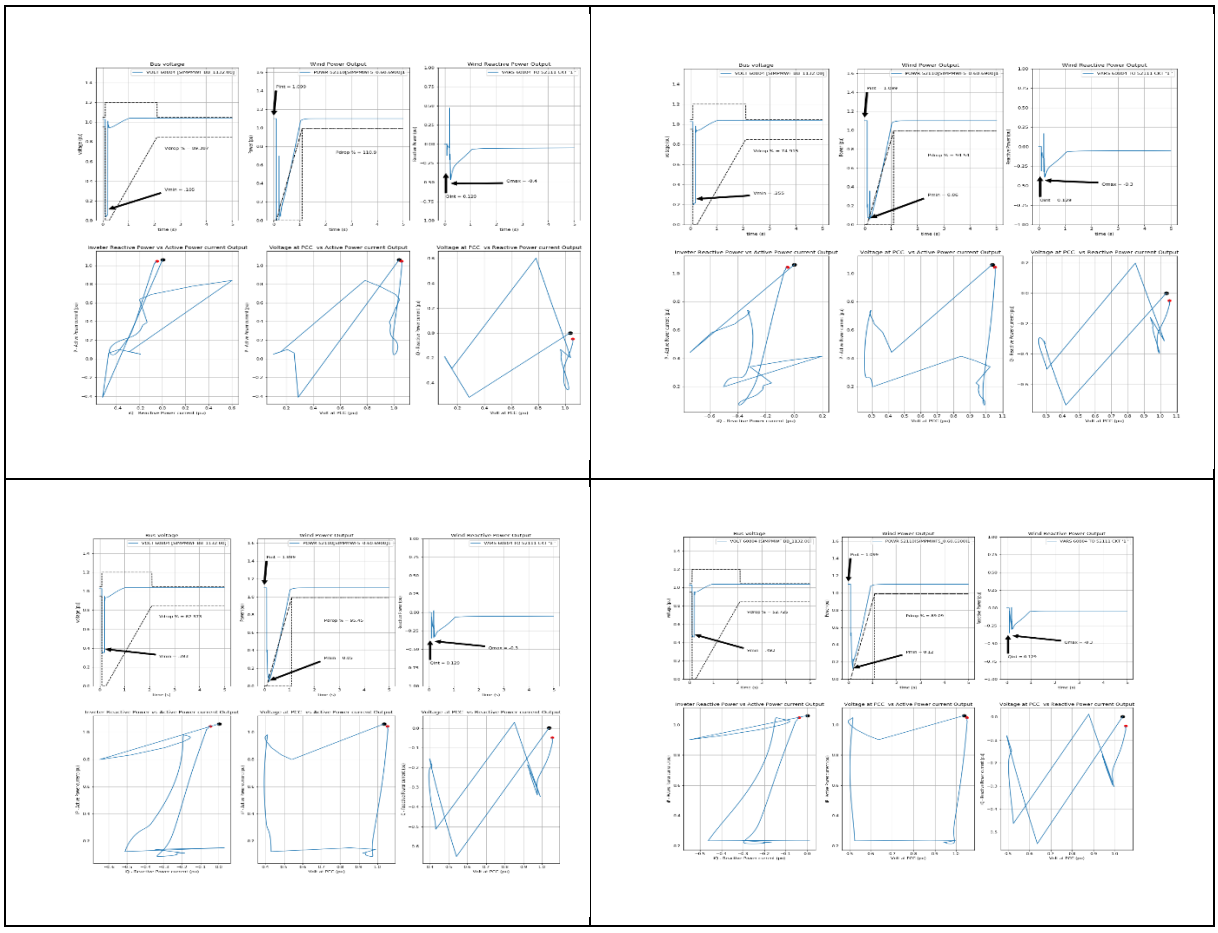

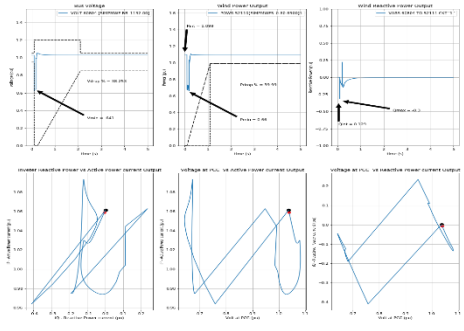

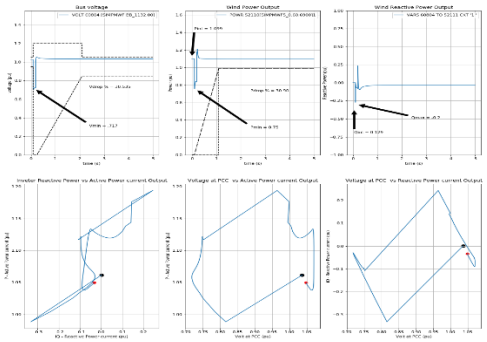

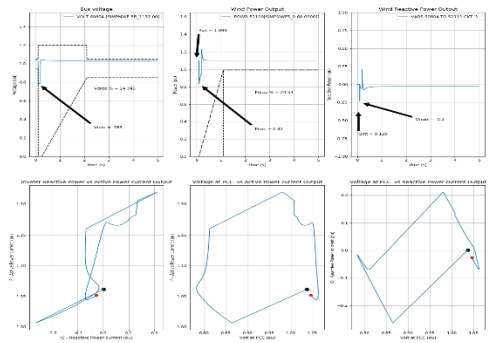

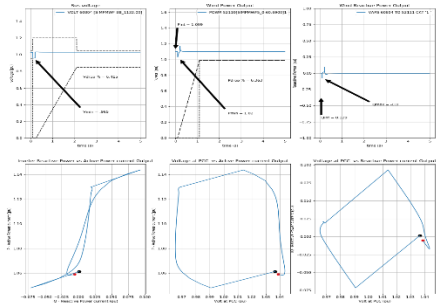

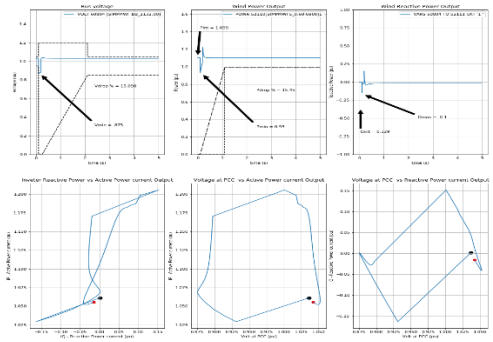

Case file:

D:\001 Ronald Data\100 Master\001 RE V_P_r2\003_M_s25_xr3_L1Var0.sav

Dyr file:

D:\001 Ronald Data\100 Master\001 RE V_P_r2\003_WECC2NewRev1EPRI_1.dyr

Faulted bus no:

590

Annexure: Voltage vs active-power for initial IBT active-power 1p.u. and 0.5p.u.

The dynamic response of 400kV voltage vs active-power output of the IBT for initial active-power output of 1p.u. and 0.5p.u. are shown in this annexure. Each dot is the results form a dynamic study with plot for 3 variation of power factor (PF) (PF=1, PF=0.95 exporting & PF=0.95 importing) and 3 variation of system strength (SCR H – High, SCR M – Medium and SCR L – low). The dynamic studies are performed for nine fault on the 400kV bus with varied admittance and 4 line distance to the IBT.

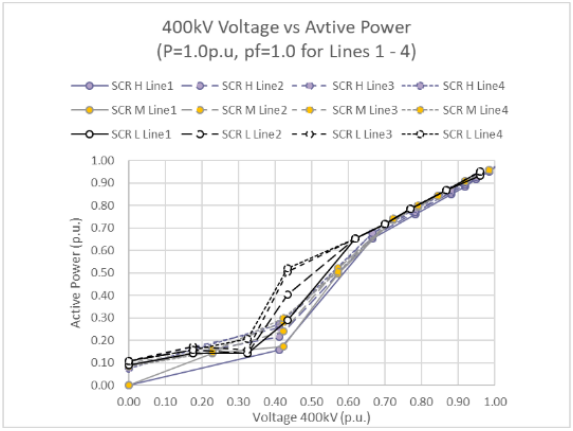

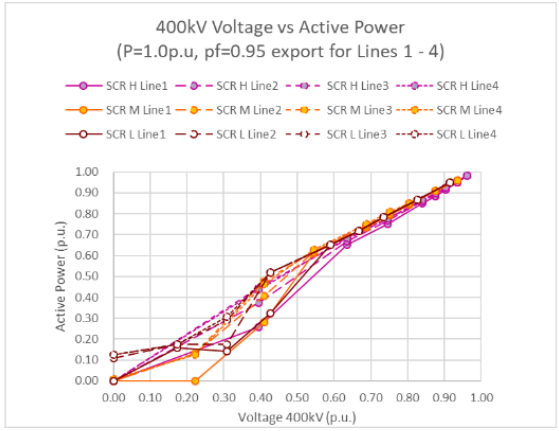

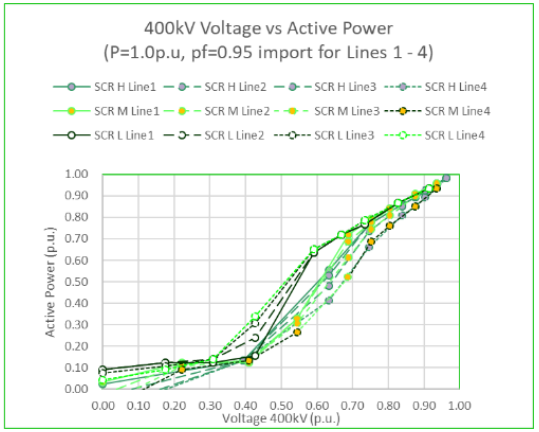

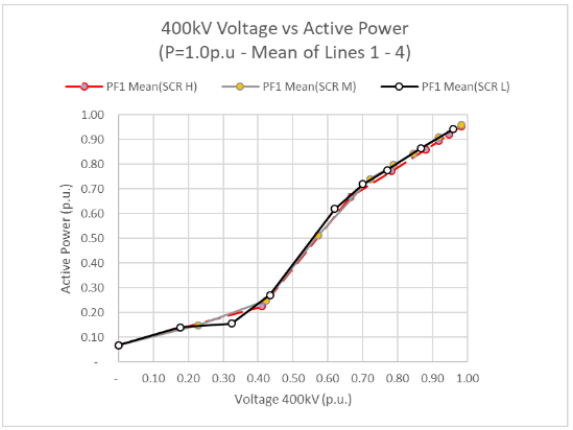

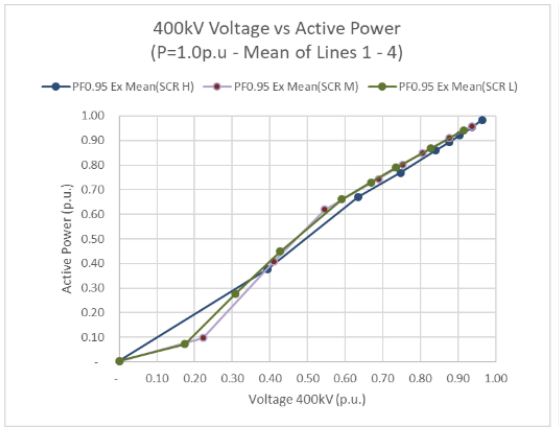

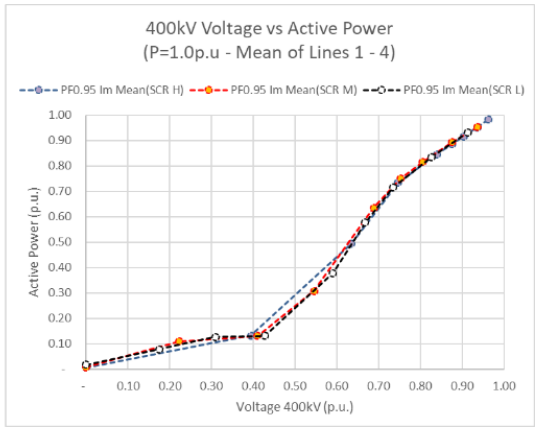

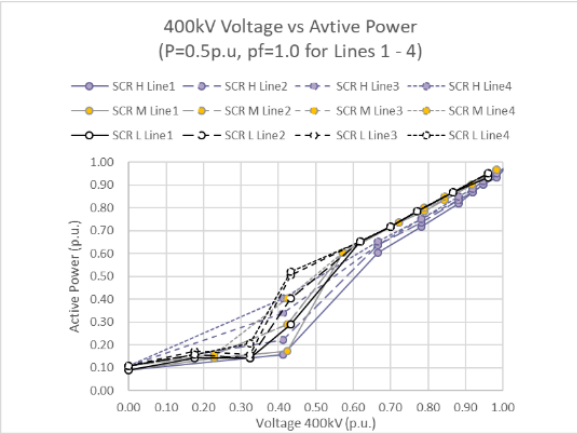
400kV Voltage vs Avtive Power
(P=0.5p.u, pf=1.0 for Lines 1 - 4)
SCR H Line1
SCR H Line2
SCR H Line3
SCR H Line4
SCR M Line1
SCR M Line2
SCR M Line3
SCR M Line4
SCR L Line1
SCR L Line2
SCR L Line3
SCR L Line4
Active Power (p.u.)
Voltage 400kV (p.u.)

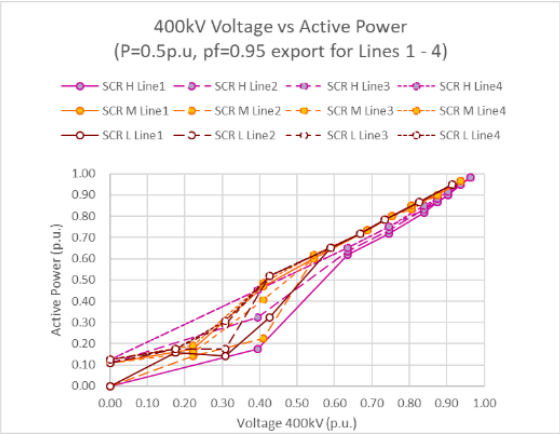
400kV Voltage vs Active Power
(P=0.5p.u, pf=0.95 export for Lines 1 - 4)
SCR H Line1
SCR H Line2
SCR H Line3
SCR H Line4
SCR M Line1
SCR M Line2
SCR M Line3
SCR M Line4
SCR L Line1
SCR L Line2
SCR L Line3
SCR L Line4
Active Power (p.u.)
Voltage 400kV (p.u.)

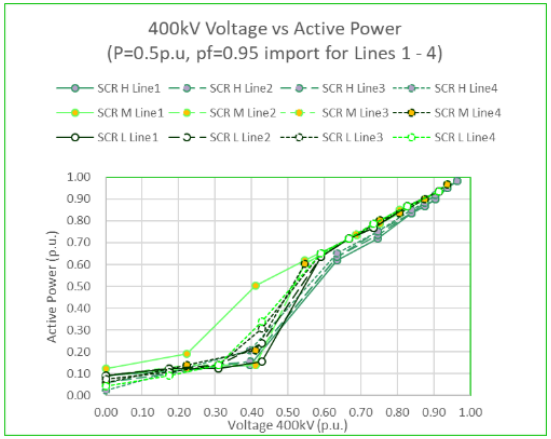
400kV Voltage vs Active Power
(P=0.5p.u, pf=0.95 import for Lines 1 - 4)
SCR H Line1
SCR H Line2
SCR H Line3
SCR H Line4
SCR M Line1
SCR M Line2
SCR M Line3
SCR M Line4
SCR L Line1
SCR L Line2
SCR L Line3
SCR L Line4
Active Power (p.u.)
Voltage 400kV (p.u.)

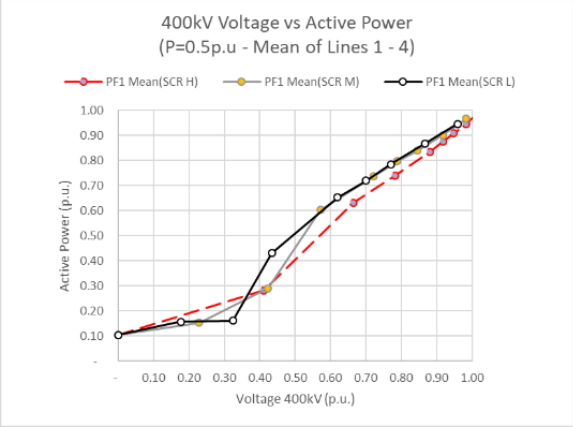
400kV Voltage vs Active Power
(P=0.5p.u - Mean of Lines 1 - 4)
PF1 Mean(SCR H)
PF1 Mean(SCR M)
PF1 Mean(SCR L)
Active Power (p.u.)
Voltage 400kV (p.u.)

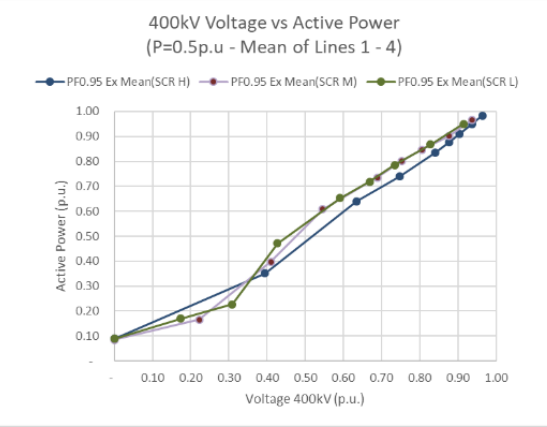
400kV Voltage vs Active Power
(P=0.5p.u - Mean of Lines 1 - 4)
PF0.95 Ex Mean(SCR H)
PF0.95 Ex Mean(SCR M)
PF0.95 Ex Mean(SCR L)
Active Power (p.u.)
Voltage 400kV (p.u.)

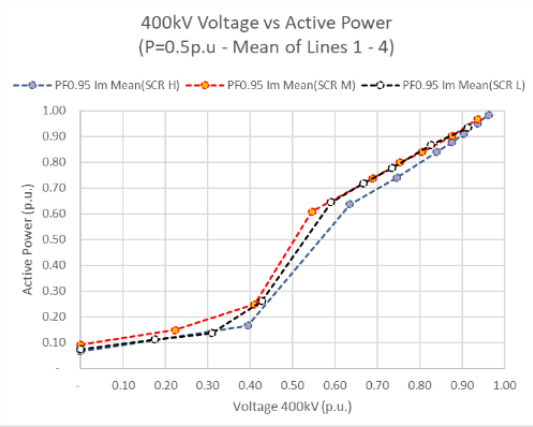
400kV Voltage vs Active Power
(P=0.5p.u - Mean of Lines 1 - 4)
PF0.95 Im Mean(SCR H)
PF0.95 Im Mean(SCR M)
PF0.95 Im Mean(SCR L)
Active Power (p.u.)
Voltage 400kV (p.u.)

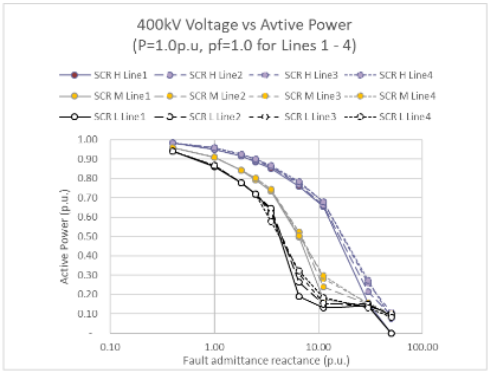
400kV Voltage vs Avtive Power
(P=1.0p.u, pf=1.0 for Lines 1 - 4)
SCR H Line1
SCR H Line2
SCR H Line3
SCR H Line4
SCR M Line1
SCR M Line2
SCR M Line3
SCR M Line4
SCR L Line1
SCR L Line2
SCR L Line3
SCR L Line4
Active Power (p.u.)
Fault admittance reactance (p.u.)

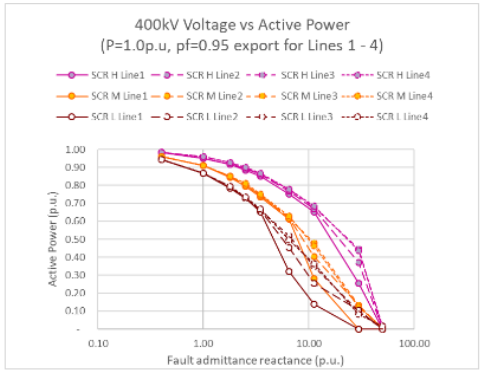
400kV Voltage vs Active Power
(P=1.0p.u, pf=0.95 export for Lines 1 - 4)
SCR H Line1
SCR H Line2
SCR H Line3
SCR H Line4
SCR M Line1
SCR M Line2
SCR M Line3
SCR M Line4
SCR L Line1
SCR L Line2
SCR L Line3
SCR L Line4
Active Power (p.u.)
Fault admittance reactance (p.u.)

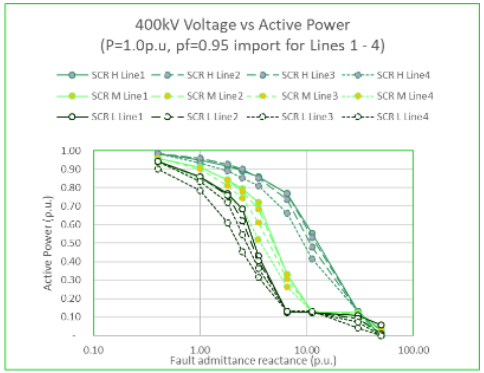
400kV Voltage vs Active Power
(P=1.0p.u, pf=0.95 import for Lines 1 - 4)
SCR H Line1
SCR H Line2
SCR H Line3
SCR H Line4
SCR M Line1
SCR M Line2
SCR M Line3
SCR M Line4
SCR L Line1
SCR L Line2
SCR L Line3
SCR L Line4
Active Power (p.u.)
Fault admittance reactance (p.u.)

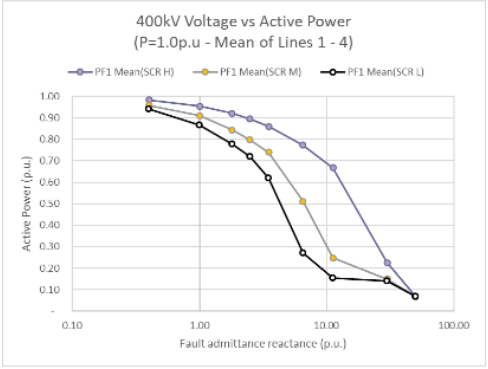
400kV Voltage vs Active Power
(P=1.0p.u - Mean of Lines 1 - 4)
PF1 Mean(SCR H)
PF1 Mean(SCR M)
PF1 Mean(SCR L)
Active Power (p.u.)
Fault admittance reactance (p.u.)

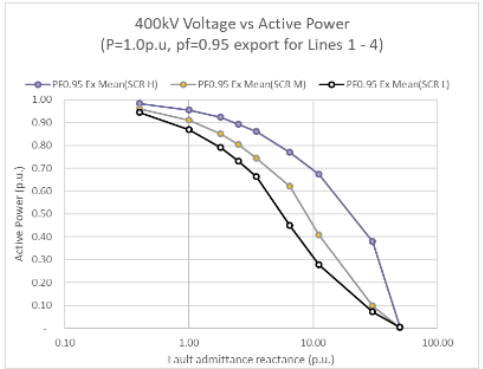
400kV Voltage vs Active Power
(P=1.0p.u, pf=0.95 export for Lines 1 - 4)
PF0.95 Ex Mean(SCR H)
PF0.95 Ex Mean(SCR M)
PF0.95 Ex Mean(SCR L)
Active Power (p.u.)
Fault admittance reactance (p.u.)

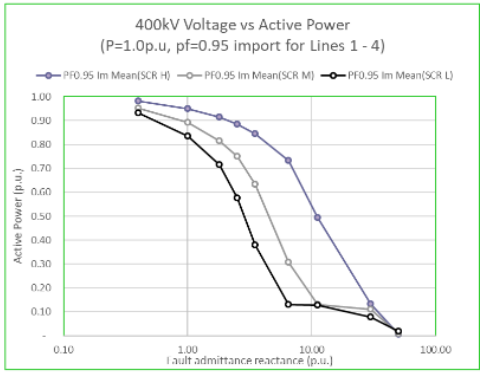
400kV Voltage vs Active Power
(P=1.0p.u, pf=0.95 import for Lines 1 - 4)
PF0.95 Im Mean(SCR H)
PF0.95 Im Mean(SCR M)
PF0.95 Im Mean(SCR L)
Active Power (p.u.)
Fault admittance reactance (p.u.)

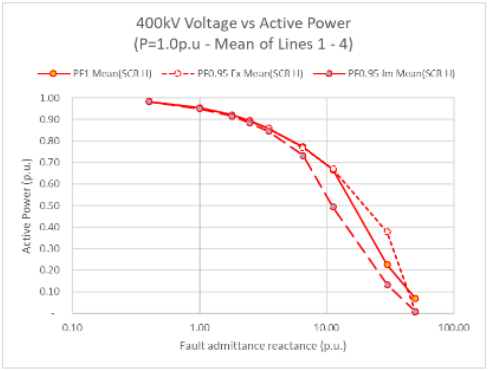
400kV Voltage vs Active Power
(P=1.0p.u - Mean of Lines 1 - 4)
PF1 Mean(SCR H)
PF0.95 Ex Mean(SCR H)
PF0.95 Im Mean(SCR H)
Active Power (p.u.)
Fault admittance reactance (p.u.)

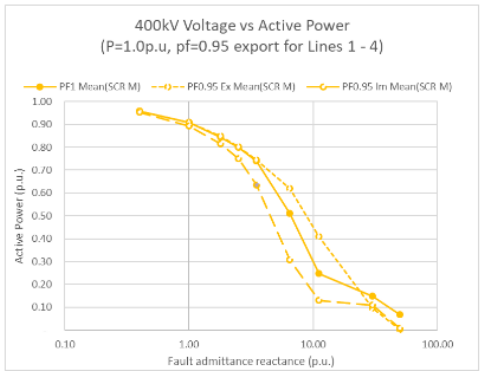
400kV Voltage vs Active Power
(P=1.0p.u, pf=0.95 export for Lines 1 - 4)
PF1 Mean(SCR M)
PF0.95 Ex Mean(SCR M)
PF0.95 Im Mean(SCR M)
Active Power (p.u.)
Fault admittance reactance (p.u.)

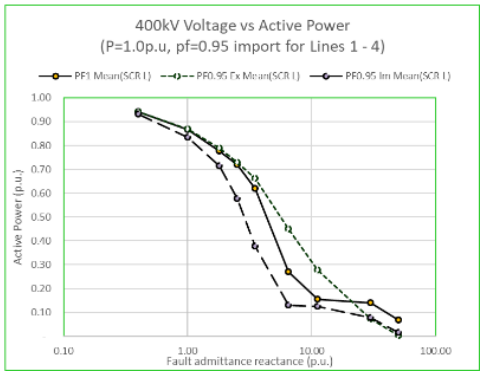
400kV Voltage vs Active Power
(P=1.0p.u, pf=0.95 import for Lines 1 - 4)
PF1 Mean(SCR L)
PF0.95 Ex Mean(SCR L)
PF0.95 Im Mean(SCR L)
Active Power (p.u.)
Fault admittance reactance (p.u.)

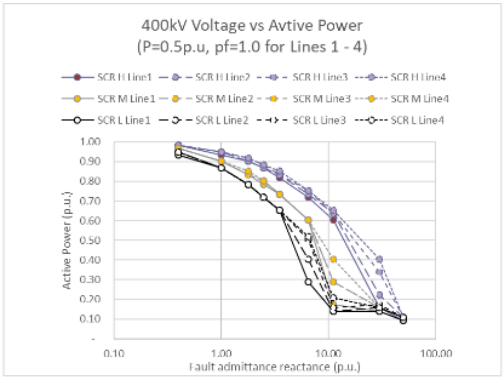
400kV Voltage vs Avtive Power
(P=0.5p.u, pf=1.0 for Lines 1 - 4)
SCR H Line1
SCR H Line2
SCR H Line3
SCR H Line4
SCR M Line1
SCR M Line2
SCR M Line3
SCR M Line4
SCR L Line1
SCR L Line2
SCR L Line3
SCR L Line4
Active Power (p.u.)
Fault admittance reactance (p.u.)

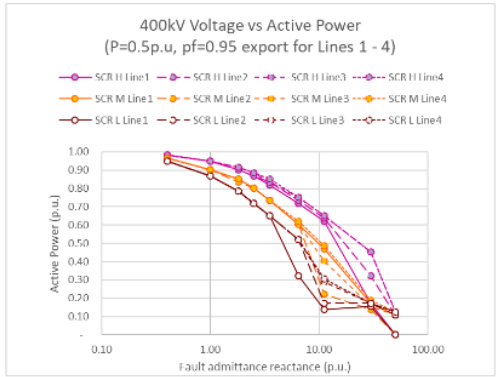
400kV Voltage vs Active Power
(P=0.5p.u, pf=0.95 export for Lines 1 - 4)
SCR H Line1
SCR H Line2
SCR H Line3
SCR H Line4
SCR M Line1
SCR M Line2
SCR M Line3
SCR M Line4
SCR L Line1
SCR L Line2
SCR L Line3
SCR L Line4
Active Power (p.u.)
Fault admittance reactance (p.u.)

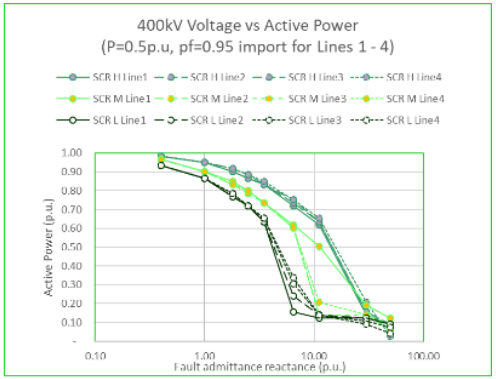
400kV Voltage vs Active Power
(P=0.5p.u, pf=0.95 import for Lines 1 - 4)
SCR H Line1
SCR H Line2
SCR H Line3
SCR H Line4
SCR M Line1
SCR M Line2
SCR M Line3
SCR M Line4
SCR L Line1
SCR L Line2
SCR L Line3
SCR L Line4
Active Power (p.u.)
Fault admittance reactance (p.u.)

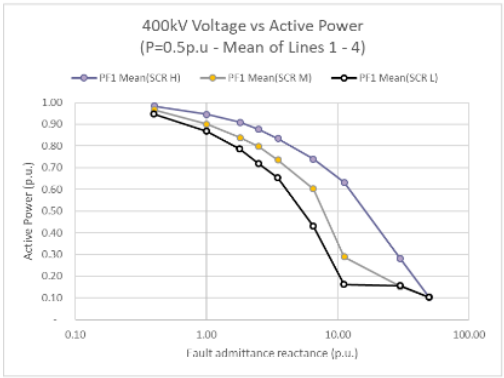
400kV Voltage vs Active Power
(P=0.5p.u - Mean of Lines 1 - 4)
PF1 Mean(SCR H)
PF1 Mean(SCR M)
PF1 Mean(SCR L)
Active Power (p.u.)
Fault admittance reactance (p.u.)

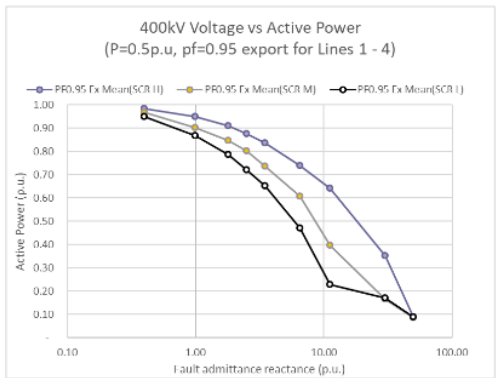
400kV Voltage vs Active Power
(P=0.5p.u, pf=0.95 export for Lines 1 - 4)
PF0.95 Ex Mean(SCR H)
PF0.95 Ex Mean(SCR M)
PF0.95 Ex Mean(SCR L)
Active Power (p.u.)
Fault admittance reactance (p.u.)

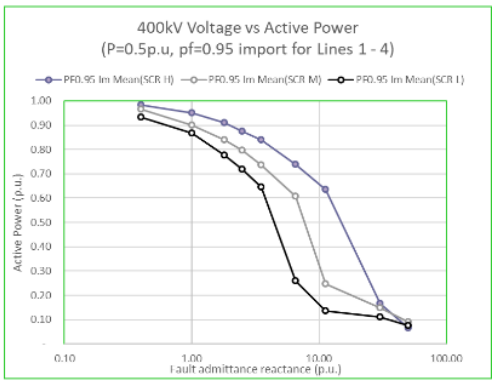
400kV Voltage vs Active Power
(P=0.5p.u, pf=0.95 import for Lines 1 - 4)
PF0.95 Im Mean(SCR H)
PF0.95 Im Mean(SCR M)
PF0.95 Im Mean(SCR L)
Active Power (p.u.)
Fault admittance reactance (p.u.)

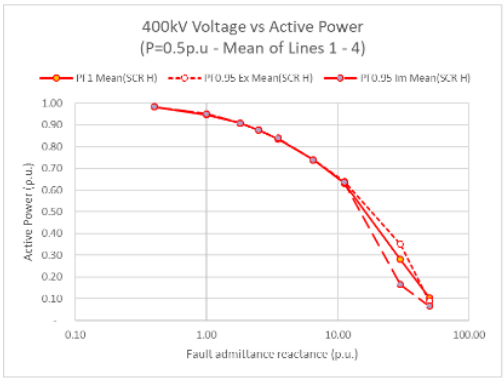
400kV Voltage vs Active Power
(P=0.5p.u - Mean of Lines 1 - 4)
PF1 Mean(SCR H)
PF0.95 Ex Mean(SCR H)
PF0.95 Im Mean(SCR H)
Active Power (p.u.)
Fault admittance reactance (p.u.)

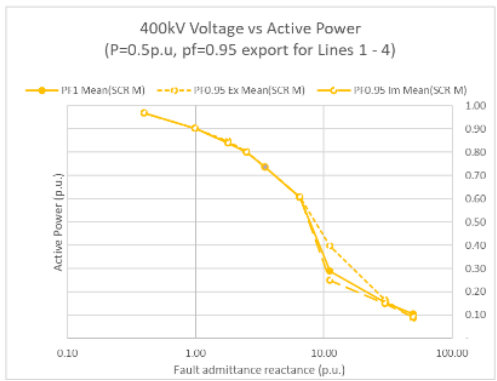
400kV Voltage vs Active Power
(P=0.5p.u, pf=0.95 export for Lines 1 - 4)
PF1 Mean(SCR M)
PF0.95 Ex Mean(SCR M)
PF0.95 Im Mean(SCR M)
Active Power (p.u.)
Fault admittance reactance (p.u.)

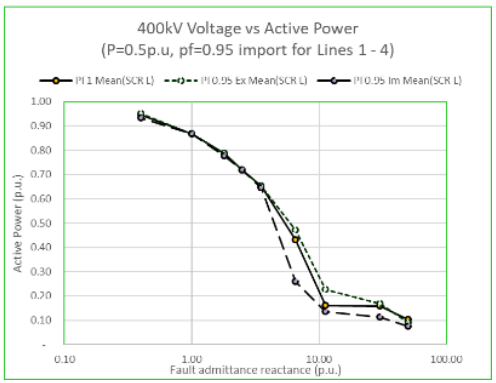
400kV Voltage vs Active Power
(P=0.5p.u, pf=0.95 import for Lines 1 - 4)
PF1 Mean(SCR L)
PF0.95 Ex Mean(SCR L)
PF0.95 Im Mean(SCR L)
Active Power (p.u.)
Fault admittance reactance (p.u.)

REFERENCES

[1] A. AL-Hinai, "voltage collapse prediction for interconnected power systems," Master, West Virginia Universiity, https://researchrepository.wvu.edu/cgi/viewcontent.cgi?article=2068&context=etd, 2000. [Online]. Available: https://researchrepository.wvu.edu/cgi/viewcontent.cgi?article=2068&context=etd

[2] C. W. Taylor, *Power System Voltage Stability* (Power System Engineering Series). McGraw-Hill, Inc., 1992.

[3] IRENA, "Renewable capacity statistics 2020," IRENA, www.irena.org, 2020 2020. Accessed: 20200221. [Online]. Available: https://www.irena.org/publications/2020/Mar/Renewable-Capacity-Statistics-2020

[4] A. D. International Renewable Energy Agency, "IRENA (2020), Renewable Power Generation Costs in 2019,," 2019 2020. Accessed: 20200221. [Online]. Available: https://www.irena.org/-/media/Files/IRENA/Agency/Publication/2020/Jun/IRENA_Power_Generation_Costs_2019.pdf

[5] C. B4.62, "Cigre TB 671 Connection of wind farms week network," CIGRE, 2016/12/01 2016.

[6] M. Sarkar, M. Altin, P. E. Sørensen, and A. D. Hansen, "Reactive-power Capability Model of Wind Power Plant Using Aggregated Wind Power Collection System," *Energies,* vol. 12, no. 9, p. 1607, 2019. [Online]. Available: https://www.mdpi.com/1996-1073/12/9/1607.

[7] P. Kundur, *Power System Stability and Control* (Power System Engineering Series). McGraw-Hill, Inc., 1993.

[8] D. Flynn *et al.*, "Technical impacts of high penetration levels of wind power on power system stability," *Wiley Interdisciplinary Reviews: Energy and Environment,* vol. 6, 06/01 2016.

[9] H. Karbouj and Z. H. Rather, "A Novel Wind Farm Control Strategy to Mitigate Voltage Dip Induced Frequency Excursion," *IEEE Transactions on Sustainable Energy,* vol. 10, no. 2, pp. 637-645, 2019.

[10] D. F. Z. H. Rather, Z. H. Rather, and D. Flynn, "Impact of voltage dip induced delayed active-power recovery on wind integrated power systems," ed: Elsevier, 2017.

[11] H. C. Xinyu Liang , Jayashri Ravishankar, "Analytical Methods of Voltage Stability in Renewable Dominated Power Systems: A Review," *MDPI electricity,* vol. 75-107, 2022. [Online]. Available: https://doi.org/10.3390/electricity3010006.

[12] T. 38.02.08, "Voltage collapse log term dyn phase 2," 1995. [Online]. Available: https://www.e-cigre.org/.

[13] T. F. 38.02.10, "Modelling of voltage collapse including dynamic phenoma.pdf," *Cigre TB075,* 1993. [Online]. Available: https://www.e-cigre.org/.

[14] T. F. 38.02.12, "Criteria and countermeasures for voltage collapse," *CIGRE,* 1995. [Online]. Available: https://www.e-cigre.org/.

[15] D. S. M. Yadav, N. Pal, "Review and Compliance of Grid Code with Renewable Energy Integration," 2015. [Online]. Available: https://regridintegrationindia.org/wp-content/uploads/sites/3/2017/09/GIZ17_189_posterpaper_Monika_Yadav.pdf.

[16] N. M. Thomas Ackermann, Tom Brown, Peter-Philipp Schierhorn (Energynautics GmbH), Francisco and F. G. a. M. A. Boshell, "scaling up variable renewable power: the role of grid codes," IRENA, 2016. [Online]. Available: www.irena.org/Publications.

[17] G. S. Anastasios Oulis Rousis, Noel Cunniffe, Sheila Nolan, Hannele Holtinnen, Caroline Bono, Ye Wang, Marie-Ann Evans, Endika Urresti Padrón, Wojciech Jaworski, Przemyslaw Kacprzak, Bernardo Silva, "State-of-the-Art Literature Review of System

Scarcities High Levels of Renewable Generation," 2018/04/27 2018.

[18] D. H. T. Breithaupt, L. Hofmann, A. Mertens, R. Meyer, N. Farrokhseresht, B. Tuinema, D. Wang, J. Rueda Torres, S. Rüberg, V. Sewdien, "MIGRATE – Massive InteGRATion of power Electronic devices - Report on systemic issues," https://www.h2020-migrate.eu/, 2016/12/15 2016.

[19] J. A. David Stenberg, "Master Development of a system protection model

against voltage collapse in PSS/E," Master Master, Department of Energy & Environment

Chalmers University of Technology, Chalmers Univercity of Technology, 2016. [Online]. Available: https://publications.lib.chalmers.se/records/fulltext/243594/243594.pdf

[20] P. Kundur *et al.*, "Definition and classification of power system stability IEEE/CIGRE joint task force on stability terms and definitions," *IEEE Transactions on Power Systems,* vol. 19, no. 3, pp. 1387-1401, 2004, doi: 10.1109/TPWRS.2004.825981.

[21] P. Kundur, J. Paserba, and S. Vitet, "Overview on definition and classification of power system stability," in *CIGRE/IEEE PES International Symposium Quality and Security of Electric Power Delivery Systems, 2003. CIGRE/PES 2003.*, 8-10 Oct. 2003 2003, pp. 1-4, doi: 10.1109/QSEPDS.2003.159786.

[22] O. Samuelsson and S. Lindahl, "Discussion of “Definition and Classification of Power System Stability”," *IEEE Transactions on Power Systems,* vol. 21, no. 1, pp. 446-447, 2006, doi: 10.1109/TPWRS.2005.861994.

[23] H. Saadat, *Power System Analysis*. WCB/McGraw-Hill, 1999.

[24] N. Hatziargyriou *et al.*, *Stability Definitions and Characterization of Dynamic Behavior in Systems with High Penetration of Power Electronic Interfaced Technologies*. 2020.

[25] F. c. N. Hatziargyriou *et al.*, "Stability definitions and characterization of dynamic behavior in systems with high penetration of power electronic interfaced technologies," *IEEE Access,* 2020/04/01 2020.

[26] J. O. O. Bukola Babatunde Adetokun, Christopher Maina Muriithi, "Application of large-scale grid-connected solar photovoltaic system for voltage stability improvement of weak national grids," *Scientific Report,* no. December 2021, 2021. [Online]. Available: https://www.researchgate.net/publication/357452354_Application_of_large-scale_grid-connected_solar_photovoltaic_system_for_voltage_stability_improvement_of_weak_national_grids.

[27] G. P. E. Josselin Fournel (EDF), Noel Cunniffe (EirGrid), Hassan Qazi (EirGrid), Sheila Nolan (EirGrid), David Corcoran (EirGrid), Peter Wall (EirGrid), Jacek Wasilewski (PSE), Mateusz Skwarski (PSE), Nuno Fulgêncio (INESC TEC), Carlos Moreira (INESC TEC), Bernardo Silva (INESC TEC), Hannele Holttinen (VTT), Jussi Ikaheimo (VTT), Hanspeter Höschle (VITO/EnergyVille), "Models for Simulating Technical Scarcities on the European Power System with High Levels of Renewable Generation," 2018.

[28] NERC, "Inverter-BasedResource Performance and Analysis Technical Workshop NERC IRPT Meeting February 2019," pp. 332 - 335.

[29] J. L. B Schowe-Von Der Brelie, M Schellschmidt, S Schrobsdorff, J Scheffer, C Kahlen, "Relevance of high-voltage-ride-through capability and testing," *23rd International Conference on Electricity Distribution,* vol. Lyon, 15-18 June 2015, p. 1391, 2015.

[30] NERC, "1,200 MW Fault Induced Solar Photovoltaic Resource Interruption Disturbance Report," *NERC Report,* 2017.

[31] AEMO, "Black system South Australia 28 september 2016," *AEMO,* 2017.

[32] NERC, "900 MW Fault Induced Solar Photovoltaic Resource Interruption Disturbance Report Southern California Event: October 9, 2017 " *NERC Report,* 2018.

[33] NERC, "900 MW Fault Induced Solar Photovoltaic Resource Interruption Disturbance Report," NERC, NERC, Altanta, 2018/02 2018. [Online]. Available: www.nerc.com

[34] Z. H. Rather and D. Flynn, "Voltage Dip Induced Frequency Events in Wind Integrated Power Systems," *IFAC-PapersOnLine,* vol. 48, no. 30, pp. 572-577, 2015/01/01/ 2015, doi: https://doi.org/10.1016/j.ifacol.2015.12.441.

[35] R. W. a. M. Kenyon, Barry A and Hodge, Brian S, "Assessment of IEEE 1547 Low-Voltage Ride-Through Criteria Impact on Bulk Power System Dynamics Following Transmission Path Fault," 2019-08-13 2019. [Online]. Available: https://www.osti.gov/biblio/1557959. Conference: Presented at the 2019 IEEE Power and Energy Society General Meeting, 4-8 August 2019, Atlanta, Georgia.

[36] EirGrid, "EirGrid Grid Code Version 6.0," EirGrid 22 July 2015 2015.

[37] NERSA. "Grid connection code for renewable power plants (RPPS) connected to the electricity transmission system (Tx) or the distribution system (Dx) in South Africa." https://www.nersa.org.za/electricity-overview/electricity-grid-code/ (accessed 2022).

[38] "Model User Guide for Generic Renewable Energy System Models," EPRI, 2018/07/01 2018. [Online]. Available: www.epri.com

[39] NERC, *NERC | Report Title | Report Date I Reliability Guideline Power Plant Model Verification for Inverter-Based Resources*. 2018.

[40] J. W. G. C4/C6.35/CIRED, "Modelling of inverter-based generation for power system dynamic studies," CIGRE, 2018/05/18 2018.

[41] WG C4.106, "Cigre TB 328 Modeling and dynamic behavior of wind generation as it relates to power system control and dynamic performance," e-CIGRE, 2007 2007.

[42] *Wind energy generation systems*, IEC, 2020.

[43] A. Ellis and E. Muljadi, "Wind power plant representation in large-scale power flow simulations in WECC," in *2008 IEEE Power and Energy Society General Meeting - Conversion and Delivery of Electrical Energy in the 21st Century*, 20-24 July 2008 2008, pp. 1-6.

[44] EPRI, "Inverter Controls and Protection Guidelines: Control Settings for the Generic Renewables Energy Resource Models to Study the Impact of Inverter-Based Resources Performance on Bulk Power System Stability and Transmission Protection.," EPRI, Palo Alto, CA, 2018/07/01 2018.

[45] P. Pourbeik *et al.*, "An Aggregate Dynamic Model for Distributed Energy Resources for Power System Stability Studies," vol. 14, pp. 38-48, 06/28 2019. [Online]. Available: https://e-cigre.org/publication/CSE014-cse-014.

[46] L. P. Thierry VAN CUTSEM, "Description, Modeling and Simulation Results of a Test System for Voltage Stability Analysis," University of Li`ege, Belgium, University of Li`ege, Belgium, 2013.

[47] S. Müller, "Development of Nordic 32 system model and performance analysis based on real operation statistics," Kungliga Tekniska högskolan (KTH), School of Electrical Engineering and Computer Science (EECS), Teknikringen 33-III, SE-114 28 Stockholm, Sweden, Kungliga Tekniska högskolan (KTH), 2019. [Online]. Available: https://www.diva-portal.org/smash/get/diva2:1395253/FULLTEXT01.pdf

[48] D. Peppas, "Development and Analysis of Nordic32 Power System Model in PowerFactory," Masters, School of Electrical Engineering Electric Power Systems, Royal Institute of Technology, KTH Electrical Engineering, 2008.